AN EXPERIMENTAL INVESTIGATION OF THE BURNING MECHANISMS OF AMMONIUM PERCHLORATE COMPOSITE SOLID PROPELLANTS

A THESIS

Presented to

The Faculty of the Graduate Division

by

Al Michael Varney

In Partial Fulfillment

of the Requirements for the Degree

Doctor of Philosophy

in the School of Aerospace Engineering

Georgia Institute of Technology

May, 1970

In presenting the dissertation as a partial fulfillment of the requirements for an advanced degree from the Georgia Institute of Technology, I agree that the Library of the Institute shall make it available for inspection and circulation in accordance with its regulations governing materials of this type. I agree that permission to copy from, or to publish from, this dissertation may be granted by the professor under whose direction it was written, or, in his absence, by the Dean of the Graduate Division when such copying or publication is solely for scholarly purposes and does not involve potential financial gain. It is understood that any copying from, or publication of, this dissertation which involves potential financial gain will not be allowed without written permission.

5/28/70

7/25/68

AN EXPERIMENTAL INVESTIGATION OF THE

BURNING MECHANISMS OF AMMONIUM PERCHLORATE

COMPOSITE SOLID PROPELLANTS

Approved:

Chairman

Date approved by Chairman: 5/29/70

ACKNOWLEDGMENTS

I would like to express my appreciation to Dr. Warren C. Strahle and Professor Edward W. Price for their suggestion of the thesis topic and for cooperation and counsel during the investigation. The many discussions with my thesis advisor, Dr. Warren C. Strahle, concerning the theoretical aspects of the investigation were both stimulating and enlightening; his guidance and encouragement are sincerely appreciated. The careful examination of the manuscript by Dr. Warren C. Strahle and the other members of my reading committee, Drs. Samuel V. Shelton and Ben T. Zinn, is appreciated.

I am grateful to Dr. R. H. W. Waesche for providing counsel and advice concerning the techniques of differential scanning calorimetry. Mr. Thom Boggs contributed significantly to the study by investigating the deflagration behavior of compacted polycrystalline ammonium perchlorate. I also appreciate the comments and advice of Dr. Arnold L. Ducoffe concerning the experimental aspects of the investigation. I wish to thank Mr. Michael D. Shapiro for numerous discussions on combustion chemistry during the research and for his critical study of the manuscript. The assistance of Mr. Calvin H. Wiser, Mr. T. Michal Dyer, and Mr. James L. Walsh in helping carry out much of the hardware fabrication and assembly cannot go unnoticed.

I am grateful for the financial assistance provided by an NDEA Title IV Fellowship, a Georgia Institute of Technology Research Assistantship, and for supplementary support from the Ford Foundation.

My wife Marolyn has provided support and assistance, both financially and morally, during my years of graduate study and worked unselfishly during her typing, editing, and proofing of this thesis; without her help, this research could not have been completed. Finally, I thank my parents, Mr. and Mrs. Alvin M. Varney, for their guidance and support during the years of my education.

TABLE OF CONTENTS

LIST OF TABLES

LIST OF ILLUSTRATIONS

LIST OF SYMBOLS

a	weighted residual length parameter
A	decomposition surface area
AN	ammonium nitrate
AP	ammonium perchlorate
b	weighted residual parameter defined in equation (16), Chapter II
B	total area enclosed under DSC thermogram
c	specific heat
CTPB	carboxy terminated polybutadiene
d	weighted residual parameter defined in equation (16), Chapter II
D	area enclosed under DSC thermogram from beginning of decomposition to temperature in question
e	internal energy
E	activation energy
f	mixing region width, Appendix I
G	diffusion coefficient
h	enthalpy
m	mass
$\dot{m}$	mass decomposition rate
MOV	manually operated valve
n	normal direction
N	degree of polymerization
NV	needle valve

O/F	oxidizer to fuel mass ratio
p	pressure
PBAA	polybutadiene acrylic acid
PS	polysulfide
PU	polyurethane
$\dot{Q}$	heating rate
r	burning rate
R	gas constant
s	dimensionless thermal penetration depth
t	time
T	temperature
u	normal velocity
v	diffusion velocity
W	residual weighting function
x	coordinate perpendicular to regression surface
X	approximate photomicrograph magnification
Y	undecomposed polymer mass fraction
Z	pre-exponential factor
α	thermal diffusivity
β	fraction of sample decomposed
δ	binder lamination thickness
ΔH	total energy of decomposition
ΔT	temperature lag
η	dimensionless temperature difference
θ	surface inclination

ξ	dummy integration variable
υ	stoichiometric coefficient
ρ	density
τ	sandwich thickness

Subscripts

DSC	differential scanning calorimeter
f	final
g	gas
i	initial
ox	oxidizer
p	polymer
pan	DSC-1B sample and reference pan material
RP	reference pan
s	surface
SP	sample pan
ST	stoichiometric
o	original, initial
∞	final, infinity

SUMMARY

In order to obtain information essential to the future success of analytical modeling of composite solid rocket propellant burning rate theory, an experimental investigation using the method of differential scanning calorimetry and the quench combustion of two-dimensional propellant sandwiches was conducted. In the first phase, the thermal decomposition characteristics of four conventional solid propellant binders -- polysulfide, polyurethane, polybutadiene acrylic acid, and carboxy terminated polybutadiene -- were determined using the method of differential scanning calorimetry. In the second phase, two-dimensional propellant sandwiches prepared from single crystals and compacted polycrystalline ammonium perchlorate were burned and quenched over a range of pressures from 300 psig to 2400 psig. The quenched samples were studied in microscopic detail to determine the effects of binder type, binder lamination thickness, binder-oxidizer ratio, oxidizer preparation method, and combustion pressure level.

The general results of the present investigation may be summarized in the following conclusions:

1. Binder kinetics and energetics obtained by the method of differential scanning calorimetry provide a qualitative understanding of binder thermal decomposition behavior which, in some cases, may be useful for combustion analysis. Caution must be exercised in extending the low pressure, low heating rate characteristics obtained by differential scanning calorimetry to actual combustion situations by investigating

the decomposition behavior in high pressure combustion tests to detect obvious anomalous behavior.

2. An effective means for compacting granular AP into polycrystalline sheets has been developed. Specimens of the compacted polycrystalline AP exhibit quantitative and qualitative deflagration behavior of pure single AP crystals over a combustion pressure range of 300 psig to 4800 psig. Also, the combustion results of sandwiches prepared with polycrystalline and single crystal AP reveal that the regression characteristics of both systems agree.

3. A reliable sandwich replica technique has been developed which permits unambiguous investigation of sandwich details.

4. Quenched combustion of propellant sandwiches prepared with PS, PBAA, CTPB, and PU polymeric binders ranging in lamination thickness from 25 to 200 microns indicated the presence of a binder melt on the oxidizer surface at combustion pressure levels from 300 psig to 2400 psig.

5. The kinetic and energetic nature of the observed binder melts has an influence on the sandwich regression behavior.

6. The presence of fuel, independent of reactive nature, was observed to augment the characteristic AP deflagration rate at a combustion pressure level of 2400 psig. Combustion at other pressure levels did not exhibit a uniform response to fuel or fuel type.

7. Smooth interfacial contours observed at the binder-oxidizer interface for every combustion pressure level indicate that significant interfacial reactions between the binder and oxidizer are not occurring.

8. The regression of two-dimensional propellant sandwiches appears to depend upon a great many interdependent events. The sandwich regression behavior was, in many cases, strikingly different, but reasonable hypotheses have been advanced to explain the observed results using the quenched sandwiches and the DSC-1B binder decomposition behavior.

9. The two-dimensional problem is extremely complex and requires more investigation than is included within the scope of this thesis. Because of the uncertainties involved in the sandwich regression time history and the actual flame structure and location, it is imperative that high speed motion pictures be taken of the sandwich combustion to provide the details unobtainable using quenching techniques.

10. Any analytical combustion models which are based upon dry propellant surfaces and/or dominant interfacial reactions are open to severe question.

11. The interpretation of the quenching results, and also of the recommended high speed photography study, would be greatly enhanced by an analytical description of the sandwich combustion which includes the effects of two-dimensional gas and solid phase heat transfer, binder surface melts, gas and solid phase chemical kinetics, and gas phase species diffusion.

CHAPTER I

INTRODUCTION

Background

Rocket motor applications impose demands for a variety of solid propellant burning rate characteristics, the attainment of which is usually achieved by costly means and with significant compromise in other performance attributes. Research has revealed a qualitative understanding of propellant combustion; it is clear that the exothermic reactions which sustain the combustion may occur in varying degrees in the gas phase, on the burning surface, or in the condensed phase. The relative importance of the different reaction steps differs according to the composition of the propellant, details of the propellant microstructure, and the environmental conditions. In most practical combustion situations, the relative importance of these steps in the combustion zone is unknown and predictive capability is largely based on experience rather than theory. The failure of analytical models is not entirely due to the complexity of the combustion process, but is enhanced by the continuing ignorance of many of the basic aspects of combustion, such as fundamental kinetics data for binder and oxidizer decomposition, gas phase reactions, and interface reactions.

Existing theories of combustion of propellants are, in most cases, based on one-dimensional models, whereas composite propellants consist of mixtures of granular, inorganic oxidizer, metal additives,

and burning rate modifiers embedded in a matrix of polymeric fuel. Existing evidence establishes that the propellant heterogeneity is a major factor in the combustion behavior, but theoretical advances have been impeded by the complexity of modeling the combustion of heterogeneous structures and ignorance of the key processes which must be included in the models. Any effective advances in the understanding of combustion of heterogeneous, composite propellants thus depends on more detailed knowledge of the multi-dimensional aspects of the phenomenon.

Review of Recent Literature

The first analytical modeling of composite propellant combustion was an extension of double base theory. Wilfong, Penner, and Daniels [1] advanced the hypothesis that, in the combustion of a double-base propellant, the rate controlling reaction occurs in the monomolecular surface layer exposed to the flame. Schultz and Dekker [2] applied this concept to the combustion of solid composite propellants in the form of a two-temperature postulate which suggested that the gasification of binder and oxidizer at the propellant surface proceeds independently of each other, and that these reactions are rate controlling. Since the surface of a burning propellant is observed to regress at some mean rate and the binder and oxidizer are kinetically different, the two-temperature postulate is physically acceptable.

Chaiken [3], in developing the thermal layer theory for composite combustion, made use of the postulate of the independence of regression rates of oxidizer and binder to delineate the important energy flow processes in the combustion of ammonium nitrate (AN) composite

propellants. Chaiken derived expressions which describe the dependence of the propellant burning rate on pressure and oxidizer particle size. Using the gas phase reactions associated with the oxidizer alone, a thermal reaction layer was assumed to exist around a spherical oxidizer particle embedded in the binder; reactions involving the binder were regarded as having no significant influence on the processes occurring at the oxidizer surface. A simplified conduction analysis provided the means for energy transfer between the AN decomposition flame and the AN surface. In a later investigation, Chaiken and Andersen [4] considered the role of the binder in composite propellant combustion and extended the thermal layer theory to ammonium perchlorate (AP) based propellants. Several cases of binder diffusion and gas phase reaction were presented in mechanistic terms, but no theoretical developments nor supporting data were given.

Analytical consideration of the flame structure in a composite propellant burning model was given by Sutherland [5]. In Sutherland's diffusion flame model, flamelets formed by the diffusive transport of oxidizer and fuel decomposition products provide the heat release necessary to support the combustion process. The model shows no explicit dependence upon the combustion pressure, but rather the surface temperature appears as the important parameter in the development. No procedure for the determination of the surface temperature, or surface temperatures as implied by a two-temperature concept, is included within the framework of the model; therefore, the model must be considered incomplete.

The most thorough examination of composite propellant combustion has been conducted by Summerfield, et al. [6] [7] [8]. Summerfield and his associates extended the earlier work of Sutherland to include the effects of pressure, oxidizer particle size, and fuel-oxidizer ratio. This extension, the granular diffusion flame (GDF) model, is a physico-chemical representation of the combustion zone including surface reaction and a gas phase flame zone which incorporates chemical reaction and diffusive mixing. The one-dimensional flame model postulates that a quasi-steady flame region exists adjacent to a dry burning surface from which the oxidizer and fuel gases are liberated directly from the solid phase by sublimation or pyrolysis. Oxidizer and fuel mixing occurs only in the gas phase, and no significant reactions occur in the interior of the solid. The vapors of the fuel are released in the form of pockets of certain mass content (related to the oxidizer particle size) and are transported into the oxidizing atmosphere where they are gradually consumed at a rate controlled by diffusive mixing and/or chemical reaction. The heat released in the combustion zone is transported by molecular conduction to the propellant surface supporting the burning process. The resulting burning rate "law" is quite novel in that it gives a two parameter representation of the classical burning rate versus pressure curve. A series of experiments [8] using AP as the oxidizer and numerous propellant fuels gave excellent correlation over a broad range of conditions. Recent investigations [9] [10] [11] show evidence that both binder and oxidizer exhibit a molten or liquid layer on the burning surface which could possibly lead to a

premixed combustion flame. These results are in conflict with the hypothesis of the granular diffusion flame theory and bear further investigation.

Nachbar [12] made use of a sandwich burning model proposed by Schultz, Green, and Penner [13] to describe the combustion of a composite propellant. The idealized sandwich model consists of a two-dimensional array of thin slabs of fuel and oxidizer from which gaseous constituents evolve from a dry solid surface. An expression for the burning rate of such an array is obtained by the Shvab-Zeldovich procedure and, consequently, is independent of gas phase reactions. When coupled with the pressure independent, surface pyrolysis laws for fuel and oxidizer decomposition, the burning rate expression obtained is also independent of pressure.

A qualitative description of composite propellant combustion was presented by Fenn [14], who visualized the combustion process in terms of flame structure. In Fenn's phalanx flame model, the dominant combustion mechanism is a flame zone located above and roughly parallel to the interfacial region between the oxidizer and fuel boundary. The flame is diffusive in nature, but the narrow tip of the mixing zone is a premixed phalanx which leads the regression through the unburned solid. The effects of pressure level, binder-oxidizer ratio, and oxidizer particle size are qualitatively predicted by the phalanx combustion model.

The theoretical development of composite propellant combustion was extended by the work of Hermance [15] [16]. Hermance presented a

physico-chemical combustion model which incorporated the surface processes of endothermic fuel pyrolysis, exothermic oxidizer decomposition, exothermic heterogeneous chemical reaction between fuel binder and oxidizer decomposition products, and gas phase combustion of the final fuel and oxidizer decomposition products. The prediction of the burning rate dependence upon pressure and oxidizer particle size agrees quite well with experimental results, although the predicted effect of oxidizer loading is in error. The model neglects gas phase diffusion and assumes a dominating interfacial reaction around the oxidizer particle producing a fissure which, in fact, has been observed only in isolated cases.

An investigation of the burning rate of composite propellants has recently been presented by Culick and Dehority [17]. The approach taken by the investigation was an inverse one which assumed the burning rate-pressure relation was known and explored the roles played by various physical and chemical propellant properties. The combustion model assumes a uniform gas phase combustion zone with heat transfer matching conditions at a reacting solid phase interface. The basic supposition is that the simultaneous influences of diffusion and kinetics interact as to produce a broad reaction zone of uniform energy release. All required thermodynamic, kinetic, and transport properties were specified and their influence upon the combustion processes and flow in the flame zone were investigated. Although the model is simply formulated and the discussion centered around flame dimensions, surface heat transfer, and reaction rates (all of which are nearly impossible

to measure), the approach appears quite useful for qualitatively exploring the influence of physical and kinetic parameters on the combustion process.

In an effort to rectify conflicting views regarding the importance of condensed phase reactions which lead to propellant surface gasification, studies of propellant energetics have been conducted by Wenograd [18], Waesche and Wenograd [19], and Waesche [20] [21] [22]. These investigations, using the method of differential scanning calorimetry, attempted the determination of the energetics and kinetics of condensed phase decomposition reactions for AP based propellants. Experiments conducted with numerous propellant combinations, with and without burning rate additives, indicate the presence of condensed phase energy release. The actual contribution of the condensed phase is not completely resolved by these experiments because the heat release attributed to the condensed phase may be partially, or totally, coming from the adjacent gas phase.

Caveny and Pittman [23] evaluated the contribution of solid phase heat release for AP based propellants and concluded that subsurface reactions are not a factor in controlling propellant burning rate at pressures above 500 psi. The results of Caveny and Pittman were based on the AP crystalline phase transition data of Beckstead and Hightower [24].

In order to better understand the combustion behavior of composite propellants, a number of studies have been conducted concerning individual ingredient decomposition. It is anticipated that ingredient

decomposition studies will elucidate the potential interactions and dominant steps in the overall combustion process. Considerable effort and analysis have been devoted to the decomposition of ammonium perchlorate by Pittman [25], Jacobs [26], Friedman [27], Powling [28], and Price [29].

Very little is currently known about the decomposition energetics and kinetics of binders currently used in solid composite propellants, particularly those conventionally used with AP as the oxidizer. General studies on polymer decomposition [30] [31] [32] [33] [34] have been made, but the results have not been directed toward solid propellant technology. The decomposition work of Howard [35], the differential scanning calorimetry work of Sammons [36], and the thermal decomposition experiments of Shannon and Erickson [37] represent the only investigations designed to produce fundamental energetics information applicable to understanding the role which the binder plays in composite propellant combustion.

Nature of the Research

The development of solid propellant burning rate theory for composite propellants has involved a broad spectrum of views in which there is a lack of general agreement. The burning rate theories, although useful in helping to guide the experiments, have had limited success in explaining many features of composite propellant combustion, particularly plateau burning, extinction, and the influence of metal additives. Analytical treatment of the combustion region -- an involved region of heat transfer processes, mass transport by laminar and

turbulent mechanisms, and a number of interdependent solid and gas phase reactions -- has generally been unsuccessful, partly due to the complexity of the combustion mechanism and partly due to ignorance of many of the basic aspects of the combustion, such as binder energetics. The principal obstacles to useful research are the experimental difficulties involved in making observations of the multi-dimensional processes in the combustion zone, and the inability to reach an optimum compromise between tractability and reality in analysis due to lack of ability to correctly specify dominant steps in the combustion mechanism.

As a compromise between the complexity of the three-dimensional combustion zone and the oversimplification of one-dimensional modeling, two-dimensional sandwich studies using simplified propellant geometries were conducted by Hightower and Price [38] [39]. The two-dimensional sandwiches, prepared by laminating a binder layer between thin sections of AP oxidizer crystals, facilitate understanding of the key combustion processes by providing direct observation of the binder-oxidizer interplay.

An experimental study of the dominant steps in composite propellant burning mechanisms will be conducted in two phases. The first phase of the study will be to establish the thermal decomposition characteristics of four conventional solid propellant binders -- polysulfide, polyurethane, polybutadiene acrylic acid, and carboxy terminated polybutadiene -- in order to provide a sound basis for interpreting observed behavioral differences in sandwich combustion characteristics. The second phase of the study will involve the quench testing of two-

dimensional propellant sandwiches in which known compositional and environmental factors can be varied. Test variables will include the type of binder, lamination thickness of the binder, binder-oxidizer ratio, oxidizer sample preparation method, and the combustion pressure.

Several significant features of the proposed research are:

1. No orderly body of data, and supporting interpretation, has been established for the thermal decomposition characteristics of conventional propellant binders. This study will attempt the determination of binder kinetics and energetics using the method of differential scanning calorimetry and test their relevance to combustion situations.

2. Past tests of sandwich burning [38] [39] [40] [41] [42] have used either single crystal sheets or sheets pressed from granular material; no single laboratory has done both. The results by the two methods appear to be critically different. This study will investigate sandwiches prepared with both kinds of oxidizer sheets.

3. The majority of the previously published work concerned oxidizer-binder sandwiches with binder layer thicknesses around 100 microns. Recent work of Hightower and Price [38] [39] with thin binder layers yielded some peculiar differences in quenched samples. Since thin binder sheets may better approximate real propellant combustion, it is important to explore the effects of binder lamination thickness and the relevance of thick binder tests to real propellants. This study will investigate a range of binder thicknesses varying between 25 microns and 200 microns.

4. Previous sandwich studies have not investigated the effects

of combustion pressure beyond 1200 psi. This investigation will double the pressure range to 2400 psi, well within the region where pure AP self-deflagration possesses a negative slope in burning rate versus pressure.

The binder thermal decomposition characteristics from the differential scanning calorimeter study will be combined with the qualitative results of the sandwich combustion tests to provide a compatible representation of the dominant steps involved in the burning mechanism.

CHAPTER II

THERMAL DECOMPOSITION CHARACTERISTICS OF FOUR CONVENTIONAL COMPOSITE SOLID PROPELLANT BINDERS

An obstacle impeding the development of an "absolute" burning rate theory for composite propellants is the lack of fundamental knowledge concerning the binder-oxidizer interplay mechanism. Simplified theories neglect the role of the binder entirely, while others consider a gas phase interaction between oxidizer and binder pyrolysis gases. No mention of surface effects resulting from a molten binder and a dry (or liquid) oxidizer interaction have been considered. Theoretical neglect of binder effects in burning rate models originates from two primary sources:

1. No experimental evidence has been provided, to date, to indicate that potential binder mechanisms are important to the overall burning rate.

2. There is a general void of pertinent binder information, particularly energetics and kinetics, on which to base sound models or interpret existing combustion data.

It would be highly desirable, but nearly impossible, to extract binder energetics and kinetics data from experiments which duplicate, as closely as possible, actual combustion situations. An alternate approach, the one chosen in this investigation, is to decompose the propellant binders under controlled laboratory conditions, and to test the relevance of the derived kinetics by comparing calculated parameters

with those which are more easily observed in combustion situations, such as propellant surface temperatures. This investigation, using the method of differential scanning calorimetry, is aimed at providing some fundamental information necessary for probing the role the binder plays in the combustion process, namely the binder thermal decomposition characteristics, including energetics and kinetics, of four propellant binders -- polysulfide (PS), polyurethane (PU), polybutadiene acrylic acid (PBAA), and carboxy terminated polybutadiene (CTPB).

Apparatus

Binder thermal decomposition characteristics were obtained using a Perkin-Elmer Differential Scanning Calorimeter linked with a Hewlett-Packard two-pen recorder. These items and the auxiliary apparatus required for sample preparation, shown in Figure 1, are described as follows.

Perkin-Elmer Differential Scanning Calorimeter, Model DSC-1B

In the DSC-1B, the temperature of a sample and a reference are maintained at the same level during a programmed temperature increase (scan) rate. The excess energy required to maintain temperature equality during thermal decomposition in a controlled atmosphere is measured and recorded, yielding a thermogram of decomposition energy requirements versus time and temperature. As will be shown later, this thermogram gives both a qualitative and quantitative description of the decomposition behavior.

The operation of the DSC-1B may be easily comprehended if the system is divided into two separate control loops, one for average

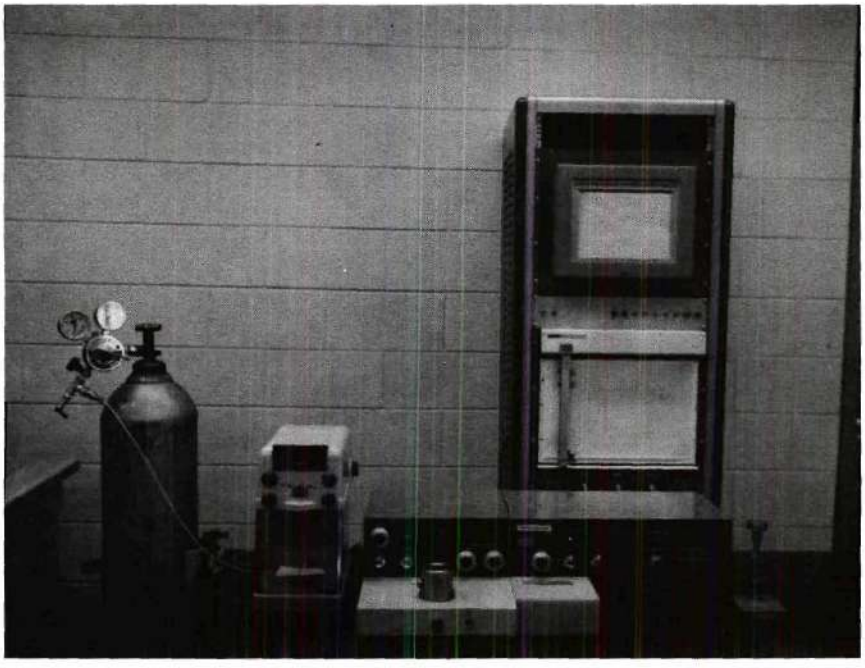

Figure 1. Binder Thermal Decomposition Experimental Apparatus.

temperature control and the other for differential temperature control. The block diagram of the DSC-1B, Figure 2, indicates the two separate control loops. In the average temperature loop, a preselected temperature scan program provides an electrical output signal which is proportional to the desired temperature of the sample and reference holders. The temperature scan information is also relayed to the recorder and appears on the abscissa scale of the recorder paper indicating the temperature events. The temperature program signal is compared with signals received from platinum resistance thermometers permanently embedded in the sample and reference holders via an average temperature computer. If the temperature called for by the temperature program is greater than the average temperature of the sample and reference holders, more power will be fed to the heaters of both the sample and reference holder, which, like the resistance thermometers, are embedded in the holders. If the average temperature demanded by the temperature program is lower than the average of the two holders, the power to the heaters will be decreased.

In the differential temperature control loop, signals representing the sample and reference temperatures are fed to the differential temperature amplifier via a comparator circuit which determines whether the reference or the sample temperature is greater. The differential temperature amplifier output will then adjust the differential power increment fed to the reference and sample heaters in the direction and magnitude necessary to correct any temperature difference between them. A signal proportional to the differential power is transmitted to

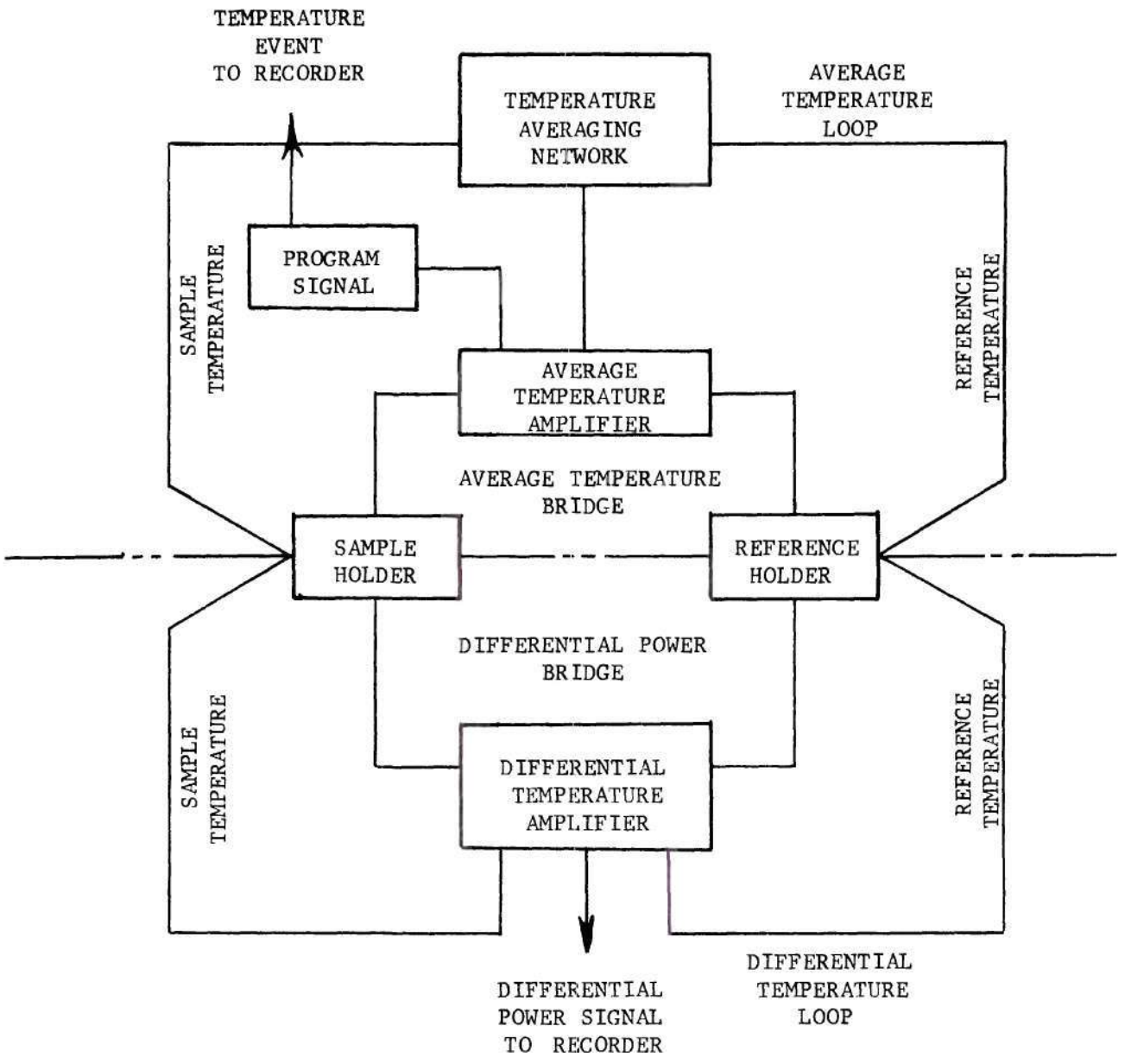

Figure 2. Block Diagram of DSC-1B Thermal Circuitry.

the recorder ordinate pen, the direction of the pen excursion depending upon whether the excess power is required by the sample or the reference holder.

The atmosphere in which binder decomposition takes place can be controlled. The sample holder cover, with a transparent viewport, seals the sample and reference holders from the ambient environment and permits an externally supplied gas to purge the sample holder vessel at a regulated rate. Flow rate adjustment is provided by a restrictor which allows one cc per minute of purge gas for each unit (psi) of input pressure. The DSC-1B is capable of operating in ascending or descending temperature scan modes, varying from 0.625 °K per minute to 80 °K per minute between the temperature extremes of 273 °K and 773 °K; operation in an isothermal mode is also provided. The power ordinate sensitivity is one millicalorie per second for a full scale deviation (10 millivolts dc), but can be varied by a six position range multiplier which is capable of decreasing ordinate sensitivity to 32 millicalories per second for a full scale deviation. Ordinate positioning and baseline slope adjustments are provided.

Hewlett-Packard Two-Pen Recorder

The recorder used in this investigation was a Hewlett-Packard Two-Pen Recorder, Model 2FRA. The Model 2FRA is a two pen, three axis graphic recorder designed to plot two cartesian coordinate curves simultaneously from dc signals representing a single independent variable. The two pens move vertically on separate carriages which travel horizontally on a single carriage. Each pen has a full scale plotting

range in both X and Y directions with ±0.1 inch horizontal separation. An electric platen accepts standard graph paper with a 10 inch by 15 inch recording area or smaller. A built-in sweep generator provides a time base on the horizontal axis for plotting two dependent variables against time. Each axis is controlled by an electrically independent servomechanism with one megohm input resistance on eleven fixed ranges. Variable range control is provided to accommodate arbitrary voltage situations. A stepless range control feature permits arbitrary full scale voltage settings on any range up to the maximum limits of the instrument.

Auxiliary Apparatus

The principal components of the binder decomposition study are the DSC-1B and the X-Y-Y recorder, but several auxiliary items were required to assure proper equipment operation and satisfactory sample preparation.

To insure accurate and reproducible operation of the DSC-1B, a constant line voltage of 117 volts (60 cps) is required by the instrument. A Sola Standard Sinusoidal Constant Voltage Transformer, Type CVS, was selected to regulate the DSC-1B input voltage. The CVS transformer is a static-magnetic voltage regulator delivering 117 volts output voltage regulated within ±one per cent, even if primary voltage variations are as great as 30 per cent.

Reproducible DSC-1B purge gas flow rates depend upon a stable pressure level being supplied to the inlet of the DSC-1B gas flow restrictor. A Matheson Two-Stage Regulator, Model 8, equipped for nitro-

gen service was used. Each unit combines two regulators: high inlet pressure is reduced automatically to a preset intermediate pressure in the first stage which feeds gas at a relatively stable pressure to the second stage. The latter stage is adjustable for the required delivery pressure which is unvarying at moderate to low flows until the supply bottle is nearly empty.

All precision weighings required in sample formulation and micro-sample preparation were made using a Mettler H6T Digital Balance. The Mettler H6T is single pan, beam balance using synthetic sapphire knife-edged bearing planes for beam support. Weight compensation is accomplished by a combination of built-in ring weights; readout is in digital form and is read optically. The weighing range of the H6T is 0-160 grams with a standard deviation precision of ± 0.05 milligrams.

The Perkin-Elmer Sample Crimper was used to encapsulate the binder specimen in a high thermal conductivity aluminum pan which facilitates sample handling and weighing.

Binder samples were cured in an Acme Laboratory Vacuum Oven, Model 43573, which has a temperature range of 35-260 °C maintained within $\pm$ one °C of the selected level. Vacuum conditions in excess of 28 inches of mercury were provided by a Welch two-stage Duo-Seal vacuum pump driven by a Craftsman one-half horsepower electric motor. The binder curing apparatus is shown in Figure 3.

Procedures

Due to the nature of the investigation and the small size of the samples involved, cleanliness was observed in every aspect of the

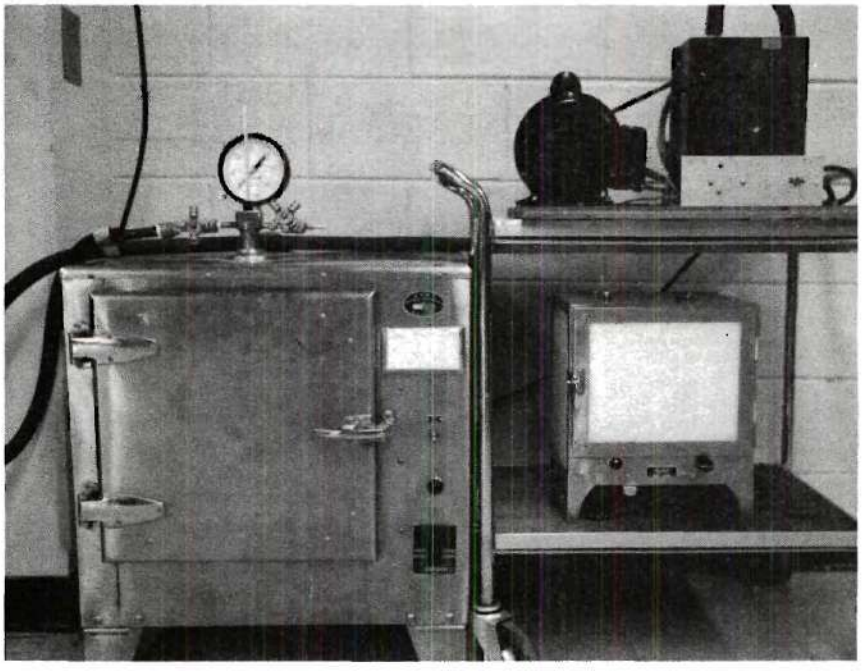

Figure 3. Binder Curing Apparatus.

investigation. General procedures included binder preparation and curing, qualitative visual decomposition tests, and quantitative decomposition tests. The DSC-1B procedures followed were those generally advised in the Instructions Manual [43] and are presented in Appendix A.

Binder Preparation and Curing

Propellant binder samples were formulated in five gram lots and cured on microscope slides in a thermostatically controlled oven. Binder ingredients were weighed, formulated in a disposable plastic cup, and manually mixed with a glass stirring rod for approximately 15 minutes. Small, elongated sections of binder were distributed in a thin layer on a microscope slide which was then placed in a thermally-soaked curing oven. The oven was sealed and curing for the first three hours was conducted under vacuum conditions in excess of 28 inches of mercury. After three hours, the vacuum was released and the samples were cured for the recommended cycle. At least three independently mixed sample batches were cured and compared to assure proper formulation. Complete binder formulation, mixing, and curing instructions are given in Appendix B.

Qualitative Decomposition

DSC-1B operation procedures follow those listed in Appendix A. A small binder specimen weighing approximately 5 milligrams was shaved from the bulk-cure sample and placed in a weighed aluminum sample pan. The sample and pan were then weighed, placed in the DSC-1B sample holder, and covered with the sample holder cover. After manually increasing the temperature to 350 $^{\circ}$K, the sample was heated at a selected

heating rate in the ascending scan mode of operation. During heating, decomposition events were observed via the sample holder viewport and the corresponding temperatures were noted. Heating was continued until the 773 °K upper temperature limit of the DSC-1B had been reached. After heating was completed, the sample pan was removed from the DSC-1B, weighed, and the pan inspected for possible reaction with the binder. Visual observations were made at several scan rates from 5 °K per minute to 80 °K per minute; at least two runs were made at each scan rate to confirm observations.

Data were generated relating the binder mass loss with temperature and scan rate using the same general procedures as the visual tests. At selected points during the heating program, the DSC-1B was switched to the isothermal mode. The sample pan was quickly removed from the sample holder and placed on a cold metal surface quenching the decomposition reaction. The sample pan was weighed, replaced in the DSC-1B, and the heating program continued until the next desired temperature level was reached. The removal, quenching, and weighing sequence was repeated at selected temperatures until the sample was decomposed.

Quantitative Decomposition

Before each series of quantitative tests, sample holder cleaning and calibration were performed according to instructions shown in Appendix A. After cleaning and calibration were completed, the nitrogen purge flow was regulated to 30 cc per minute, and the DSC-1B and the X-Y-Y recorder were allowed to warm-up for thirty minutes. During the

warm-up period, aluminum sample pans and covers were cleaned in acetone and air dried. After the warm-up period, the X-Y-Y recorder voltage ranges were selected and a piece of 11 inch by 17 inch graph paper was aligned and positioned on the electrostatic platen. Using tweezers for handling, an aluminum sample pan and cover were weighed. A small binder specimen was then shaved from the bulk-cure sample and placed in the sample pan. The aluminum sample cover was placed over the sample, and the sample container was weighed prior to encapsulation. After encapsulation, another weighing was taken and compared with the pre-encapsulated weight; if the weights were identical, indicative of no contamination during the crimping process, the encapsulated sample was placed in the sample cup of the sample holder. Another carefully weighed empty sample pan and cover were crimped and placed in the reference cup to facilitate thermal matching. Both the sample and reference cups were covered with domed aluminum cup covers to enhance baseline linearity and run to run reproducibility. The dome covering the sample cup had a small hole drilled in the top which allowed decomposition products to readily escape. After securing the sample holder enclosure, the temperature was manually programmed to 400 $^{\circ}$K. During a short thermal stabilization period of approximately thirty seconds, the zero positions of the X-Y-Y recorder were adjusted. The temperature was then increased at a programmed scan until reactions of interest were completed or the 773 $^{\circ}$K upper temperature limit of the DSC-1B had been reached. The aluminum sample pan was removed and weighed. The DSC-1B was manually programmed down to 350 $^{\circ}$K and allowed to stabilize. If the sample holder appeared

to be clean, and the previous run did not exhibit a noisy or otherwise abnormal trace, the DSC-1B was considered to be ready for another run. Two runs were conducted at each scan to insure duplicate behavior.

Data Reduction

DSC-1B data are in the form of a thermogram representing the instantaneous rate of heat absorption or release as a function of absolute temperature. The heating rate signal from the DSC-1B is the differential power required to maintain temperature equality between the sample and reference materials. The law of conservation of energy for a control volume requires

$$\begin{pmatrix}\text{Rate of accumulation of internal and kinetic energy}\end{pmatrix} = \begin{pmatrix}\text{Rate of internal and kinetic energy in by convection}\end{pmatrix} - \begin{pmatrix}\text{Rate of internal and kinetic energy out by convection}\end{pmatrix} + \begin{pmatrix}\text{Net rate of heat addition}\end{pmatrix} - \begin{pmatrix}\text{Net rate of work done by system on surroundings}\end{pmatrix} . \quad (1)$$

If the sample and reference holders are considered separately and the conservation of energy applied, the heating rates to the sample and reference holders are given, respectively, by

$$\frac{d}{dt}\left[m_{SP}e_{SP} + m_p e_p\right] = \dot{Q}_{SP} - \dot{m}_g h_g \quad (2)$$

and

$$\frac{d}{dt}\left[m_{RP}e_{RP}\right] = \dot{Q}_{RP} ,$$

where $\dot{m}_g$ is the gaseous evolution rate of binder decomposition products, h_g is the enthalpy of the binder gaseous products, and the remaining terms are defined in the List of Symbols. If the DSC-1B output signal is defined as positive for an exothermic reaction occurring in the sample pan, the net instantaneous heating rate is

$$\dot{Q}_{DSC} = \dot{Q}_{SP} - \dot{Q}_{RP} \ . \tag{3}$$

Since the volume of the decomposition container (sample pan) is quite small and the binder decomposition relatively slow, it seems reasonable to assume that the evolution rate of the gaseous products is equal to the negative of the polymer decomposition rate, $\dot{m}_p$,

$$\dot{m}_g = -\dot{m}_p \ . \tag{4}$$

No interaction was observed between the sample container and the polymer products during decomposition; consequently, equations (1) through (4) can be combined to express the net DSC-1B heating rate in terms of the scan rate and binder thermodynamic properties

$$\dot{Q}_{DSC} = c_{pan} \frac{dT}{dt}\left[m_{SP} - m_{RP}\right] + \left[\frac{d}{dt}\, m_p e_p\right] - \dot{m}_p h_g \ , \tag{5}$$

where $\frac{dT}{dt}$ is the DSC-1B scan rate. Invoking the definition of enthalpy and performing the differentiation, equation (5) becomes

$$\dot{Q}_{DSC} = \dot{m}_p\left[h_p - h_g + \frac{p}{\rho_p}\right] + \frac{dT}{dt}\left[c_{pan}\left(m_{SP} - m_{RP}\right) + m_p\left(c_p + \int_{T_o}^{T} \frac{dc_p}{dT}\, d\xi\right)\right] \ . \tag{6}$$

Since p/ρ_p is small compared to the total binder decomposition energy, ΔH, the DSC-1B heating rate is

$$\dot{Q}_{DSC} = -\dot{m}_p \Delta H + \frac{dT}{dt}\left[c_{pan}\left(m_{SP} - m_{RP}\right) + m_p\left(c_p + \int_{T_o}^{T} \frac{dc_p}{dT}\, d\xi\right)\right] , \qquad (7)$$

where ΔH has been defined as positive for an exothermic reaction. The last term in equation (7) represents a shift in thermogram baseline position due to temperature scan rate and changes in polymer heat capacity and can be removed by proper construction of the thermogram baseline (see Appendix C). After the corrected baseline position is established, the DSC-1B heating rate and the polymer decomposition rate are related by

$$\dot{Q}_{DSC} = -\dot{m}_p \Delta H . \qquad (7a)$$

Assuming that an in-depth pyrolysis is occurring, and that the kinetics obey an Arrhenius law, the sample decomposition rate is related to the sample mass remaining by

$$\dot{m}_p = -Z m_p \exp\left[-\frac{E}{RT}\right] , \qquad (8)$$

where Z is the pre-exponential factor, E the activation energy, and m_p the sample mass remaining at any temperature.

Referring to Figure 4, the sample mass remaining at any temperature can be determined directly from the thermogram using the following procedure. The mass decomposed at any temperature is assumed to be

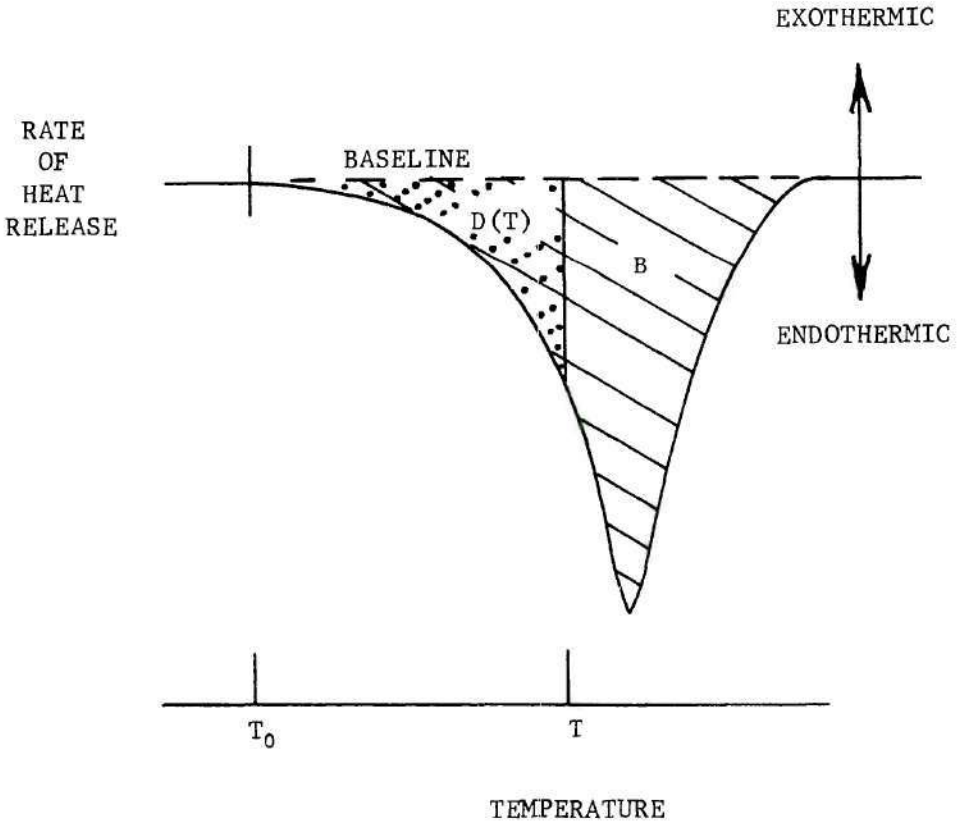

Figure 4. Graphical Determination of Binder Decomposition Mass Loss.

proportional to the enclosed area, D(T), under the thermogram from the beginning of decomposition up to the temperature in question. The fraction of the sample decomposed, β, up to the temperature T is given by the area ratio

$$\beta = \frac{D(T)}{B} , \tag{9}$$

where B is the total area enclosed under the thermogram. The sample mass remaining at any temperature is thus

$$m_p = m_o - \beta(m_o - m_f) , \tag{10}$$

where the subscripts $(\ )_o$ and $(\ )_f$ refer to initial and final conditions respectively. If the sample decomposes entirely during the temperature program, the mass remaining is given by

$$m_p = (1 - \beta)m_o . \tag{11}$$

β is determined quite simply with a planimeter directly from the thermogram for as many values of the temperature as may be required to adequately determine the mass remaining versus temperature curve.

Equations (7a) and (8) may be combined to give an expression for the heating rate per unit mass of sample remaining in terms of the binder kinetics and energetics,

$$\frac{\dot{Q}_{DSC}}{m_p} = (\Delta H)(Z)\ \exp\left[-\frac{E}{RT}\right] . \tag{12}$$

Equation (12) may be plotted versus reciprocal temperature on semi-logarithmic graph paper as a straight line with slope of negative E/R and intercept of $\exp[(\Delta H)(Z)]$. Data correlation with a straight line fit provides a check as to the validity of the assumed rate and kinetics relations.

The total heat of decomposition, assumed independent of temperature (later verified experimentally), is proportional to the total area enclosed under the thermogram and is determined using a planimeter following the procedure given in Appendix C. The pre-exponential factor and activation energy are most easily determined algebraically by repeated application of equation (12) using several data points. The data reduction analyses were performed using an external standard method to calibrate the area response of the DSC-1B/X-Y-Y recorder in terms of energy units. Area measurements, made with a planimeter from the thermogram, were reduced to energetics data using indium transition properties [44]. These procedures are given in Appendix C.

Effect of Sample Geometry

Quantitative performance of the DSC-1B is quite sensitive to sample size and shape, particularly where endothermic decomposition of low thermal conductivity materials is concerned. A thermal lag in the sample temperature and extreme baseline variation were both observed during the binder decomposition study, the former being the more serious problem.

Due to the very low thermal conductivity [45] of the binders investigated, the average sample temperature can be somewhat below the

digital temperature indicated on the DSC-1B readout, the lag being greater as the programmed temperature rate increases. For sample sizes which were as thin as practical handling techniques would permit, approximately one millimeter, a transient heat transfer analysis [46] showed that the average sample temperature could lag the indicated temperature by as much as 25 °K. The kinetic data presented for PS and PU have been corrected for a thermal lag; that is, the temperature used for the data correlation was a corrected value which reflected the average sample temperature. The PS thermal lag was based on a transient heating analysis and the PU thermal lag was referenced with respect to the well defined melt transition temperature using the 5 °K per minute scan as a base. Both thermal lag analyses are given in Appendix D.

Effect of Scan Rate

Quantitative results obtained from the DSC-1B are not affected by the temperature scan rate, although the qualitative characteristics of the thermogram are affected. The decomposition processes observed are kinetic in nature; consequently, a change in the sample heating rate also implies a change in the sample reaction rate history. Differentiating equation (12) with respect to time, the location of the reaction peak $\left(\frac{d\dot{Q}_{DSC}}{dt} = 0\right)$ can be seen to depend upon both the kinetics and the scan rate according to the relation

$$T^2 = \frac{m_p}{\dot{m}_p} \frac{dT}{dt} . \qquad (13)$$

The uniqueness of the kinetics is tested by the degree of success

achieved by the data correlation. If unique kinetics are found to govern the decomposition, the location of the reaction peak should be displaced to higher temperatures with increased scan rates as can be seen by inspection of equation (13).

Results

The four binders considered in this study exhibited widely different endothermic decomposition behavior. PS and PU binders rapidly decomposed at relatively low temperatures, less than 700 °K, and good quantitative data were obtained at scan rates up to 80 °K per minute. PBAA and CTPB binders decomposed near the 773 °K upper temperature limit of the DSC-1B unit, and good quantitative data were obtained at scan rates up to 5 °K per minute. The temperatures of the various events reported below, being kinetic in nature, do of course vary with the scan rate but are indicated as rough measures of activity at low scan rates. Typical thermograms and characteristic events as described below are shown in Figures 5 and 6 for the four binders under consideration.

Qualitative Decomposition

Polysulfide. Polysulfide binder was decomposed at scan rates from 5 °K per minute to 80 °K per minute. Initial low temperature decomposition is characterized by the binder specimen relaxing into a viscous fluid at 475 °K. The binder specimen remains quite viscous, undergoing a slow outgassing until 530 °K when decomposition activity rapidly increases. Peak decomposition, a violent bubbly action in a highly viscous fluid, occurs at 565 °K with the entire sample being decomposed by 575 °K. During decomposition, the sample was in a molten

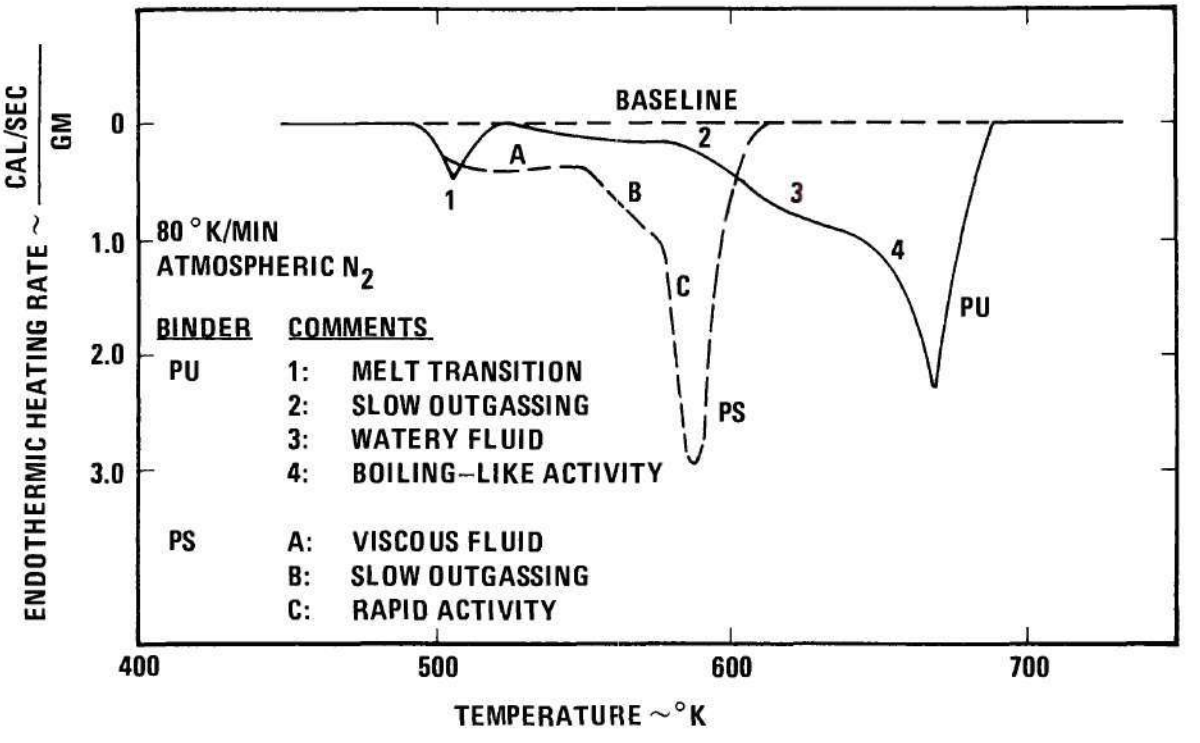

Figure 5. DSC-1B Thermogram for Thermal Decomposition of PS and PU Binders.

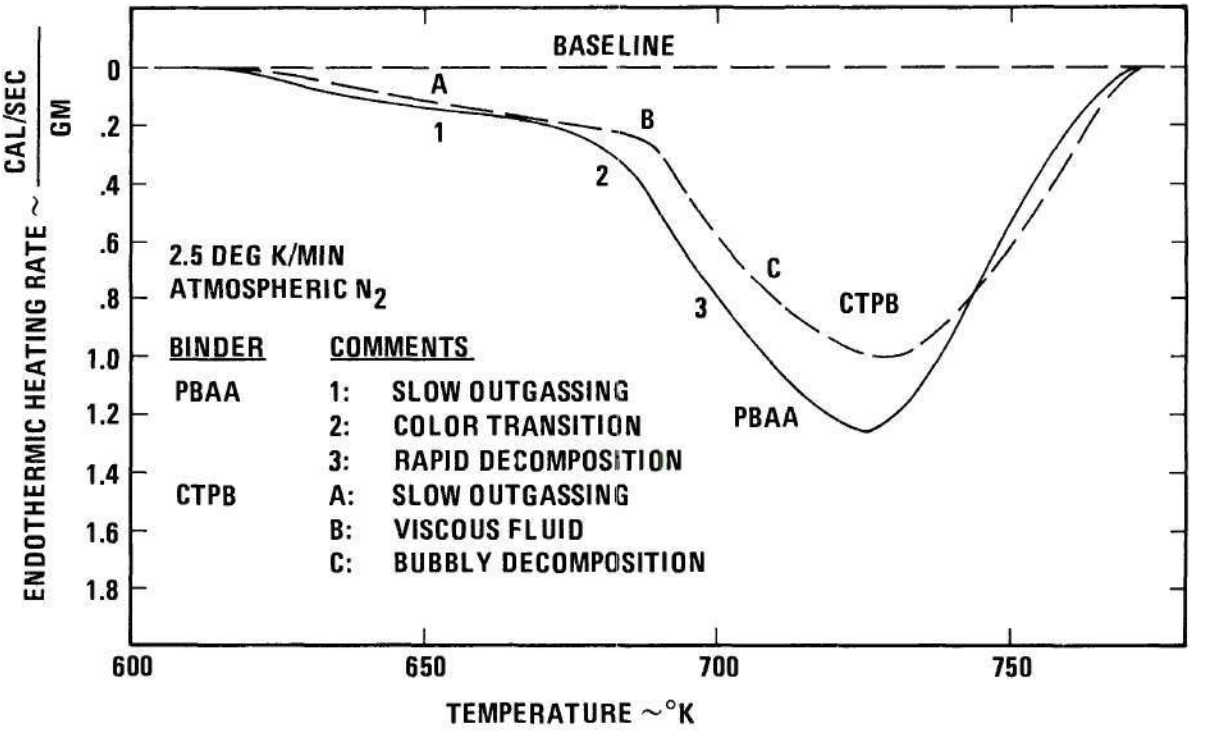

Figure 6. DSC-1B Thermogram for Thermal Decomposition of PBAA and CTPB Binders.

state and did not exhibit any tendancy to run, but rather tended to maintain itself in a hemispherically shaped puddle. As decomposition activity increased, gaseous decomposition products emanating from the lower portion of the sample could be seen coalescing while rising to the surface. Upon reaching the surface, the larger bubbles ruptured giving rise to a small amount of binder spatter. During the peak activity, large volumes of smoky decomposition gases evolved and no binder spattering was observed. A small amount of black ash-like residue was observed in the visual decomposition tests; this residue was "weightless" within the accuracy of the analytical balance, even when the original sample size was as large as 10 milligrams.

Polyurethane. Polyurethane binder was decomposed at scan rates from 5 °K per minute to 80 °K per minute. PU exhibits a well defined melt transition at 495 °K followed by a slow outgassing and gradual loss of viscosity which continued until 615 °K. At 615 °K, the liquid binder becomes very dilute, followed by a very active boiling-like activity. Peak decomposition activity occurs at 635 °K, and sample decomposition is complete by 640 °K. In the early stage of decomposition, the binder fluid has the appearance of a viscous liquid, but before the period of peak decomposition, the fluid loses its viscous appearance and has an unusually good wetting ability. During the boiling-like peak activity period, large quantities of off-white smoke were emitted. Following decomposition, the sample pan was slightly discolored, but no visible residue remained.

Polybutadiene Acrylic Acid. PBAA binder was decomposed at scan

rates from 1.25 °K per minute to 80 °K per minute. Decomposition at the lower and higher scan rates was qualitatively the same, with the exception of the final stages.

At the slower scan rates of 1.25, 2.5, and 5 °K per minute, low temperature outgassing was noted at 610 °K and continued until 680 °K. At 685 °K, the originally amber clear sample became very dark but maintained its physical size and shape. The rate of decomposition increased, as evidenced by the evolution of large volumes of smoke, reaching a peak at 725 °K. By 770 °K, the sample was "massless" but a fragile, ash-like shell remained which was the same size and shape as the original sample before decomposition; decomposition had occurred from within the shell and the gaseous decomposition products had escaped through the porous outer surface.

At the higher heating rates, the sample became a quivering mass at the color transition temperature and became a viscous liquid during the high temperature portion of the decomposition. No visible residue remained after decomposition at the higher heating rates.

Carboxy Terminated Polybutadiene. CTPB binder was decomposed at scan rates from 1.25 °K per minute to 80 °K per minute. At lower scan rates of 1.25, 2.5, and 5 °K per minute, slight degassing was noted at 610 °K and continued until 690 °K. At 690 °K, the sample relaxed into a highly viscous fluid, and decomposition increased rapidly from the the binder fluid. Peak decomposition occurred at 730 °K and was complete by 770 °K. No residue remained after decomposition.

Qualitative observations made at higher scan rates indicated a

rapid melt followed by a violent, foamy boiling action during the high temperature portion of the decomposition.

Quantitative Decomposition

In all cases, the binders decomposed according to a first order decomposition mechanism, although correlation with a two-thirds power rate law could be achieved with slightly more data scatter. Implications of both mechanisms will be discussed in a later section, but the kinetics presented in this section were reduced according to the first order analysis previously given.

Kinetic data for the thermal decomposition of PS and PU binders are shown in Figure 7. The data correlate quite well for all scans from 5 °K per minute to 80 °K per minute. It should be noted that the higher temperature data for a given scan overlap the lower temperature data of the next higher scan providing a continuous data pattern with the same slope. This, of course, is expected where unique kinetics are involved.

Kinetic data for the thermal decomposition of PBAA and CTPB are given in Figure 8. Both PBAA and CTPB decomposed near the upper temperature limit of the DSC-1B, and good quantitative data were obtained for scans of 1.25, 2.5, and 5 °K per minute. Data correlation was considered to be good over the range investigated.

The calculated values for the pre-exponential factor, total energy of decomposition, and activation energy of the binders thermally decomposed in this study are listed in Table 1.

The quantitative results listed in Table 1 depend quite heavily on the determination of the sample mass remaining during decomposition

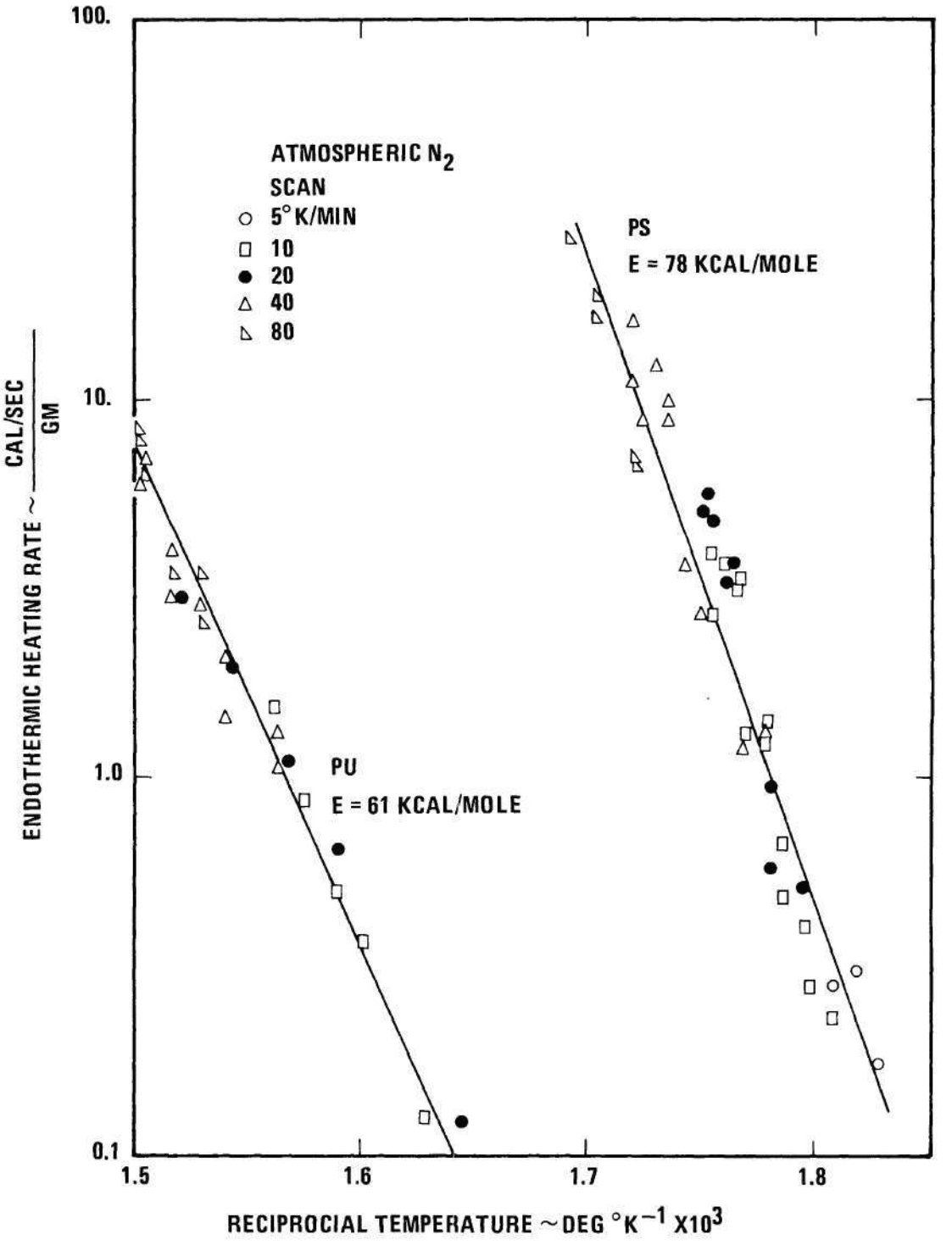

Figure 7. Thermal Decomposition Kinetics of PS and PU Binders.

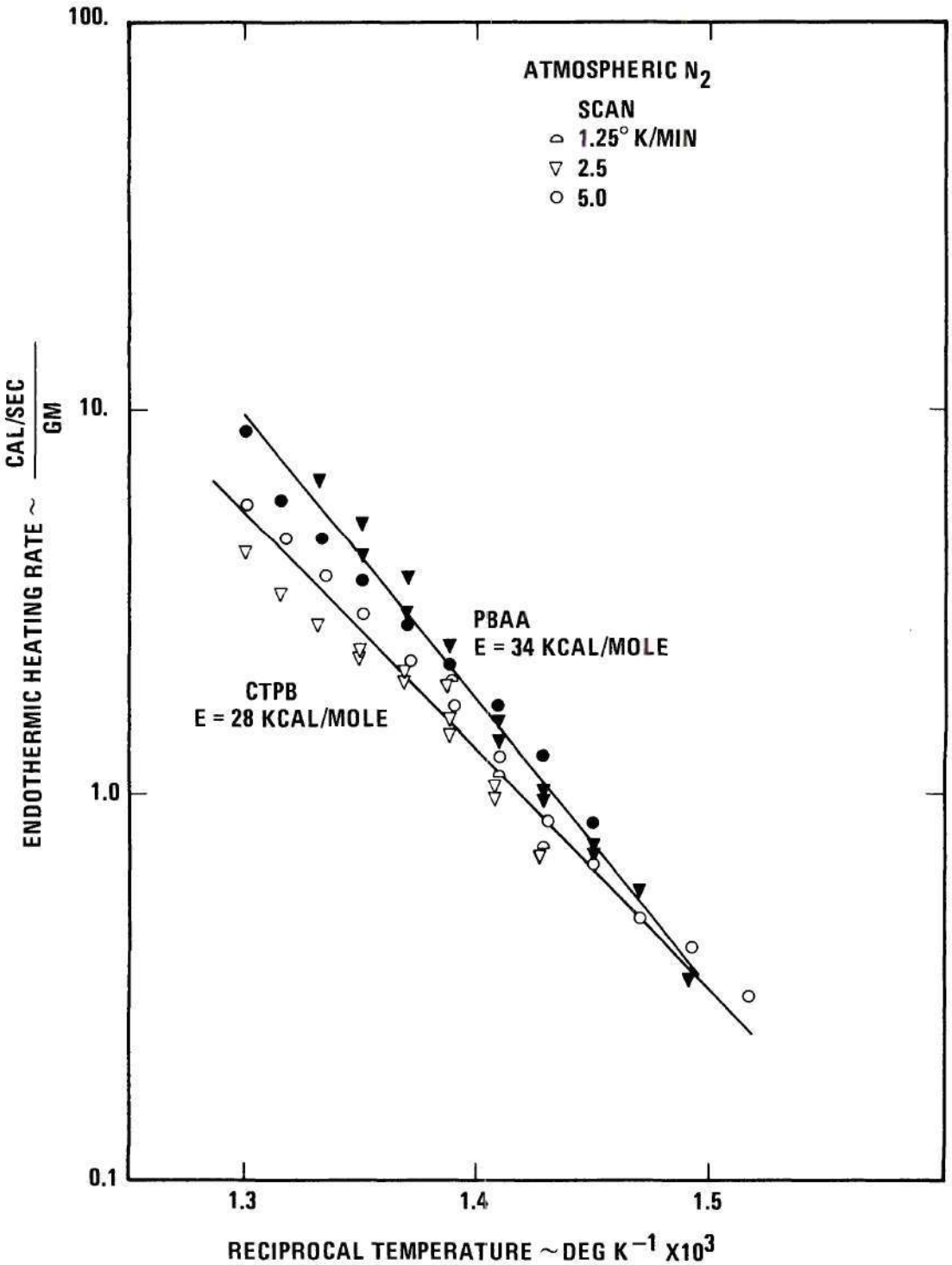

Figure 8. Thermal Decomposition Kinetics of PBAA and CTPB Binders.

(see Data Reduction). The results of the mass loss quenching tests were compared with the mass loss information obtained by the procedure discussed in the Data Reduction analysis. Figures 9, 10, 11, and 12 show that the experimental data points fall considerably below the curves calculated using the thermogram area ratio method and that the general shape of both curves agree. The differences in the mass loss values are a result of continued decomposition during the removal and quenching of the binder sample; this is substantiated by the fact that the data points lie below the calculated curves. If the sample could be very rapidly quenched, it is felt that the resulting data and the calculated curves would be in good agreement.

Table 1. Binder Decomposition Energetics and Kinetics

Binder	Pre-Exponential Factor (Z, sec^{-1})	Energy of Decomposition (ΔH, cal/gm)	Activation Energy (E, kcal/mole)
Polysulfide	2.3×10^{28}	66	78
Polyurethane	7.4×10^{18}	77	61
PBAA	2.0×10^{7}	1950	34
CTPB	3.4×10^{5}	1910	28

Complete DSC-1B decomposition data, including thermograms and data reduction calculations are presented in Appendix E.

Relevance of the Generated Kinetic Data

If the generated kinetic data are relevant to solid propellant combustion, one obvious item of agreement should be the predicted and the

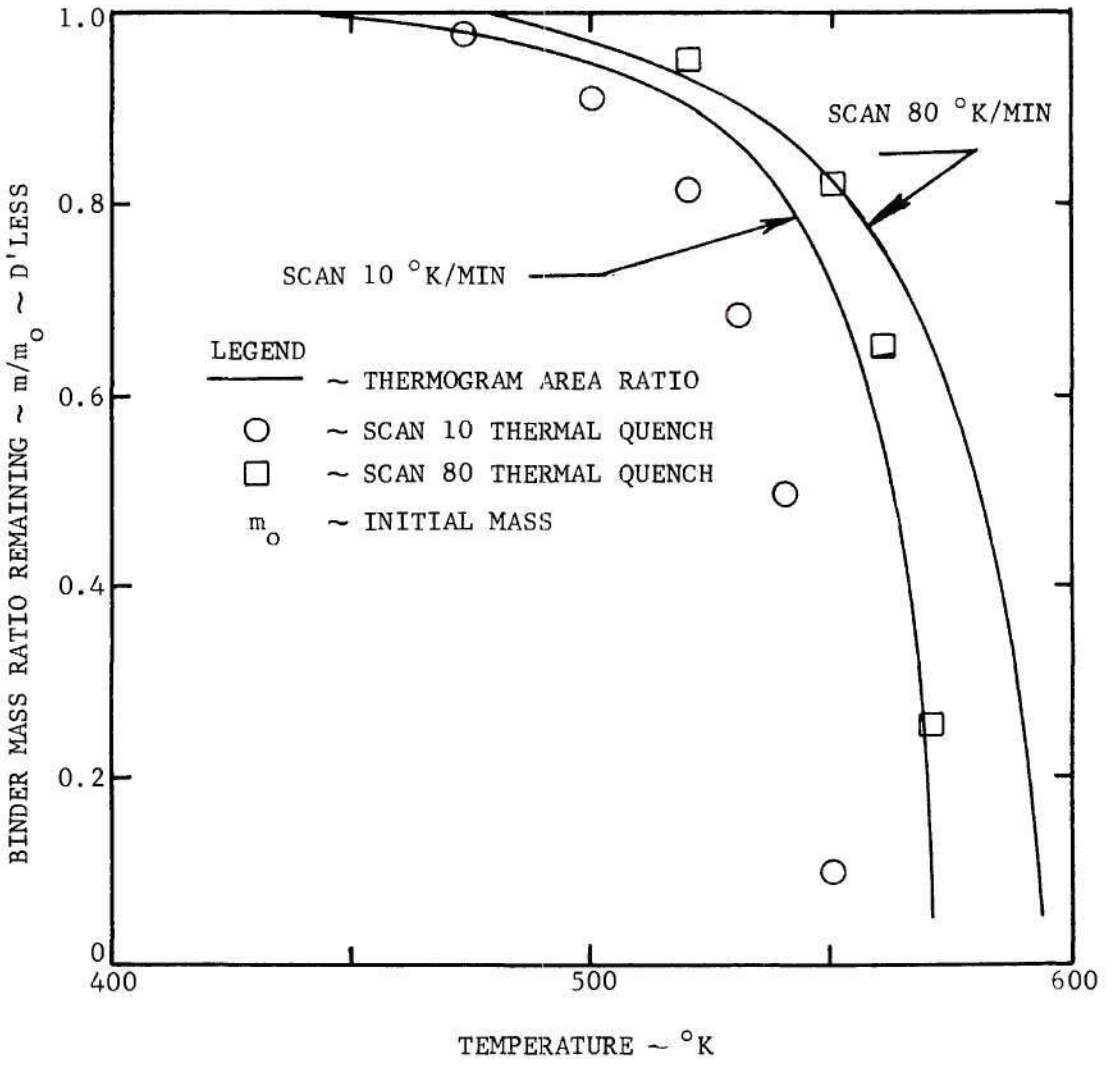

Figure 9. Thermal Decomposition Mass Loss for PS Binder.

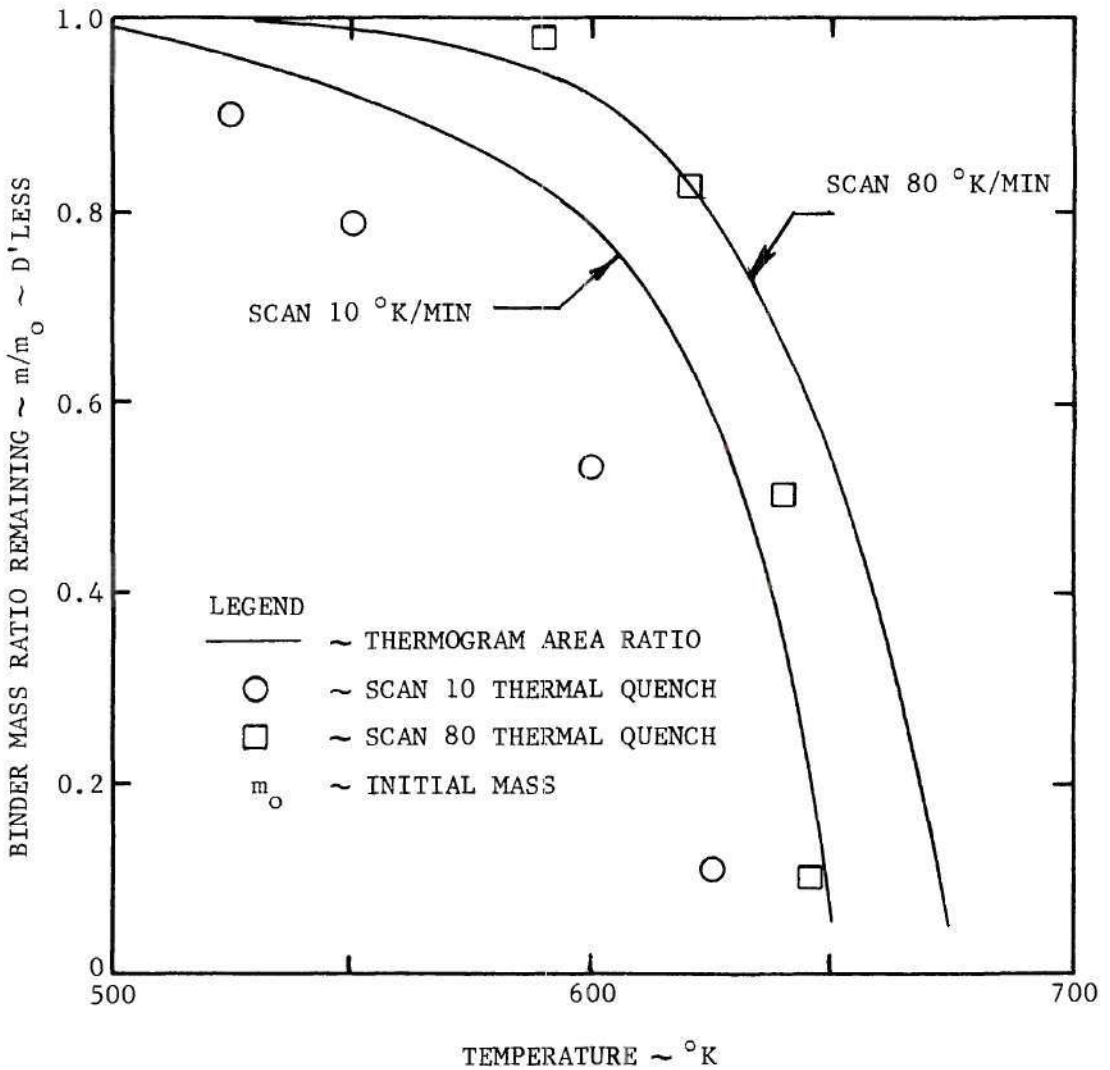

Figure 10. Thermal Decomposition Mass Loss for PU Binder.

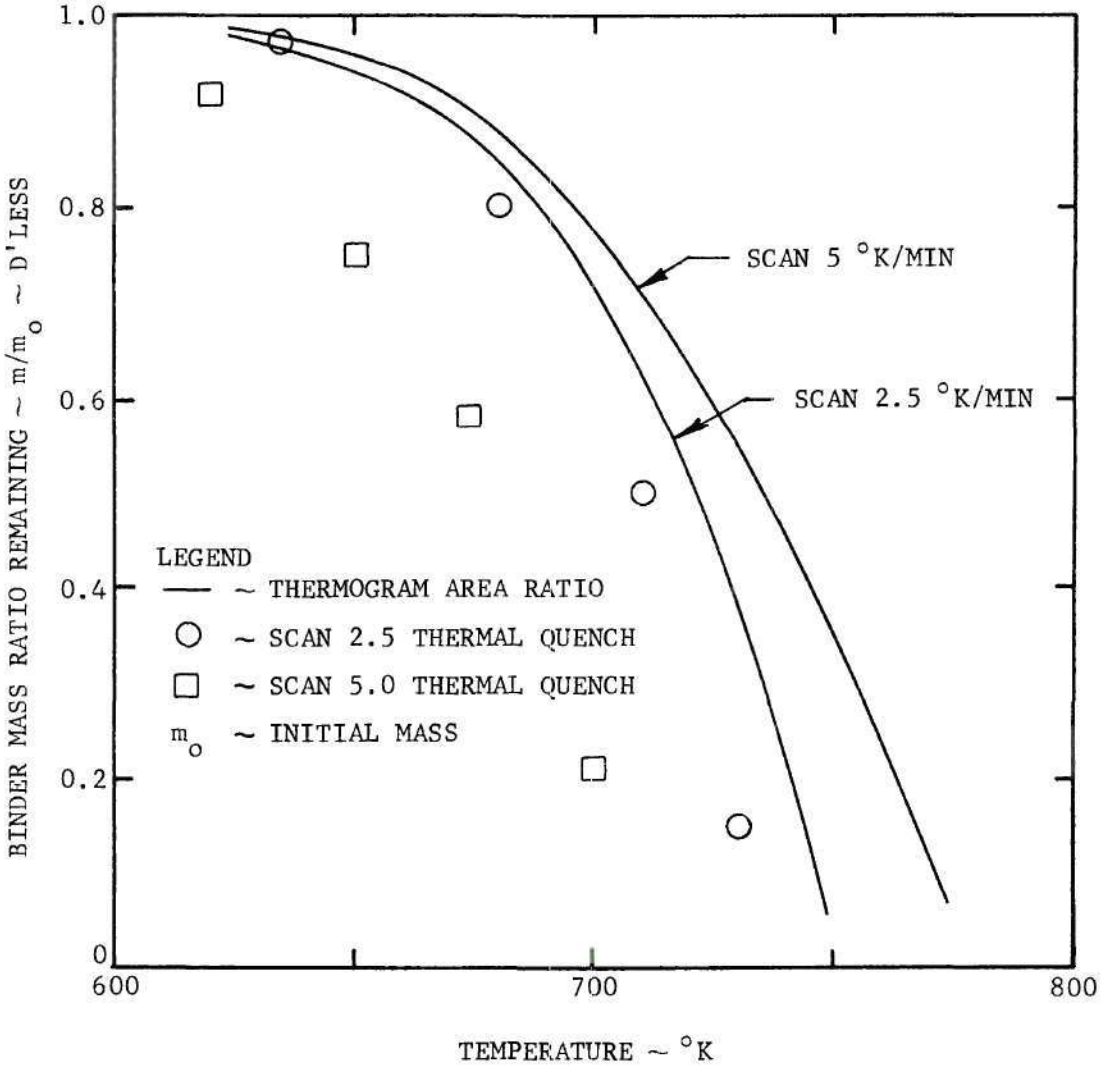

Figure 11. Thermal Decomposition Mass Loss for PBAA Binder.

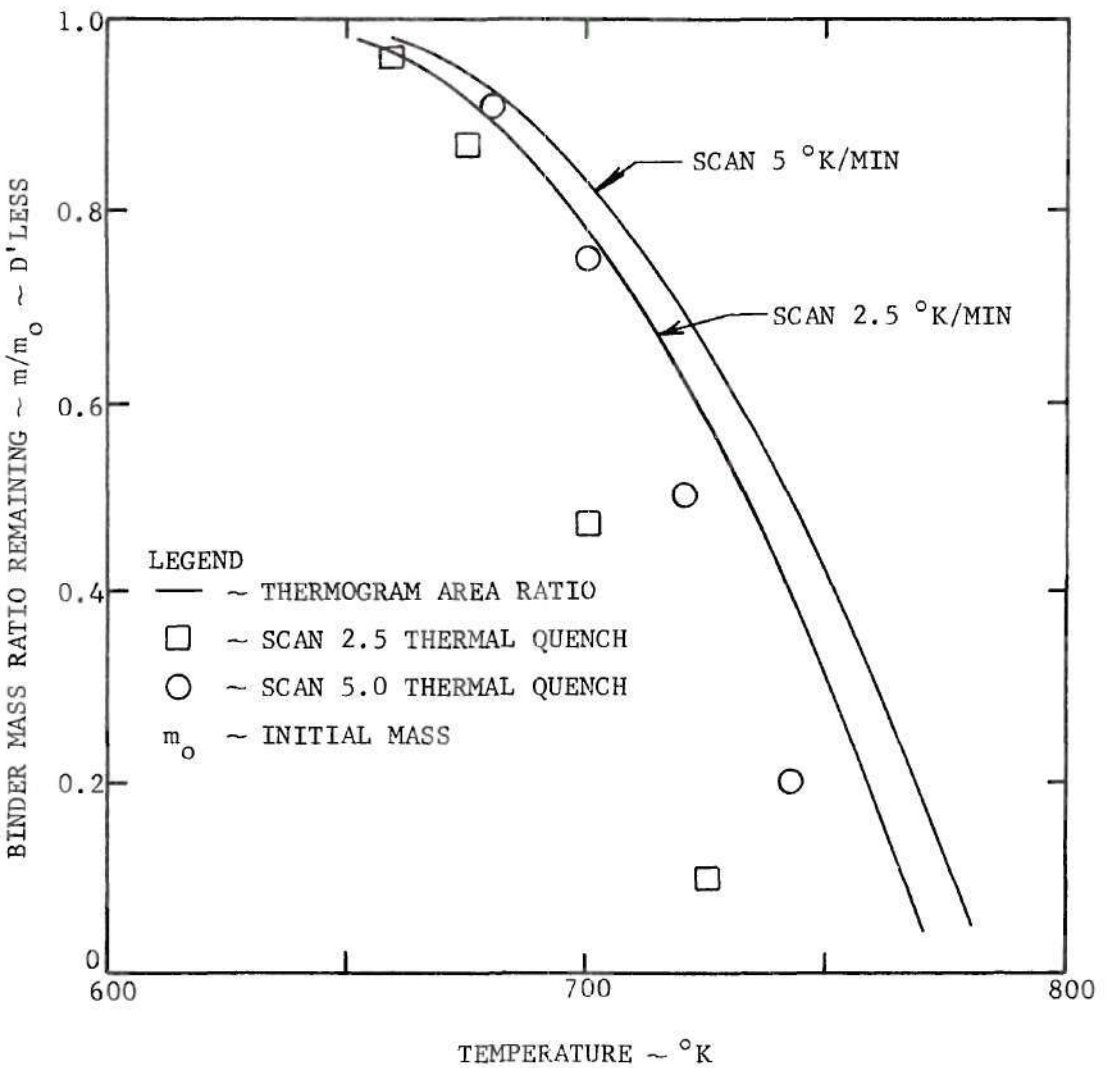

Figure 12. Thermal Decomposition Mass Loss for CTPB Binder.

observed binder surface temperature during deflagration. A difficulty immediately appears since only some apparent average surface temperatures, including the oxidizer, have been measured [8]. Nevertheless, an order of magnitude comparison can be made from a knowledge of the average surface temperature, a rough knowledge of the pure ammonium perchlorate surface temperature, and the mass ratio of binder to oxidizer.

The data of this investigation reveal an uncertainty concerning the type of rate process occurring. If an in-depth pyrolysis is occurring, a first order decomposition process is a reasonable assumption; if a surface escape process is occurring, then the data should be correlated by a two-thirds order rate law. Since the data presented here could have been correlated either way, with slightly more data scatter for a two-thirds law, it must presently be left open concerning which, if either, is the dominant process. The surface temperature calculations below indicate, however, that a surface process may be occurring.

For a first order process and a one-dimensional regression model, the mass fraction, Y, of undecomposed material should obey the differential equation and boundary condition

$$\frac{dY}{dx} = -\frac{Z}{r}\, Y\, e^{-\frac{E}{RT}}, \tag{14}$$

where $Y(0) = 0$ and $x = 0$ at the surface. The length scale for decomposition may adequately be predicted by the constraint that the mass fraction approaches unity as x approaches negative infinity. Equation (14) may not be solved exactly; the approximate method used is the method of

weighted residuals [47]. Assume $Y = (1 - e^{ax})$ which satisfies the boundary conditions with an as yet unknown length parameter, a. Assuming most of the reaction takes place near the surface in the highest temperature region, $e^{-E/RT}$ is approximated by de^{bx} where the value of this fraction and its first derivative are matched at x = 0. Since an overall energy balance at the regressing surface yields

$$\left.\frac{dT}{dx}\right]_{x=0} = \frac{r}{\alpha}\left[T_s - T_0 + \frac{\Delta H}{c_p}\right], \tag{15}$$

the matching criteria for b and d are

$$b = \frac{E}{RT_s^2}\frac{r}{\alpha}\left[T_s - T_0 + \frac{\Delta H}{c_p}\right] \tag{16}$$

and

$$d = e^{-\frac{E}{RT_s}}.$$

Errors in the unknown length parameter, a, and in the residual matching parameter, b, have little effect on the calculated value of the surface temperature since the surface temperature determination is dominated by the exponential Arrhenius factor, $\exp(-\frac{E}{RT})$. Two independent relations for "a" and "b" (i.e., T_s) can be obtained by weighting equation (14) with two linearly independent weighing functions and integrating over the semi-infinite domain. Due to the insensitivity of the calculations upon the values of "a" and "b", the selection of the weighting functions W = 1 and W = x will be chosen solely for the resulting algebraic simplicity.

Multiplying equation (14) by W = 1 and integrating between $-\infty$ and 0 gives

$$\frac{Zd}{rb}\left[\frac{a}{a+b}\right] = 1 \ . \tag{17}$$

Multiplying equation (14) by W = x and integrating between $-\infty$ and 0 yields

$$\frac{Zd}{r}\left[\frac{a^2 + 2ab}{b^2(a+b)^2}\right] = \frac{1}{a} \ . \tag{18}$$

The unknowns are T_s and a in equations (17) and (18), presuming r is given. Assuming r = 1 cm/sec, c_p = 0.3 cal/gm °K, T_0 = 300 °K, $\alpha = 10^{-3}$ cm^2/sec, and the Z, E, and ΔH as given from the data of this study, equations (17) and (18) have been solved for T_s; the results are shown in Table 2.

Now assuming a surface process, the rate expression is

$$\dot{m} = ZA\, e^{-\frac{E}{RT}} \ . \tag{19}$$

For simplicity, the relation of A to m is chosen as that for a sphere, although the precise relation is unknown in these experiments. Then for a one-dimensional regression,

$$r = \frac{Z}{\rho_s}\, e^{-\frac{E}{RT_s}} \ . \tag{20}$$

The value of Z for a surface process is computed from the data through equation (19) and is shown in Table 2. Equation (20) is then used to calculate the surface temperature and this is also shown in Table 2.

Table 2. Computed Surface Temperatures for a One cm/sec Plane Regression Rate

	Pre-Exponential Factor		Surface Temperature	
Binder	First Order (Z, sec^{-1})	Surface Process (Z, $gm/sec\text{-}cm^2$)	First Order (T_s, °K)	Surface Process (T_s, °K)
Polysulfide	0.23×10^{29}	0.51×10^{27}	715	641
Polyurethane	7.4×10^{18}	1.42×10^{17}	871	773
PBAA	0.20×10^{8}	0.37×10^{6}	2170	1404
CTPB	0.34×10^{6}	0.97×10^{4}	3070	1648

Since for both polysulfide and polyurethane the indicated temperatures are close to the range experimentally studied, it is concluded that the thermal decomposition results may be relevant to solid propellant deflagrations. The results for PBAA and CTPB are less clear, however. If a first order process is involved, the CTPB results must be discarded because the temperature would be in excess of the overall flame temperature in many systems. Alternatively, if a surface process is governing, the temperature is more reasonable. Nevertheless, since the indicated temperatures for both PBAA and CTPB are substantially above those achieved in the experiments [8], there must exist

doubt concerning the relevance of the deduced kinetics given here. It should be pointed out that doubt will always exist concerning results deduced from DSC experiments since the heating rates achieved are orders of magnitude lower than those experienced in actual combustion situations.

CHAPTER III

QUENCH COMBUSTION OF TWO-DIMENSIONAL PROPELLANT SANDWICHES

The potential of simplifying the study of composite solid combustion by utilizing two-dimensional propellant systems has been explored theoretically by Nachbar [12] and Fenn [14] and experimentally by several investigators, primarily Hightower and Price [38] [39] and Nadaud [42]. The relative ease of preparing two-dimensional propellant samples with different binder types and binder thicknesses makes propellant sandwiches an ideal tool for observing and interpreting the binder effects in the combustion zone.

Propellant sandwiches were prepared from cleaved AP crystals and pressed AP polycrystalline discs laminated together with a thin binder layer, the thickness of which was varied over a range of approximately 25 to 200 microns. Propellant sandwiches were burned at pressures from 300 to 2400 psig and the combustion process rapidly interrupted in order to allow microscopic examination of the quenched sample. Particular attention was given to the sandwich surface for evidence of the binder forming a melt and flowing.

An ancillary study was conducted by the U.S. Naval Weapons Center (NWC) to establish the deflagration behavior of pressed polycrystalline AP specimens supplied by this laboratory. Also, a determination was made early in the investigation of the time scale required to obtain a steady burning state.

Finally, the results of the quench combustion study and the information obtained from the binder thermal decomposition investigation were formulated into a qualitative argument in order to elucidate the physico-chemical steps occurring in the sandwich combustion zone.

Apparatus

The experimental investigation was conducted in the Aerospace Engineering Propulsion Laboratory using facilities modeled after the solid combustion laboratory at the U.S. Naval Weapons Center. Principal components of the facility are a high pressure, variable flow combustion system and associated apparatus required for sample preparation and data analysis.

High Pressure Combustion System

The high pressure combustion system, Figure 13, is designed to accommodate the ignition and combustion of a two-dimensional propellant sandwich in an inert, pressurized environment, either stagnant or flowing, and to permit interruption of the burning process by rapid depressurization of the combustion section. A description of the high pressure combustion system, schematically shown in Figure 14, follows. Gaseous nitrogen is supplied from pressurized containers to a three-station collector manifold, where positive system on/off control is provided by a quarter-turn ball valve. Nitrogen flow is then directed to a stainless steel combustion vessel via a dome-loaded pressure regulator which provides for environmental combustion pressure control. Nitrogen purge flow through the combustion section is regulated by two metering valves located in parallel exit lines which exhaust combustion

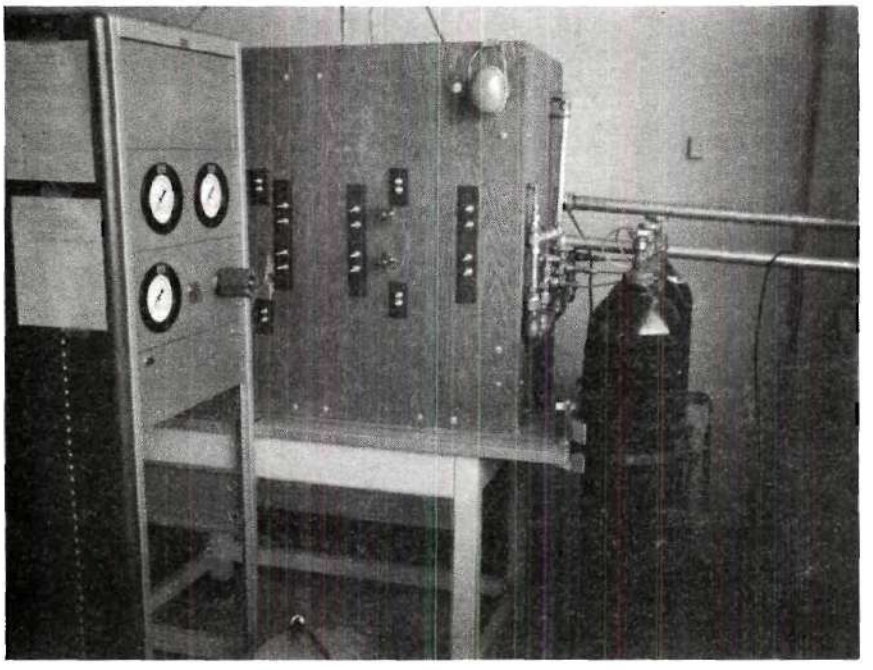

(a) Control Panel and Nitrogen Supply.

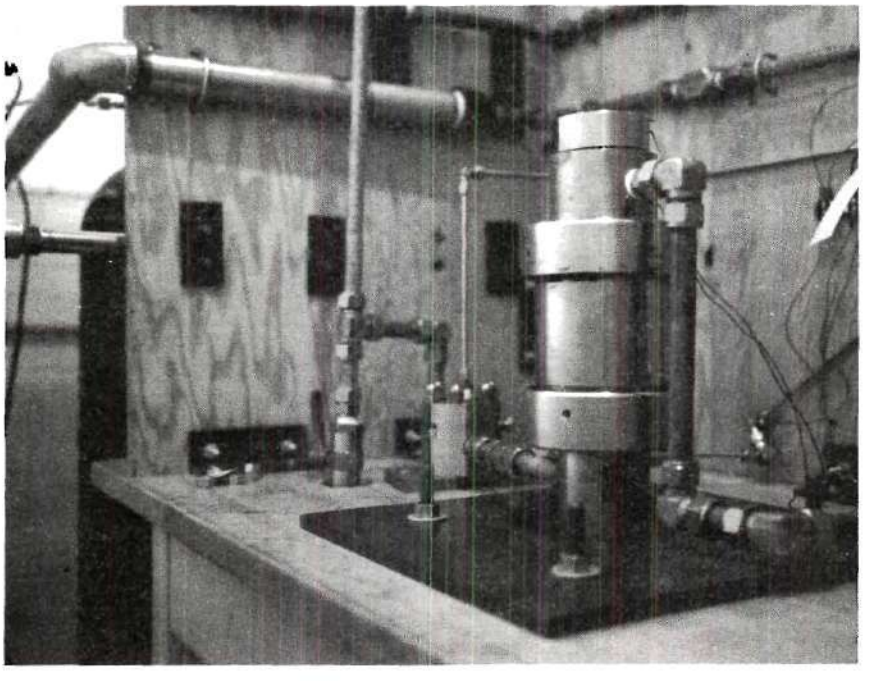

(b) Combustion Vessel and Associated Plumbing.

Figure 13. High Pressure Combustion System.

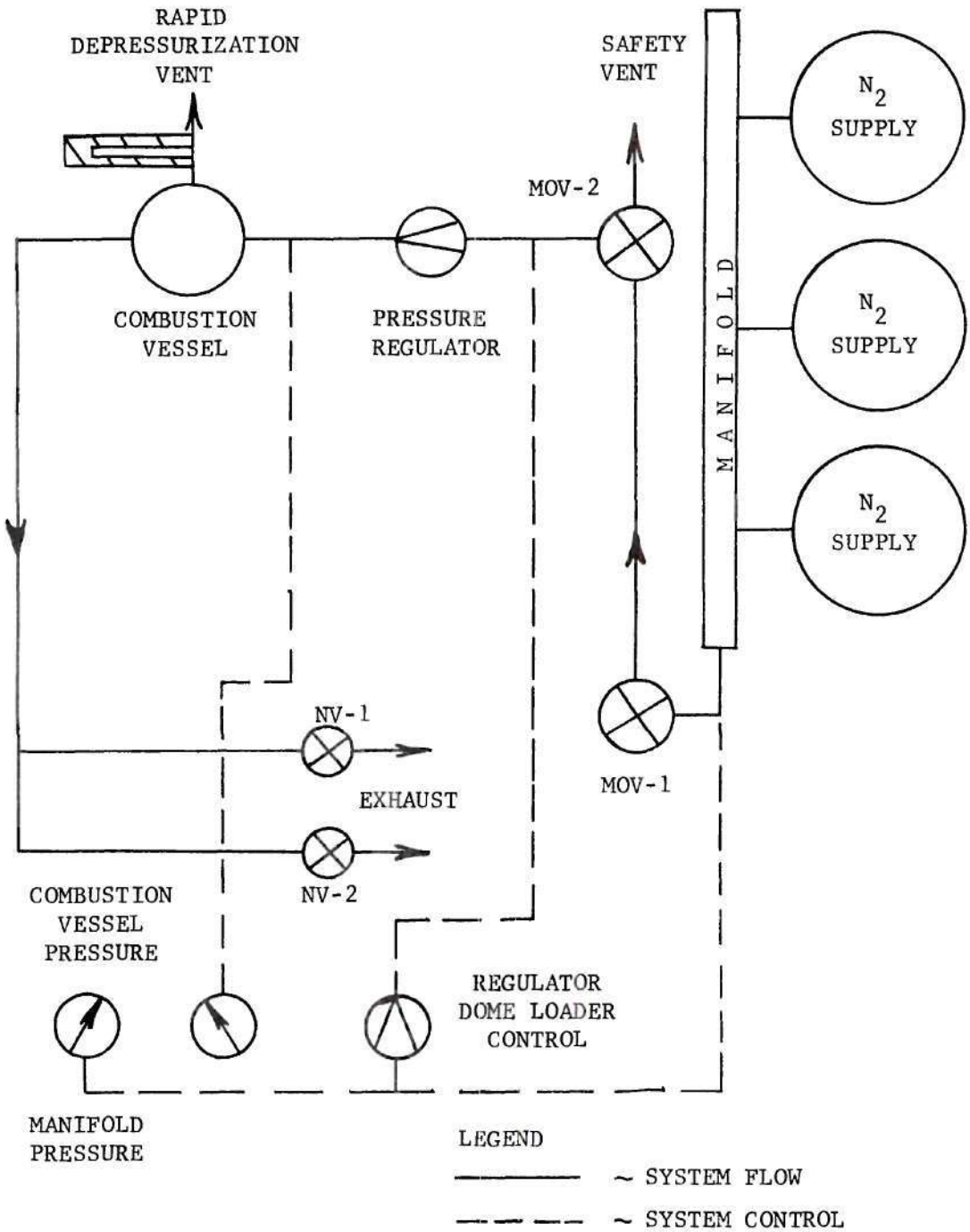

Figure 14. High Pressure Combustion System Schematic.

flow from the laboratory. The combustion vessel is equipped with electrical circuitry for sample ignition and with a rapid pressure relief device for interruption of burning.

In addition to the primary flow system, a control panel was provided for the selection of the desired combustion pressure level, display of manifold and combustion pressure, regulation of gas flow, and activation and proper sequencing of the ignition and quenching apparatus.

The combustion system components were assembled on a laboratory test bench and isolated from the control panel and nitrogen supply containers by a three-fourths inch thick plywood enclosure which also provided plumbing support and tie-down. A ten inch O.D. closed steel tube with one-half inch walls, Figure 15, was lowered around the combustion vessel during testing and served as a safety shield. An itemized description of the combustion system components follows.

A three-station, single row brass manifold supplied by the Matheson Company was used to collect gaseous nitrogen from the pressurized cylinders. The manifold, rated for 3500 psig safe working pressure, was wall mounted on the combustion system enclosure. High purity, dry nitrogen (Linde) supplied in cylinders containing 300 standard cubic feet at 2600 psig was used as the environmental medium in this investigation.

The combustion pressure level was maintained by a Victor Controls dome-loaded pressure regulator, Model GD 68. The Model GD 68, a diaphragm operated, balanced poppet regulator with 316 stainless steel body

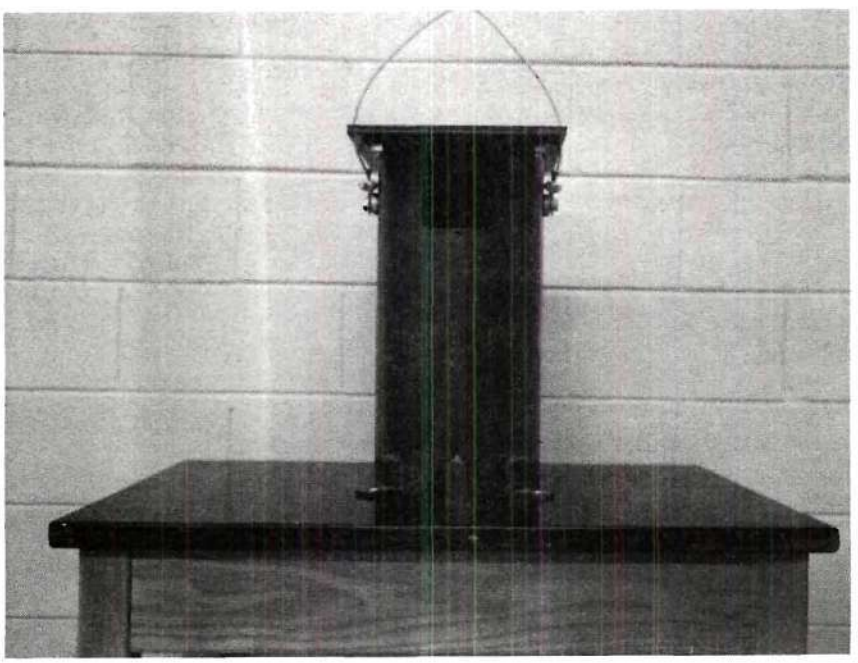

Figure 15. Combustion Vessel Safety Shield.

and springs and "Viton" diaphragm and seals, is rated for 10,000 psig service.

A stainless steel ventilated pressure vessel was used for control of the combustion atmosphere. The combustion vessel, schematically shown in Figure 16, is a three piece assembly with provisions for sample ignition and quenching:

1. The lower section provides an inlet for the nitrogen pressurization flow, houses the ignition circuitry, and serves as a base for the sample holder assembly.

2. The center section serves as the combustion section.

3. The top section provides an exit for the exhaust flow, both primary and quench, and houses the quenching mechanism.

The three piece combustion vessel is retained by upper and lower stainless steel, threaded collar rings on the O.D. of the combustion section and utilizes rubber "O"-rings for leak proof pressure control.

The sample holder assembly, Figure 17, is attached to the lower section of the combustion vessel and serves three functions:

1. Provides a means for sample support in the combustion section.

2. Initiates smooth flow past the combustion sample via a 20 micron, sintered stainless steel porous plate which serves as the floor of the holder assembly.

3. Provides an extension of the ignition circuitry to the proximity of the combustion sample.

Sample ignition was accomplished by electrically heating a single strand

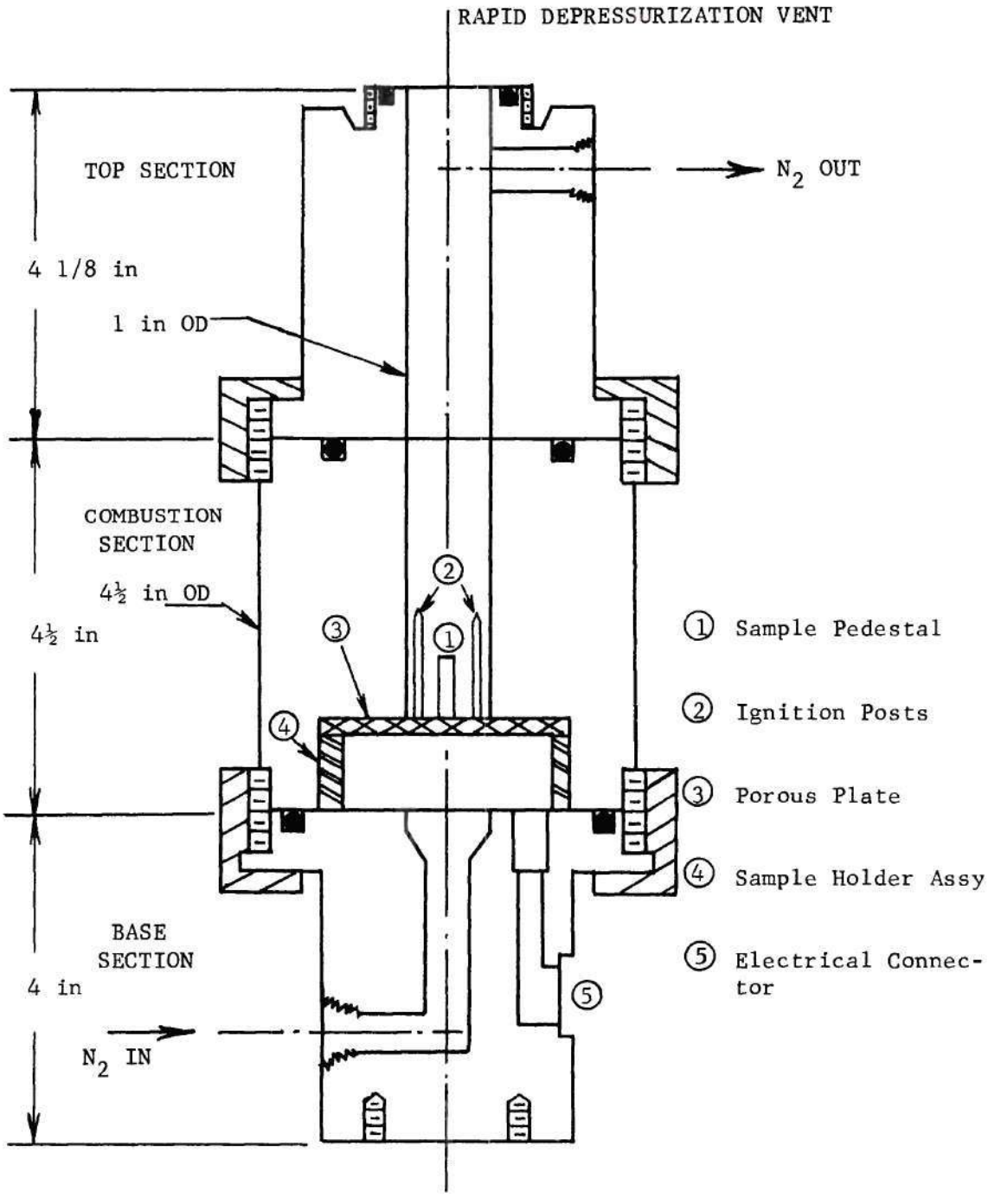

Figure 16. Combustion Vessel Schematic.

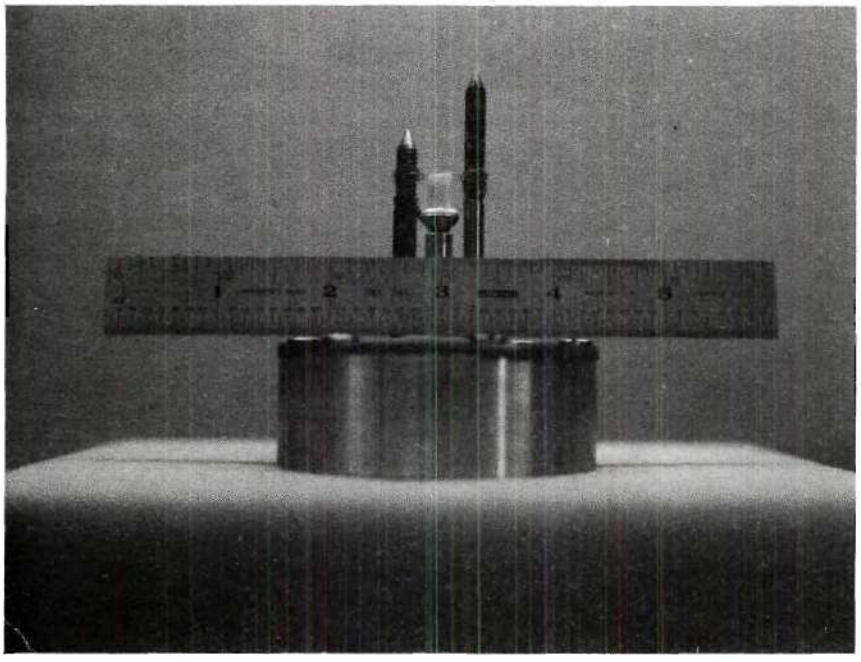

Figure 17. Sample Holder Assembly.

of 10 mil nichrome wire positioned on the upper sandwich surface. Ignition power was supplied by two 12 vdc dry cell batteries wired in series.

The quenching mechanism is attached to the upper portion of the combustion vessel and permits, upon an electrical signal, the rapid depressurization of the combustion section.

Two quenching mechanisms were used during this investigation. The first design, Figure 18, was modeled after a NWC design and accomplished depressurization by rapidly opening a trap door which covered the one inch diameter combustion section. The device consists of three moving parts: two locking toggles and a release trap door. The mechanism is activated by a solenoid which releases the locking toggles, allowing the trap door to be opened by the combustion vessel pressure. Mechanical failures with this type mechanism occurred at pressures above 1200 psig.

The second quenching device, Figure 19, utilized several laminae of 2 inch diameter, 5 mil mylar discs held in place over the top section of the combustion vessel by a ported retainer cap. Rupture was initiated by electrically heating a 10 mil nichrome hot wire, positioned as shown in Figure 19, with two 12 vdc dry cell batteries wired in series. The bulged shape of the diaphragm containing the rupture wire is the shape assumed during run conditions; in this case, the diaphragm contained 9 laminae of 5 mil mylar discs and was pressurized to 2000 psig. Also shown is a similar diaphragm after rupture at 2000 psig.

Two Hoke Roto-Ball 303 stainless steel valves were used in the

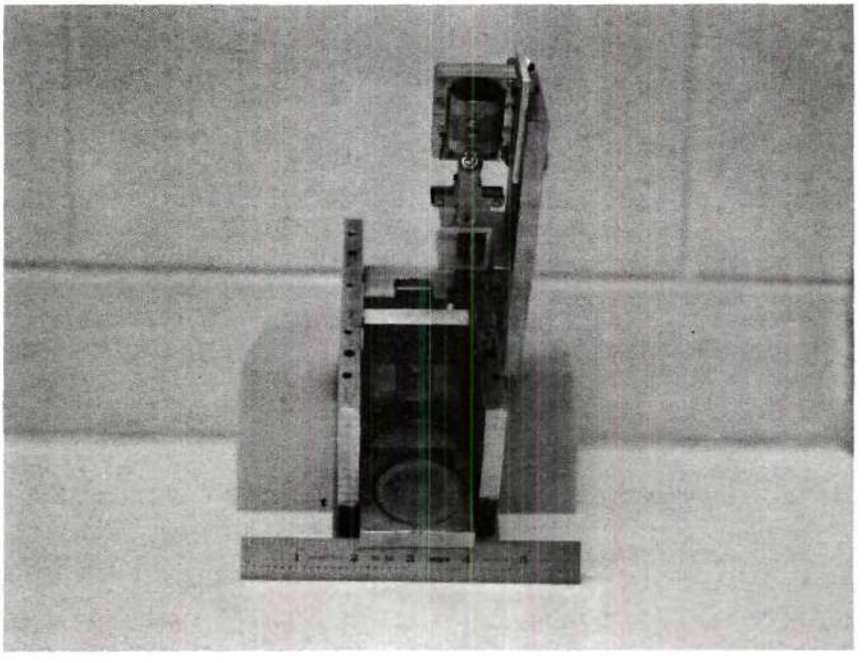

Figure 18. Mechanical Pressure Relief Device.

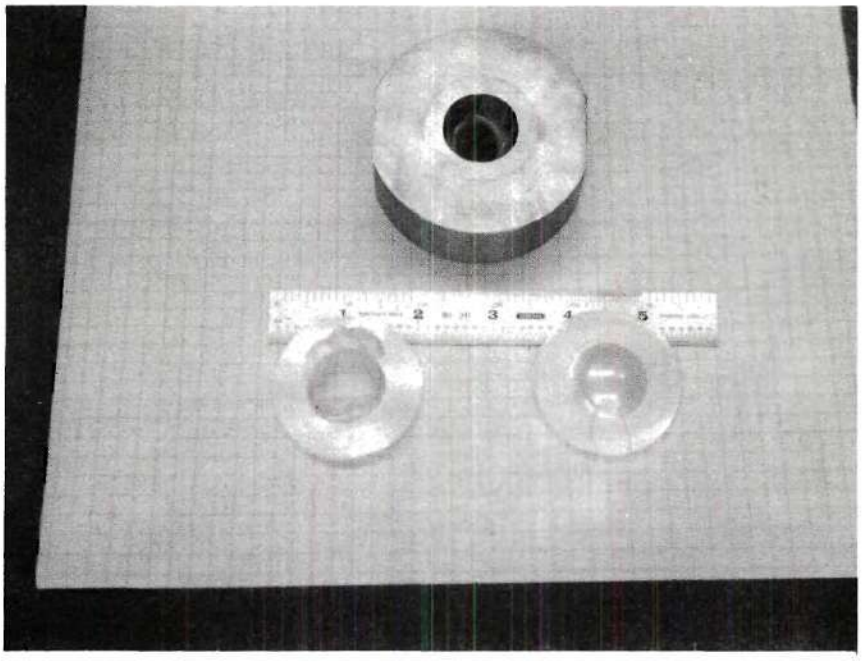

Figure 19. Mylar Diaphragm Pressure Relief Device.

primary flow portion of the combustion system upstream of the combustion vessel. Referring to Figure 14, the valve designated MOV-1 was used for off/on control in the high pressure system. The valve designated MOV-2 provided an upstream nitrogen bleed capacity in case of a regulator lock-up or other unforeseen difficulties in the pressurization system.

Smooth regulation of combustion vessel purge flow was provided by two Hoke 270 Series needle valves, NV-1 and NV-2, arranged in parallel in the exhaust portion of the flow system.

Nitrogen flow lines were constructed with PATCO seamless 316 stainless steel tubing having a three-fourths inch O.D. with a 0.120 inch wall thickness. Leak proof connections were made using Crawford "Swagelok" 316 stainless steel tube fittings.

Principal components of the control console, Figure 20, were a pressure regulator control, pressure gauges, and a multichannel cam timer used for sequencing the ignition and quenching operations.

The Model GD 68 is an externally gas dome loaded regulator requiring a pressure control device to maintain the proper dome loading. This role was performed by a Victor Controls LR series pressure reducing regulator. The LR series regulator is a low flow, high pressure regulator for the control of pressure up to 10,000 psig. The LR regulator is self-relieving and has hand wheel control operated by a single control in the console.

Manifold and combustion pressure levels were monitored on Marsh Type 210 pressure gauges. The Type 210 gauges are Bourdon tube type,

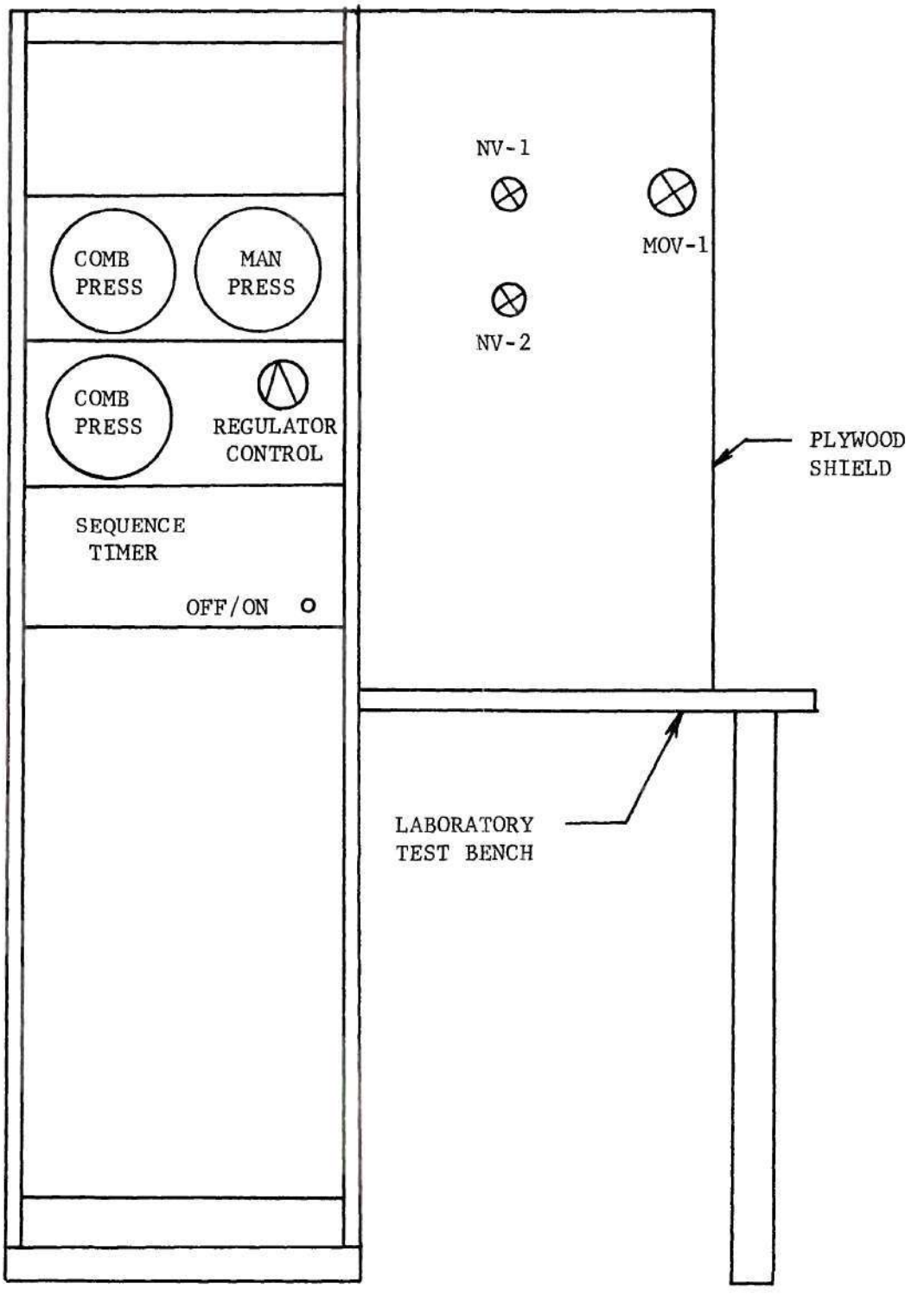

Figure 20. Control Panel Schematic.

stainless steel throughout, and have an accuracy of one-fourth of one per cent of the maximum dial reading. A dial pressure range of 0-5000 psig was used for manifold pressure while a 0-3000 psig gauge was used to monitor combustion pressure level.

Activation and proper sequencing of the ignition and quenching apparatus were accomplished by a ten-channel, electro-mechanical cam timer, Model RC-2, manufactured by the Industrial Timer Corporation.

Control panel instrumentation lines were prepared with Superior Tube Company 316 stainless steel tubing having a one-fourth inch O.D. with a 0.049 inch wall thickness; leak tight connections were made with Crawford "Swagelok" 316 stainless steel tube fittings.

Auxiliary Laboratory Facilities

Auxiliary laboratory facilities and apparatus required for sample preparation and data analysis are described below.

Sample Preparation Apparatus. A heavy glass mortar and pestle were used to thoroughly grind crystalline AP into a fine powder. AP polycrystalline compaction was achieved using a six piece mold in a Carver Laboratory Hydraulic Press, Figure 21. Binder preparation was accomplished using the apparatus described in Chapter II.

Data Analysis Apparatus. Microscopic examination of the quenched propellant sandwich was achieved using a Bausch & Lomb Dynazoom Laboratory Microscope and the lighting apparatus shown in Figure 22. The Dynazoom permits fixed magnifications ranging from 40X to 1000X with a continuously variable 1X to 2X zoom magnification within each fixed setting. Basic illumination is achieved by a base mounted, variable

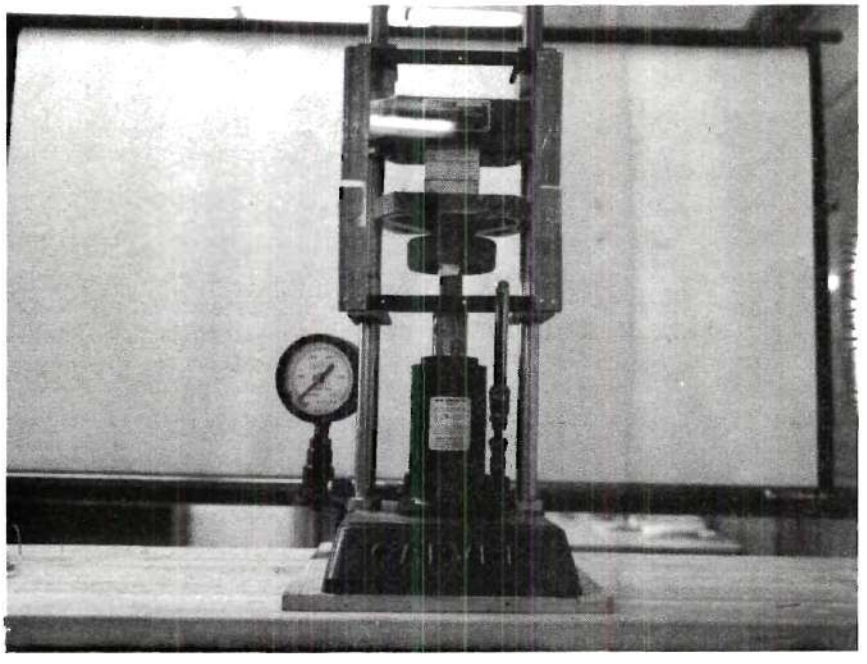

(a) AP Mold Assembled and Loaded in Press.

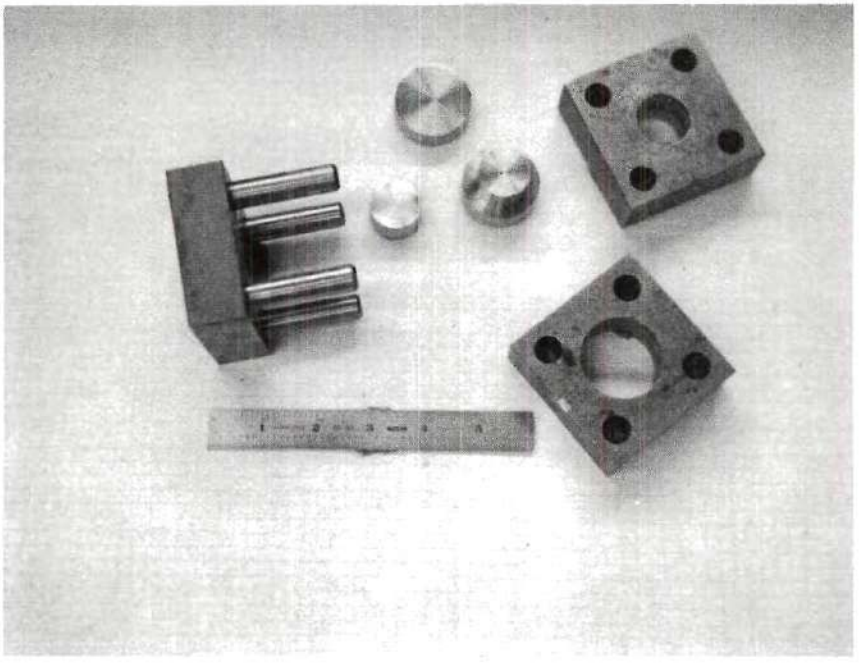

(b) AP Mold Component Parts.

Figure 21. Polycrystalline AP Compaction Apparatus.

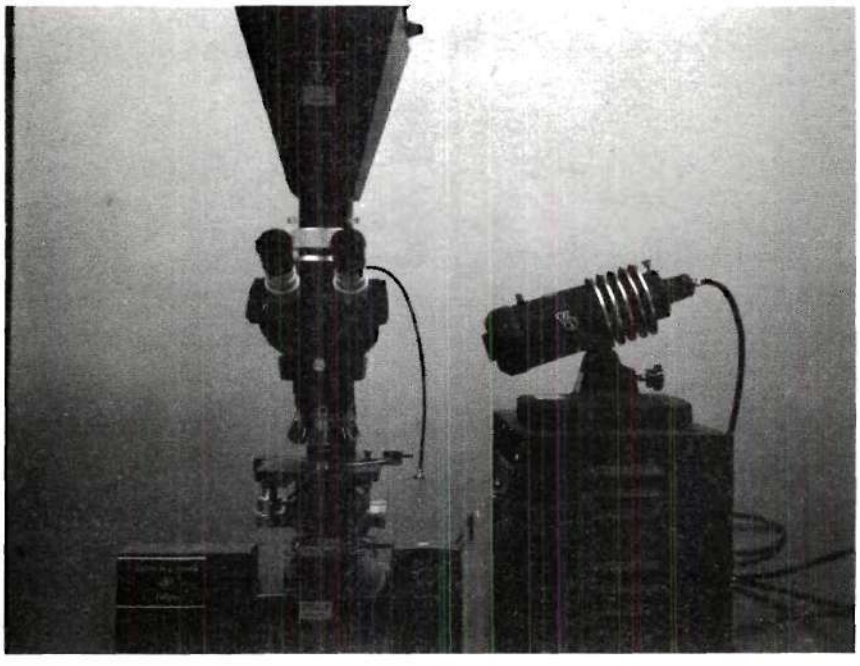

Figure 22. Sandwich Data Analysis Apparatus.

output illuminator coupled with an Abbe condenser system. Photomicrographs can easily be made with the Dynazoom microscope which incorporates provisions for several camera assemblies. For this investigation, a 4 X 5 camera, supplied by Bausch & Lomb, was installed on the Dynazoom microscope. The 4 X 5 camera is equipped with a Graflok back which will accept a wide variety of film holders, including the Polaroid 500 sheet film holder which was used in this study. Sandwich photomicrographs presented in this investigation were made using Polaroid Type 55 P/N film (black and white) and Polaroid Type 58 film (color) in the 4 X 5 camera.

To insure fine quality photomicrographs, external illumination was required to complement the basic illumination system. A Fish-Schurman "Zirconarc" photomicrographic lamp and power supply were selected to augment the basic illumination. The "Zirconarc" is basically an arc lamp, but its electrodes are fixed and sealed within a glass bulb containing an inert atmosphere. The character of the light is such that no color correction filters are required for color exposures. The illuminating light beam is aimed at the microscope sample by means of a non-slip adjusting screw which controls the angle of the beam with the horizontal. Beam focusing is accomplished by a condenser system with an extremely short focal length. The power supply and lamp starter are a separate, self-enclosed unit operating from a standard 110 vac current source.

Experimental Procedures

In order to successfully conduct an experimental investigation

involving new or untested techniques, procedures must be developed and evaluated at each stage of the program. The procedures and techniques discussed are those which produced successful results and contributed to achieving the goals of the investigation. These procedures include the successful compaction of a near crystalline density, polycrystalline AP disc from laboratory grade AP, moderately successful control of binder layer lamination thickness, success in achieving rapid depressurization quenching at elevated pressures, and successful development of a sample replica technique which permits unambiguous investigation of the quenched sample.

Ammonium Perchlorate Compaction Procedure

A small amount of certified laboratory grade AP weighing approximately 1.3 grams was ground in a mortar and pestle for ten minutes producing a fine, talc-like powder. The ground AP was transferred to a mold fixture, Figure 21, for compaction. The mold loading procedure, schematically shown in Figure 23, was as follows:

1. The ground AP was transferred to the partially assembled mold fixture and evenly distributed on the stainless steel lower cavity plug.

2. The upper cavity plug was positioned and used to lightly compact the powdered sample insuring uniform distribution.

3. The upper cavity retainer and compression plug were located completing the mold assembly.

The completed mold assembly was loaded in a hydraulic press for compaction under a load equivalent to 27,000 psi for a period of 24 hours.

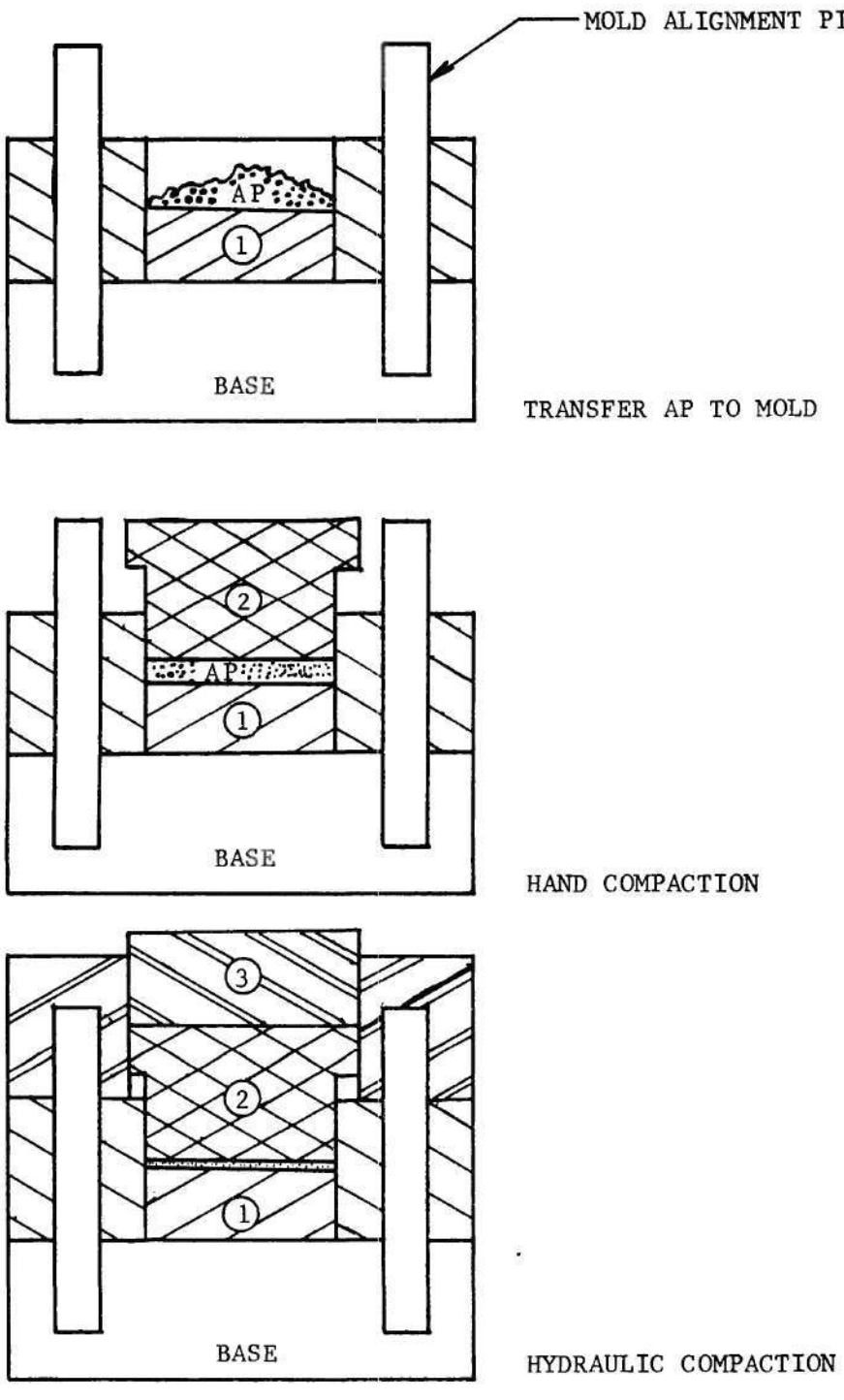

Figure 23. Procedure for Assembling AP Compaction Mold.

After compaction, the disc was removed from the mold and stored in a desiccator.

Sandwich Preparation Procedures

Propellant sandwiches were prepared from selected polycrystalline discs or from crystal segments (cleaved as matched pairs) by laminating a thin layer of uncured binder between the oxidizer sections. A small portion of binder material, prepared as indicated in Chapter II, was placed between two AP discs which were gently pressed together to uniformly spread the binder over the discs' mating surfaces. Very thin lamination thicknesses were achieved by separating sandwich halves before curing and matching each half with a new AP disc. Thick lamination layers were accomplished by using a larger portion of binder material and applying slight pressure to insure a uniform binder spread. Sandwich preparation techniques for pure crystals were similar to those described for pressed discs. The uncured propellant sandwiches were placed in a thermally soaked laboratory oven, and the binder curing cycle followed. After cure, the propellant sandwich disc was cut into six sandwiches, Figure 24, which were typically one centimeter by one-half centimeter and of varying thicknesses depending upon the binder lamination thickness.

Propellant sandwiches were weighed, dimensions taken, and then vertically mounted on flat-head machine screws using Dow Corning 732 adhesive. After curing in a desiccator, the mounted sample unit was weighed and screwed into the upper portion of the sample pedestal (the center post of the sample holder assembly, Figure 17). A single strand

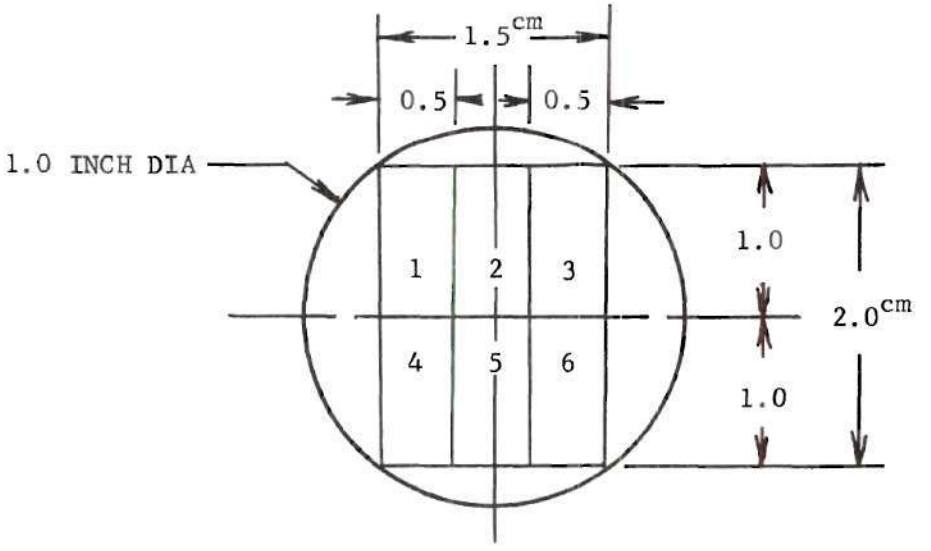

Figure 24. AP Disc Cutting Template.

of 10 mil nichrome wire was positioned on the upper sandwich surface along the binder-oxidizer interface and attached to the ignition posts, the two outer posts of the sample holder assembly. The completed assembly, Figure 17, was attached to the lower section of the combustion vessel; the center and upper vessel sections were then positioned and tightened. The quenching device was located on the top section of the combustion vessel and fastened in place. External wiring connections were made, thus arming the ignition and quenching circuits; circuit continuity and cam timer sequences were verified using an ohm meter. The cylindrical steel safety shield was lowered into place and fastened to the combustion vessel support plate.

Prior to initiating the combustion sequence, a preliminary check of all system valves was made to insure proper positioning, as shown in Appendix F. The run sequence was begun by opening the nitrogen cylinders and charging the manifold. After noting the manifold pressure, the system control valve, MOV-1 in Figure 14, was fully opened, admitting nitrogen to the upstream side of the regulator. The pressure level in the combustion vessel was then adjusted using the hand loader control on the instrument console. The combustion pressure level was noted, and a gentle nitrogen purge flow established by using needle valve(s) NV-1 (and/or NV-2). The cam timer was activated by a control switch on the instrument console, sequencing the sandwich ignition and quenching events. After quenching, characterized by a very loud discharge, the nitrogen flow through the system was terminated by closing the system control valve, MOV-1. After closing the nitrogen cylinder valves, the

upstream bleed valve, MOV-2, was opened, permitting the system pressure level to be reduced to ambient pressure.

After removing the safety shield and disconnecting the electrical circuits, the combustion vessel was disassembled and the quenched sample removed for weighing and investigation.

Sandwich Replica Technique

To facilitate the unambiguous study of sandwich burning profiles and to eliminate possible impairment of interfacial details, the feasibility of encapsulating the quenched sample and producing a reliable replica was considered.

A series of silicone potting and encapsulating materials was submitted by the Dow Corning Corporation for investigation. Preliminary screening was conducted to eliminate those materials which did not possess favorable color, low uncured viscosity, and relatively short cure time with nil shrinkage. The list of candidate materials was further reduced after the physical nature of the cured material was evaluated, particularly the ease with which the cured sample could be reliably sectioned with a razor blade. The final list of candidate materials -- Dow Corning RTV's 3110, 3112, 3120, and "Sylgard" 184 -- were tested for compatibility and good bonding with each other; no bad performance was noted, however, RTV's 3110, 3120, and "Sylgard" 184 proved to be excellent. A final evaluation of the three materials, in fact the most critical evaluation, was to check the solubility of AP and the binder materials in the encapsulating compounds. Intricate AP and binder shapes were potted and cured in the encapsulants; post-cure

examination revealed no loss of detail or sample distortion.

A quenched sandwich sample was glued upright in the bottom of a 30 milliliter disposable plastic medicine cup with Dow Corning 140 RTV adhesive. After the adhesive had cured, either RTV 3120 (red) or "Sylgard" 184 (clear) encapsulant was prepared according to Dow Corning instructions. The mixing container and its contents were placed in a vacuum chamber to remove the entrapped air. A vacuum in excess of 28 inches of mercury was maintained for five minutes and released to collapse any further entrapped bubbles; vacuum was reapplied and maintained for five more minutes. Fifteen milliliters of the de-aired encapsulant were gently poured into the cup around the quenched sample. The potted sample was placed in the vacuum chamber and the de-airing cycle repeated. After de-airing, the potted sample was allowed to cure at room temperature for three days. Following RTV curing, the plastic cup was removed and a small hole was cut in the base of the RTV "cup" replica exposing the lower portion of the encapsulated propellant sandwich. The RTV "cup" replica was placed in a container of warm water dissolving the AP portion of the sandwich via the hole in the base of the "cup." Following drying, the voids representing the leached AP portion of the sandwich were hypodermically filled with RTV 3110 (white) and allowed to cure for three days. The final encapsulated replica, Figure 25a, being entirely rubber, was very easy to cut into thin sections for microscopic investigation. The red RTV (3120) was easier to cut and provided a better background for photography, but the clear "Sylgard" encapsulant afforded better quality control during encapsula-

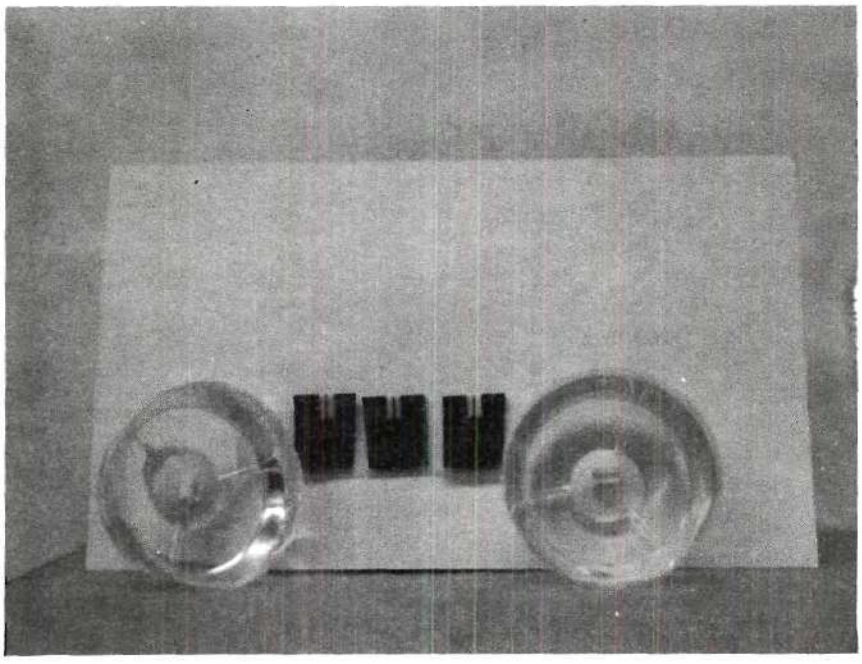

(a) Encapsulated Replicas (Left and Right) and Sectioned Replica (Center).

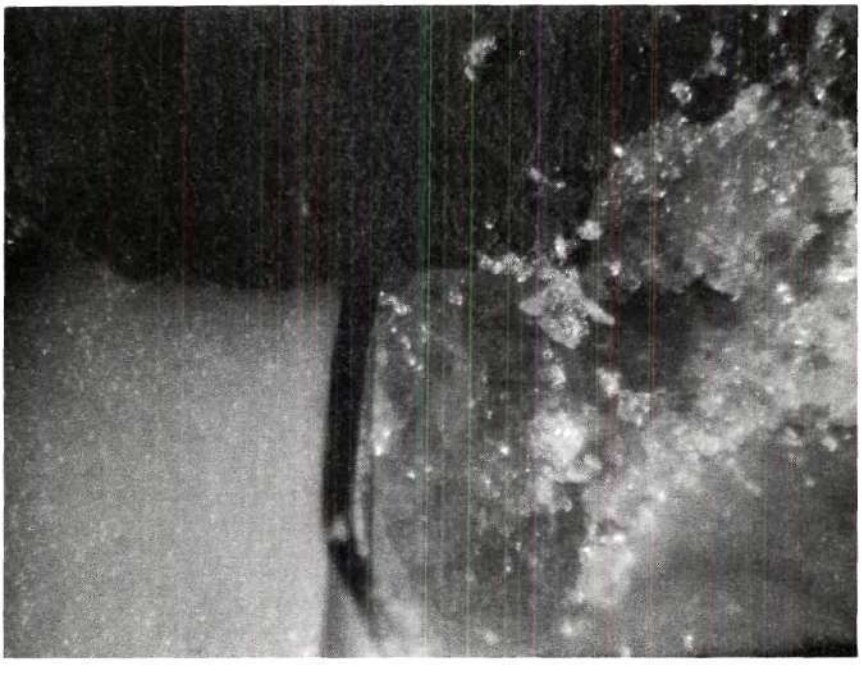

(b) Sectioned Sandwich with Replica AP (Left) and Polycrystalline AP (Right).

Figure 25. Silicone Rubber Replicas of Quenched Sandwiches.

tion and a thorough post-encapsulation inspection.

The quenched propellant sample shown in Figure 25b clearly indicates the loss of detail which can result from sectioning a polycrystalline sandwich. The AP in the left portion of Figure 25b has been leached and filled with RTV, while the right side was shielded from contact with the water. The surface and interfacial details for the silicone rubber portion are well defined, whereas the unpotted details are obscured.

Results of Ancillary Studies

The quench combustion investigation of two-dimensional propellant sandwiches was conducted in an orderly fashion by developing and evaluating techniques at each stage of the program. Accurate interpretation of the quenched sandwich characteristics depended upon a knowledge of the decomposition behavior of both the fuel and oxidizer and the assumption that a steady burning state was achieved before quenching. In order to provide a sound foundation for interpreting the quench combustion results, the decomposition behavior of polycrystalline AP and the reliability of achieving sandwich ignition and extinction were investigated.

Behavior of Polycrystalline Ammonium Perchlorate

It is desirable to use polycrystalline AP in the fabrication of two-dimensional propellant sandwiches because of the availability of commercial AP (as compared to the paucity of sources for large AP crystals) and because several identical combustion specimens can be made from a single propellant formulation (limited only by the size of

an acceptable compacted AP sheet). Several criteria by which the success of a polycrystalline AP compaction technique can be measured are obvious:

1. Does the compaction technique produce a specimen which exhibits physical characteristics (appearance, density, and resistance to penetration by binder) which approximate those of crystalline AP?

2. Does the compaction technique produce a specimen with a reproducible deflagration behavior which approaches that of crystalline AP?

Upon removal from the hydraulic press, the compacted AP specimen, a one-inch diameter disc approximately 50 mils in thickness, varied slightly in physical appearance. Some samples were transparent after pressing, but the majority were translucent; however, the transparent samples became translucent after storage. Large polycrystalline discs and smaller laminated sandwiches appeared to be macroscopically homogeneous, but as can be seen in the scanning electron microscope micrographs [48], Figure 26, individual grain boundaries and voids between the compacted AP particles are evident. The surface finish of the compacted AP disc was moderately smooth, the surface roughness generally ranging less than one micron as determined microscopically with a General Electric surface comparator. The final compacted density (calculated) of a large number of samples ranged from 1.862 gm/cm^3 to 1.922 gm/cm^3, which is approximately 97 $\pm$ 1 per cent of crystalline density. Compacted AP discs were thermally baked at 72 $^{\circ}C$ for a 96 hour period to determine if any sample degradation might occur during

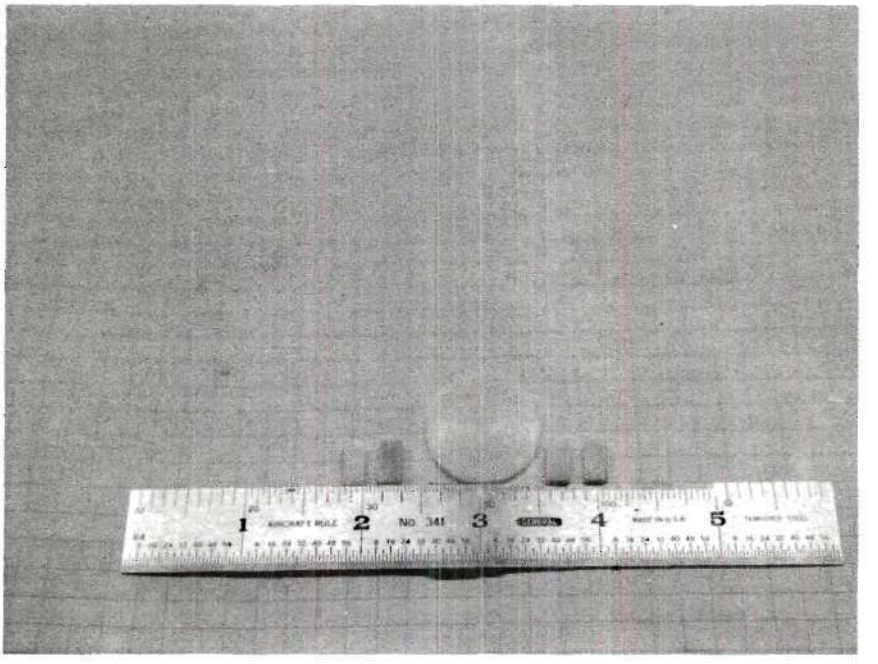

(a) Compacted Disc and Propellant Sandwiches.

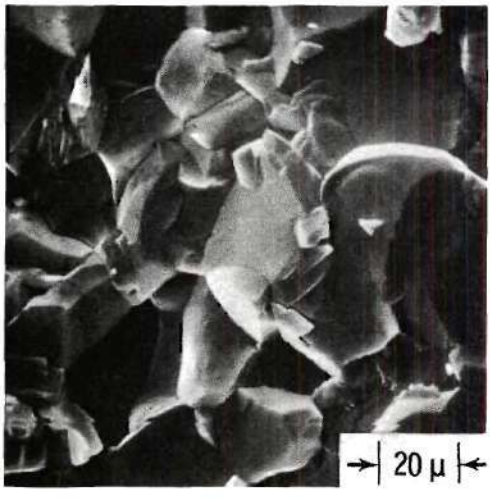

(b) Scanning Electron Microscope Micrograph of Unreacted Disc.

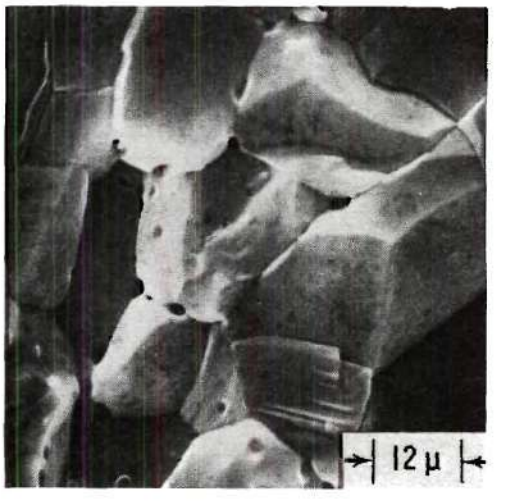

(c) Scanning Electron Microscope Micrograph Showing Individual Grain Boundaries.

Figure 26. Compacted Polycrystalline AP.

the binder curing cycle. No changes in specimen mass or physical dimensions were observed, although the disc was less translucent after the bake cycle (the sample shown in Figure 26 has been subjected to the thermal bake cycle).

Several AP discs were laminated with the propellant binders used in this investigation and cured according to the specified cycles. Peel tests made on several of the cured samples indicated good bonding between binder and disc, and that a uniform binder layer had been achieved. Sandwich samples microscopically viewed "edge on" did not show any binder permeation into the AP disc surface; the sandwich combustion results discussed later support this finding.

The deflagration rate versus pressure data for polycrystalline AP prepared in this laboratory and pure, single crystal AP are presented in Figure 27. The agreement between the polycrystalline pressed samples and the Naval Weapons Center single crystals is quite good considering the difference in sample preparation and physical characteristics.

The surface characteristics of pure AP single crystals thermally quenched during deflagration in a nitrogen atmosphere are well documented over a pressure range of 300 to 6200 psia [11]. Recently, Boggs and Zurn [48] [49] have investigated the surface characteristics of polycrystalline AP specimens prepared by this laboratory over a pressure range of 400 to 4800 psia using the same techniques as used in the single crystal combustion investigations. The surface structure of the polycrystalline samples is remarkably similar to the surface of single

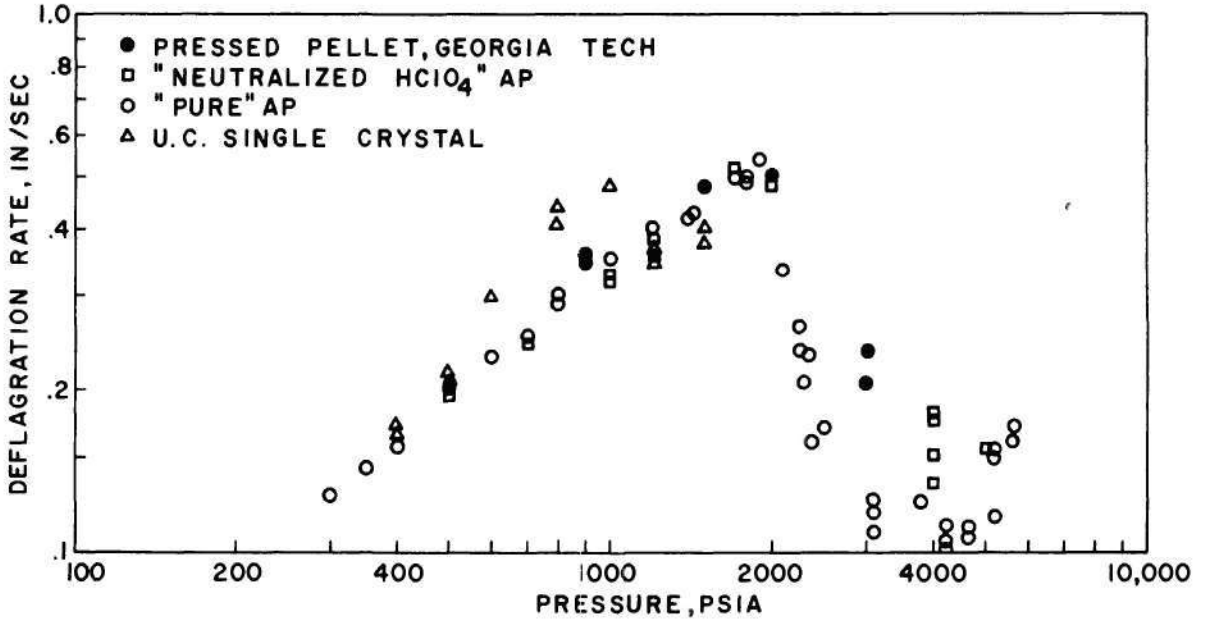

Figure 27. Deflagration Rate Behavior of Polycrystalline and Single Crystal AP.

crystals quenched at all pressure levels. The froth and bubble-like formations, characteristic of pure AP deflagrating at low pressures, are evident for polycrystalline AP samples thermally quenched at 400 psia, Figure 28, and 600 psia, Figure 29. A polycrystalline sample quenched at 1200 psia, Figure 30, displays a pattern of ridges and valleys characteristic of AP deflagration between 1000 psia and 2000 psia. The subsurface structure of a specimen quenched at 4800 psia, Figure 31, exhibits the intricate layer of needles typical of pure AP deflagrating at elevated pressures. Since the surface structures of polycrystalline and single crystal AP deflagration samples are almost identical, the agreement of the burning rate data between the two systems is not surprising. The results indicate that the deflagration behavior of polycrystalline AP duplicates single crystal behavior remarkably well.

Sandwiches prepared using both polycrystalline and single crystal AP were burned and quenched at 300 psig and the results compared. Primary attention was given to the interfacial details for evidence of binder permeation into the polycrystalline surface during curing. The sandwich profiles, Figure 32, were similar and preferential regression was not observed to occur along the interfacial region. The surface features of the quenched sandwiches exhibit the bubble and froth pattern typical of AP deflagration. The oxidizer surface near the interfacial region appears to be affected to the same extent by the binder melt in both cases. PS sandwiches prepared with both pressed and single crystal AP were also quenched at 1000 psig and were in good

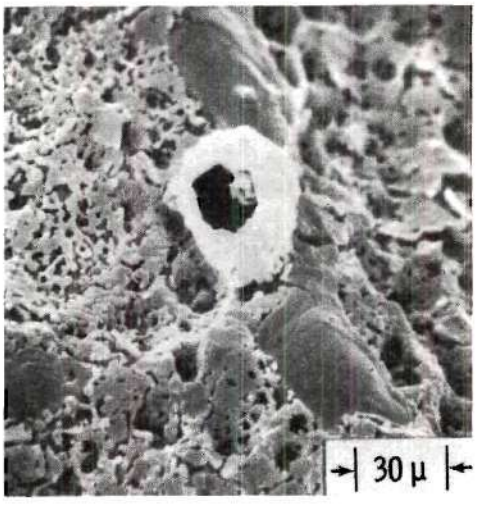

(a) Bubble and Froth Formation.

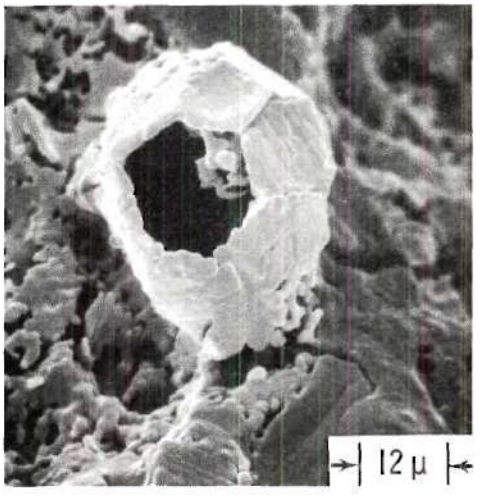

(b) Details of Large Bubble.

Figure 28. Surface Characteristics of Polycrystalline AP Burned and Quenched at 400 psia.

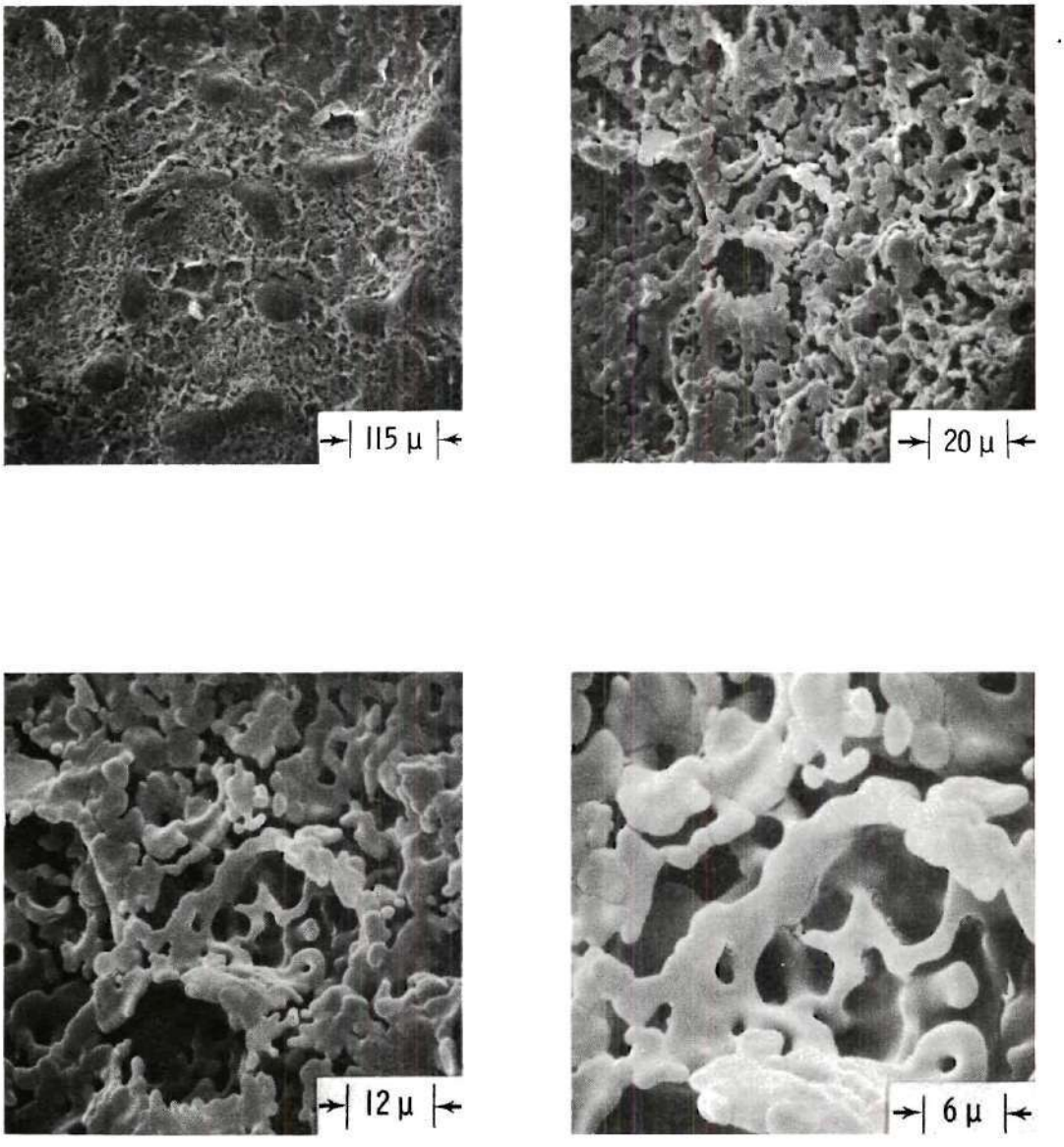

Figure 29. Surface Characteristics of Polycrystalline AP Burned and Quenched at 600 psia.

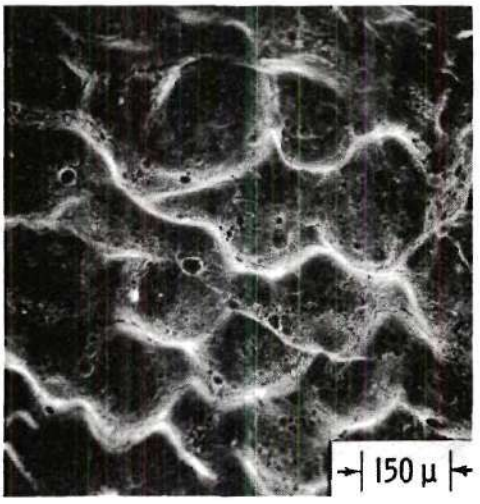

(a) Pattern of Ridges and Valleys.

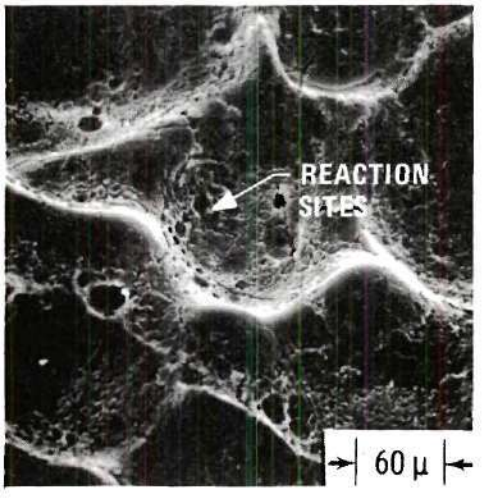

(b) Reaction Sites on Valley Floor.

Figure 30. Surface Characteristics of Polycrystalline AP Burned and Quenched at 1200 psia.

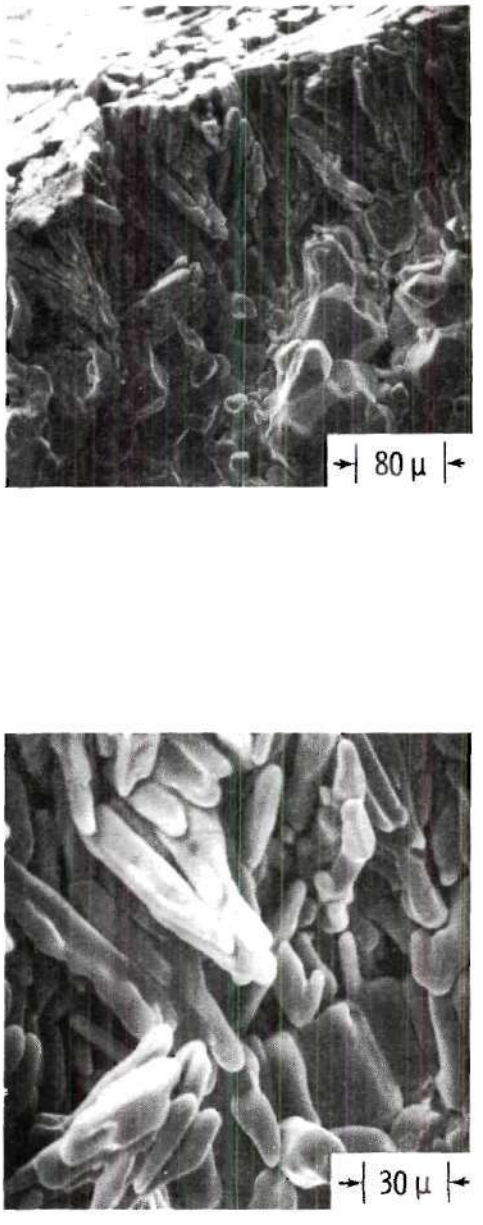

Figure 31. Subsurface Structure of Polycrystalline AP Burned and Quenched at 4800 psia.

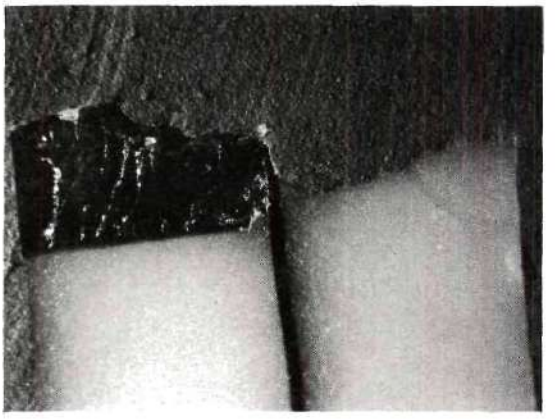

(a) Sandwich Profile (Crystal).

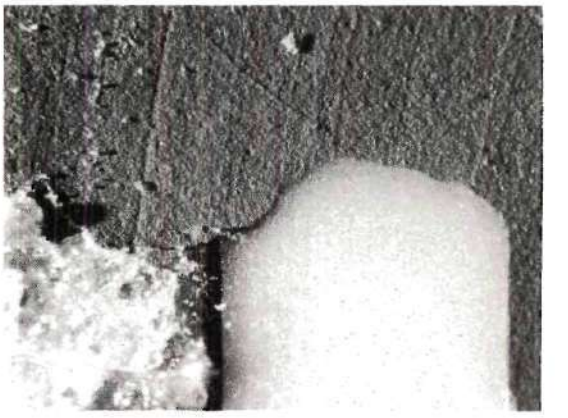

(b) Sandwich Profile (Pollycrystalline).

(c) Sandwich Surface (Crystal).

(d) Sandwich Surface (Polycrystalline).

Figure 32. Polycrystalline and Single Crystal PS Sandwiches Burned and Quenched at 300 psig.

agreement. Because the deflagration behavior of polycrystalline AP duplicated single crystal behavior well and no evidence of interfacial fuel-oxidizer penetration during cure was observed, it was concluded that nothing significant could be obtained by an extensive comparison between polycrystalline and single crystal sandwich characteristics; therefore, the remainder of the investigation would be conducted using polycrystalline AP.

Attainment of Steady State and Quenching Reliability

In order to determine if a steady state was in fact achieved, sandwiches were ignited at several pressure levels and the combustion time varied. At least three different tests were conducted at 300, 600, and 1000 psig using PS and PBAA sandwiches. Combustion mass losses were observed to lie between 30 per cent and 90 per cent of the original mass. The sandwich profiles were observed to be qualitatively the same for all burn durations at pressure levels of 600 and 1000 psig. The profiles at 300 psig were generally different and indicate that a steady AP deflagration is not achieved. The mass burning data correlation is less clear. An average mass loss rate was determined using the sample mass loss and the burn time. Since the sandwich dimensions were similar, the average mass loss rate was initialized with respect to the original mass to facilitate run to run burning rate comparison. These results are shown in Table 3.

The results indicate that a steady burning state is probably achieved, but are not conclusive. Burning rates obtained using high speed motion pictures are recommended to accurately determine the

Table 3. Sandwich Steady State Determination

Binder	Pressure (psig)	Original Mass (gm)	Mass Loss (gm)	Mass Burned (per cent)	Burn Time (sec)	Average Mass Loss Rate ($\frac{gm/gm}{sec}$)
PBAA	300*	0.3410	0.2070	61	1.5	0.41
	300	0.3696	0.1342	36	2.3	0.16
	300	0.2912	0.0919	32	2.7	0.12
	600	0.3902	0.1561	40	0.75	0.53
	600	0.4212	0.3836	91	1.5	0.61
	600	0.4138	0.3200	78	1.5	0.52
	1000	0.2872	0.1868	65	0.5	1.3
	1000*	0.3050	0.2145	70	0.75	0.94
	1000	0.2237	0.2092	94	1.0	0.94
PS	300	0.3150	0.1730	55	1.5	0.37
	300	0.3405	0.1775	52	1.5	0.35
	300*	0.2885	0.1705	59	1.5	0.39
	600	0.4475	0.2168	48	1.0	0.48
	600	0.3371	0.2043	61	1.0	0.61
	600	0.3877	0.3674	95	1.5	0.63
	1000	0.3835	0.2460	64	0.75	0.85
	1000	0.4190	0.3287	79	0.75	1.05
	1000	0.3976	0.3818	96	1.0	0.96

NOTE: *Sandwich prepared with single crystal

sandwich regression history.

Early investigators [50] [51] [52] have demonstrated that a burning solid propellant can be reliably quenched by depressurizing the combustion chamber at a rate which is fast enough to arrest the rate limiting step in the combustion process. Experimentally determined depressurization rates [50] for successful propellant extinction vary between 50,000 psi per second at 400 psi to 250,000 psi per second at 1500 psi. Depressurization rates using the NWC version of the quenching device used in this investigation have been measured and found to be in the range of 10^4 to 10^6 psi per second [39]. The mechanical depressurization device, Figure 18, is similar to the NWC device and was used for quench combustion tests up to and including pressures of 1000 psig. The mylar diaphragm device, Figure 19, was used to extend the combustion pressure-quench range to 2400 psig. The depressurization rates of this device were not measured, but redundant tests were conducted at 600 psig and 1000 psig using both quenching devices to establish quenching similarity. The quenched samples obtained using the mylar device (Figure 33a and c) reproduce the results obtained using the mechanical mechanism (Figure 33b and d), both in surface detail and observed experimental burning rate. The mylar evaluation results and a schematic of the mylar quenching device are presented in Appendix G.

Experimental Error in Mass Loss Data

The mass loss data generated during the quench combustion study were used to calculate an average sandwich regression mass flux for comparison with pure AP deflagration characteristics. The calculated

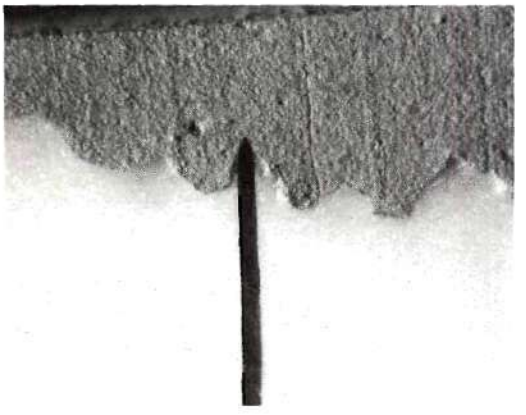

(a) PBAA Sandwich (Mylar).

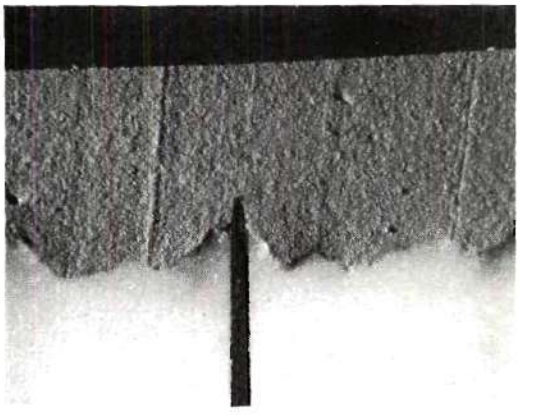

(b) PBAA Sandwich (Mechanical).

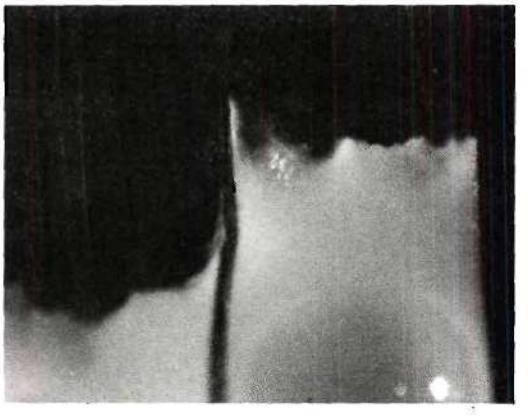

(c) CTPB Sandwich (Mylar).

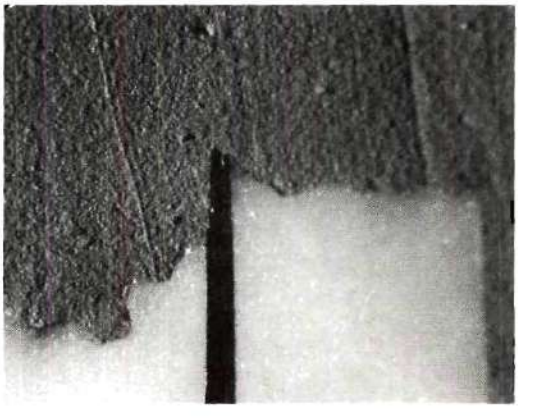

(d) CTPB Sandwich (Mechanical).

Figure 33. Comparison of Redundant Quenching Results Using The Mechanical and Mylar Devices for Sandwiches Burned and Quenched at 600 psig.

flux was based on the experimental mass loss data, sample burn time, and a sandwich regression area calculated from the quenched profiles.

The mass loss data were based on actual sample weighings before and after combustion. The possibility that the sudden depressurization process used to quench the combustion might entrain an appreciable portion of the sandwich surface was considered. Two observations tend to indicate that no appreciable mass loss can be attributed to the quench process:

1. The surface details of the quenched sandwich surface displayed the same characteristics as deflagrating AP quenched using a heat sink device [11].

2. Microscopic examination of the quenched samples never revealed any large scale surface irregularities which would be indicated if portions of the sandwich were being ripped off during quench.

A possible error in the sample burn time was introduced by the efficiency in which ignition and quenching were achieved. Sample ignition with a single strand nichrome hot wire and quenching with the mechanical device previously discussed have been investigated using high speed photography and were found to be very effective [39]. Although excellent sample quenching was achieved using the mylar diaphragm technique, a time lag between the cam timer signal and the actual mylar rupture was observed. To determine the magnitude of this time lag, a dual beam oscilloscope was wired into the quench electrical circuitry in conjunction with a B&K condenser microphone and microphone amplifier. The oscilloscope sweep was triggered automatically by the

cam timer quench signal and the quenching event was recorded with the B&K microphone. Runs were made at 300 psig and 2000 psig with the same number of mylar discs as used in the quench combustion program. The results shown in Figure 34 indicate that a time lag of 225 ± 5 milliseconds existed between timer activation and mylar rupture. The error in using an uncorrected burn time would be considerable at high pressures since the total burn program only requires 250 milliseconds. The corrected burn time based on the cam timer signal and mylar delay introduces an error of ±3 per cent in the mass flux calculations.

Errors are encountered in determining the sandwich regression area because of the uneven surface topology of the quenched sandwich and variations in sandwich size. The sandwich thickness was determined with a micrometer to one ten-thousandth of an inch, but the sandwich width was determined by a template used to cut sandwiches from the larger propellant disc. The pre-cut sandwich width indicated by the disc template was 0.5 cm, but the "cut" dimension varied between 0.35 cm and 0.45 cm. The surface topology and final sandwich width errors tend to compensate, but, nevertheless, an uncertainty of ±13 per cent is involved. To facilitate calculations, the mass flux area was based on a sandwich width of 0.40 cm and the measured sandwich thickness. The uncertainty involved in the mass flux calculations, therefore, varies from ±13 per cent at low pressures to ±16 per cent at high pressures.

Results

Character of the Quenched Sandwich Surface

Prior to encapsulating the propellant sandwich, the quenched

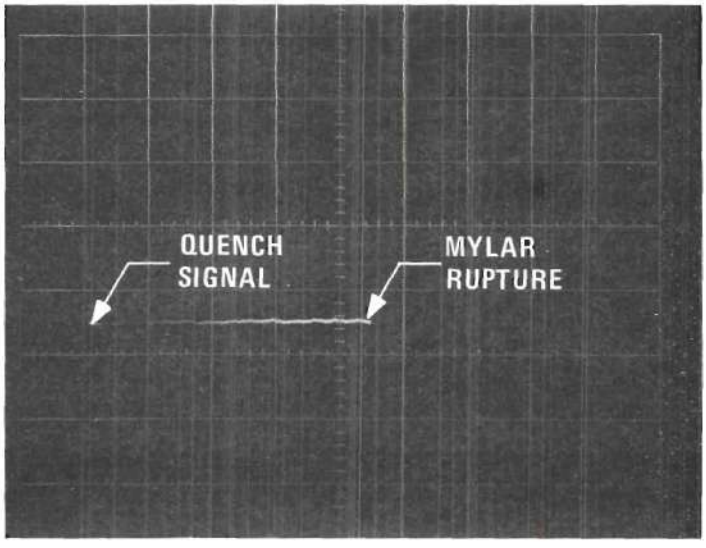

(a) Rupture at 300 psig.

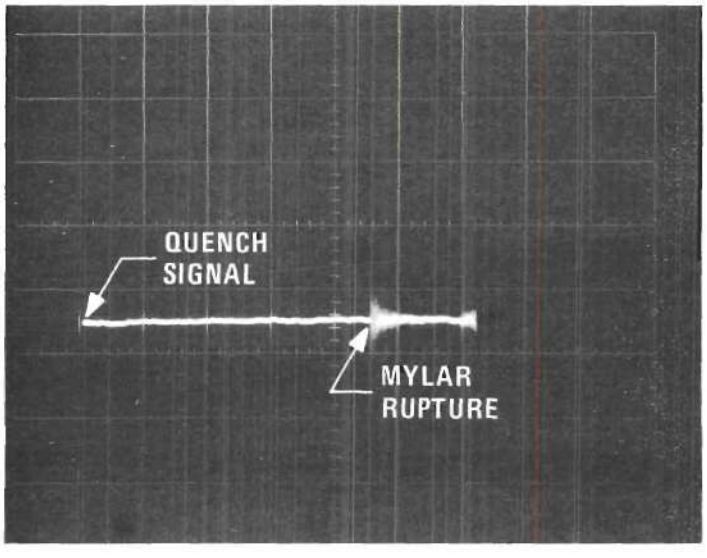

(b) Rupture at 2000 psig.

Figure 34. Mylar Diaphragm Rupture Time Delay.

samples were microscopically examined using various types of illumination to reveal the character of the burned surface. The surface characteristics were carefully noted and documented with photomicrographs for comparison with the surface characteristics of AP self-deflagrating at the same pressure level. Particular attention was given to the evidence and extent of binder melts forming on the sandwich surface.

The surface pattern of the quenched propellant sandwiches generally exhibited the pressure dependent characteristics observed for the deflagration of AP, particularly for sandwiches constructed with thin binder lamination layers. Binder melts were observed to exist on the AP surface for all binder types investigated at every combustion pressure level.

Several comments relevant to better understanding the presentation of the quenched sandwich details are now given. During the data presentation, the terms binder lamination layer, binder melt, and carbonaceous residue are frequently used; these items are indicated on Figures 35 and 36, but have been omitted on the remaining figures for the sake of clarity. Other pertinent comments have been placed on some figures to indicate details referred to in the text. Also, the binder lamination layer has been located near the lower border of the photomicrograph in the section pertaining to the surface details; this orientation should assist the reader in noting the details presented in the discussion of the data. During the reproduction of this thesis, it was necessary to reduce the photomicrographs to facilitate data presentation. The approximate magnification shown in the figure

captions represents the magnification of the photomicrograph before reduction. If scaling from the photomicrographs is to be employed, the following reductions must be considered: 50 per cent for Figures 39, 42f, and 50d and 40 per cent for the remaining figures (except Figure 45, which has not been reduced).

Burned Surface, 300 psig. The polycrystalline and pure crystal PS sandwiches, Figures 35a and 35b, exhibit a bubble and froth pattern typical of AP self-deflagration at low pressures over a major portion of the sandwich surface. Adjacent to the oxidizer-binder interface, the oxidizer surface is covered with a molten binder layer which extends for approximately 100 microns. The typical froth and bubble pattern does not extend into the surface region covered by the binder melt, but diminishes rather abruptly as the affected region is approached. The AP surface far from the binder was very clean, with a few dark specks of carbonaceous residue being observed.

Effects of a PBAA melt, shown in Figure 35c, are far reaching and can be seen extending for approximately 300 microns from the oxidizer-binder interface. AP surface decomposition is occurring in localized regions which are predominately aligned with but displaced from the interface. The oxidizer surface near the binder interface is coated with a very heavy molten layer of binder which can be seen to possess large cracks. These cracks appear as a fractured surface layer and may be the result of the quenching process. The implication that the binder is flowing over the oxidizer surface is enforced. The inclined oxidizer surfaces on the outer portion of the sandwich are coated with a fine,

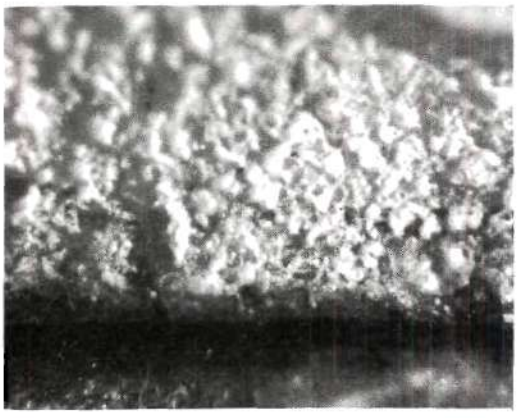

(a) PS (Crystal) Sandwich (60X).

(b) PS Sandwich (60X).

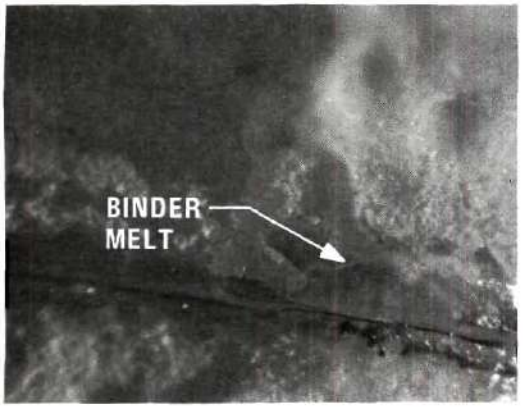

(c) PBAA Sandwich (60X).

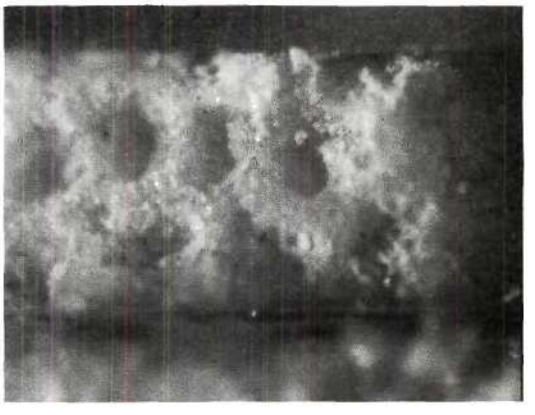

(d) CTPB Sandwich (60X).

Figure 35. Burned Surface of Sandwiches Quenched at 300 psig.

brownish residue which extends along the surface for approximately 600 microns.

The oxidizer surface of the CTPB sandwich, Figure 35d, exhibited large craters which were typically 200 microns wide and 50 microns deep. The oxidizer surface within 300 microns of the binder interface was lightly coated with a brown, misty residue. The brown surface coating was also observed on the walls and floors of the craters in this region indicating that the craters were present during combustion and were not produced by the quenching process.

Burned Surface, 600 psig. The oxidizer surface of a PS sandwich quenched at 600 psig, Figure 36a, is characterized by numerous 150-300 micron craters. The craters within 250-300 microns of the binder interface were lightly coated with a dark residue. The dark regions in the crater floors are shadows produced by the indirect lighting used to illuminate the samples. A large crater adjacent to the binder is shown in Figure 36b using more direct illumination; note the reaction sites on the walls and the large bubbles on the crater floor. A very dense molten binder layer extended 50-75 microns from the binder interface.

Large craters are also noted on the surface of a PBAA sandwich, Figure 36c. The surface is very dirty, exhibiting a carbonaceous residue which is seen on the crater surfaces. Sandwiches with thin PBAA binder layers (approximately 20 microns) exhibited a very clean oxidizer surface but still possessed the crater-like structure. A molten binder layer was observed to extend for 50-75 microns from the binder interface.

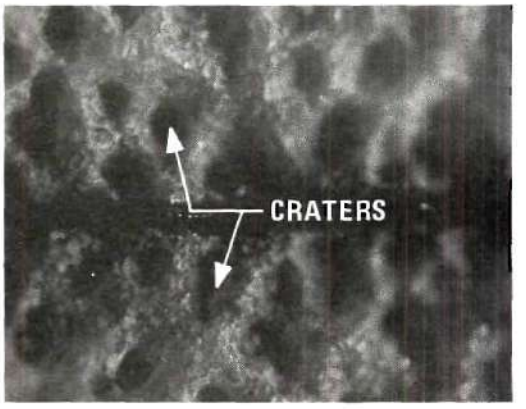

(a) PS Sandwich (40X).

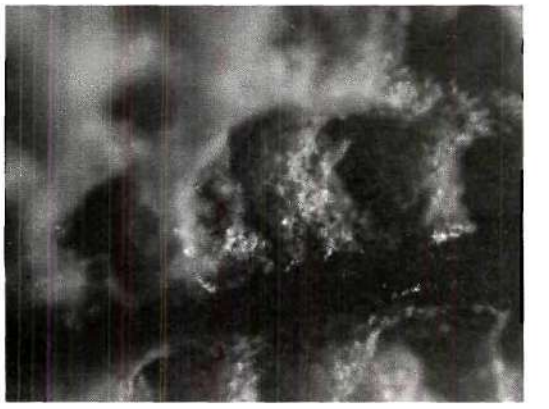

(b) PS Sandwich (60X).

(c) PBAA Sandwich (60X).

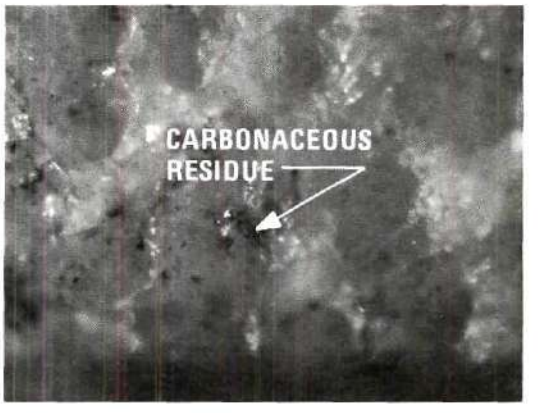

(d) CTPB Sandwich (60X).

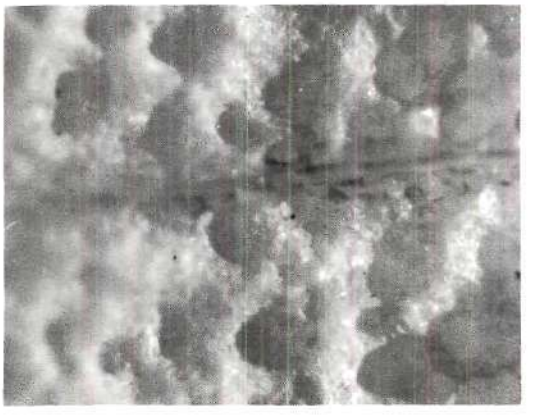

(e) PU Sandwich (40X).

Figure 36. Burned Surface of Sandwiches Quenched at 600 psig.

The CTPB sandwich surface, Figure 36d, is cratered and coated with a very fine glossy residue which extends for 400-500 microns from the binder interface. A heavy carbonaceous residue is superimposed on the residue coating and also extends to the outer portion of the sandwich (approximately 1200 microns). A very dense melt exists adjacent to binder interface extending only 25-50 microns, but could possibly extend for 400-500 microns if the glossy surface residue observed were in fact a thin melt layer.

The oxidizer surface of the PU sandwich, Figure 36e, possesses the cratered surface similar to the other 600 psig quenched samples, but in contrast to the other specimens, the AP surface is very clean except for a light film on some of the crater walls. A light intensity binder melt extends approximately 100 microns from the binder interface.

Burned Surface, 1000 psig. A surface pattern of ridges and valleys (darker portions of surface) is beginning to form on the PS sample shown in Figure 37a. The surface is moderately clean with a few dark specks of carbonaceous residue being observed. A very dense molten binder layer extends for 100-150 microns onto the oxidizer surface where it terminates rather abruptly.

The PBAA sample surface shown in Figure 37b exhibits an emergent pattern of ridges and valleys similar to the PS sandwich, although the surface is considerably more contaminated with a carbonaceous residue. The oxidizer surface adjacent to the binder is covered with a dense melt for approximately 150 microns.

The surface pattern for CTPB and PU, Figures 37c and 37d,

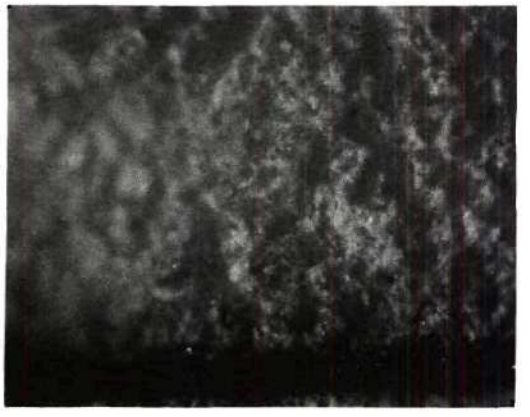

(a) PS Sandwich (60X).

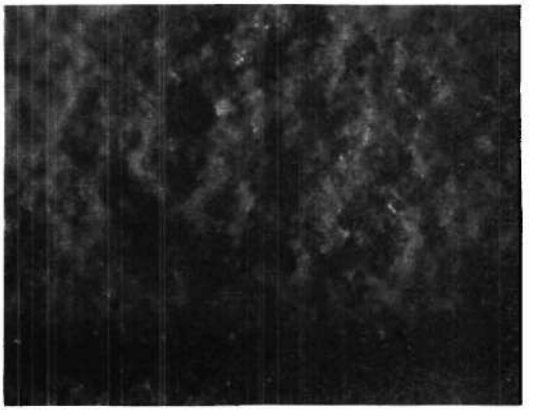

(b) PBAA Sandwich (60X).

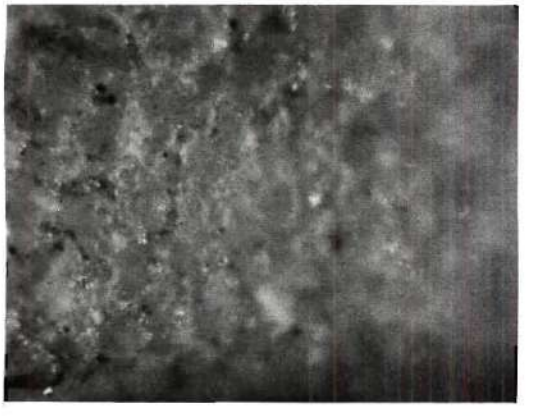

(c) CTPB Sandwich (60X).

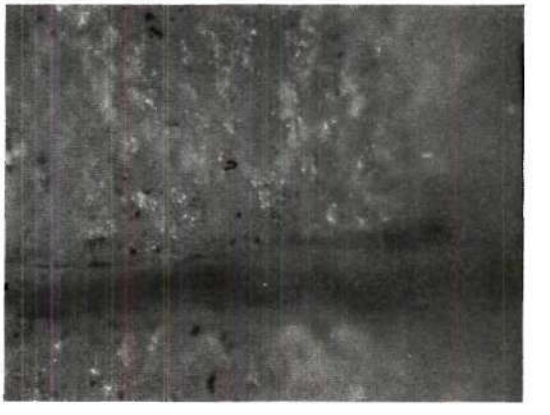

(d) PU Sandwich (60X).

Figure 37. Burned Surface of Sandwiches Quenched at 1000 psig.

respectively, is a poorly defined pattern of ridges and valleys with both surfaces being rather heavily contaminated with carbonaceous residue. Both sandwiches show a very narrow molten binder region extending 50-75 microns from the binder interface.

Burned Surface, 1500 psig. The surface of the PS, PBAA, and CTPB sandwiches, Figures 38a, 38b, and 38c, respectively, is a well defined pattern of ridges and valleys and is very clean except for a few random deposits of carbonaceous residue observed on the CTPB and PBAA sandwiches. Each sandwich possessed a molten binder which extended 75-100 microns onto the oxidizer surface.

The PU sandwich surface, Figure 38d, is very glossy and appears to be coated with thin binder melt extending 250-300 microns from the binder interface. The surface pattern of ridges and valleys is not well formed and seems to be inhibited by the binder coating.

Burned Surface, 2000 psig. The oxidizer surface of the PS sandwich, Figure 39a, is clean with only a few random carbonaceous deposits. The pattern of ridges and valleys is more refined than the 1500 psig surface, but begins to lose its character as the melt region is approached. The binder melt clearly extends for 100-150 microns and affects the oxidizer surface pattern for another 200 microns.

The PBAA surfaces shown in Figures 39b and 39c are for thick (150 microns) and thin (30 microns) binder layers, respectively. The surface pattern of ridges and valleys is common to both specimens, but the carbonaceous residue contamination is considerably more dense and farther reaching on the surface of the thicker binder layer sample.

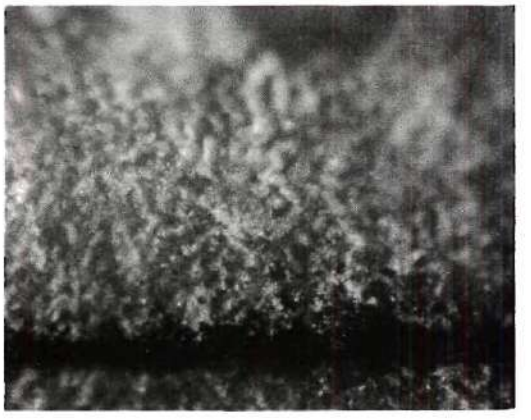

(a) PS Sandwich (60X).

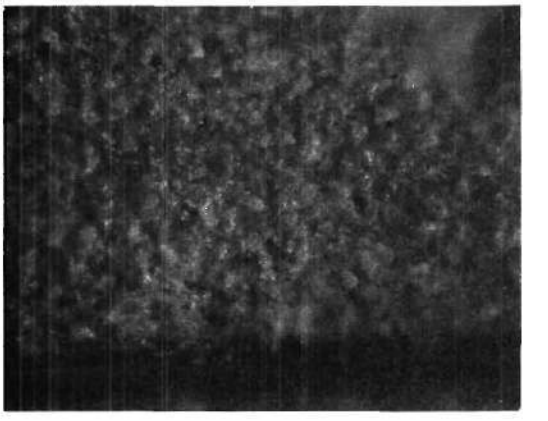

(b) PBAA Sandwich (60X).

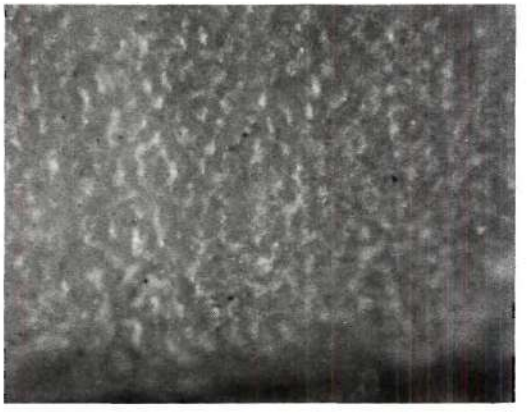

(c) CTPB Sandwich (60X).

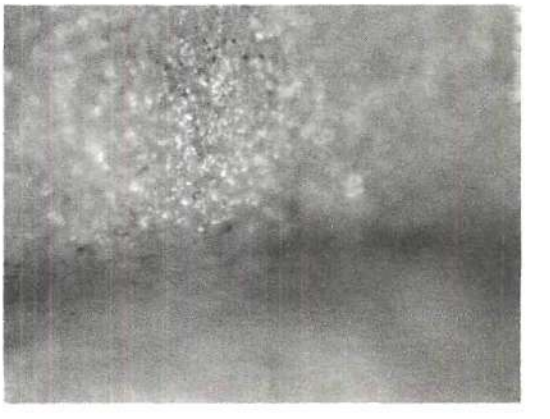

(d) PU Sandwich (60X).

Figure 38. Burned Surface of Sandwiches Quenched at 1500 psig.

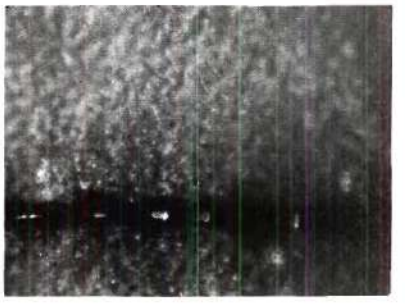

(a) PS Sandwich (60X).

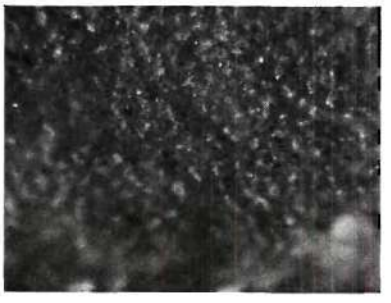

(b) PBAA Sandwich (60X).

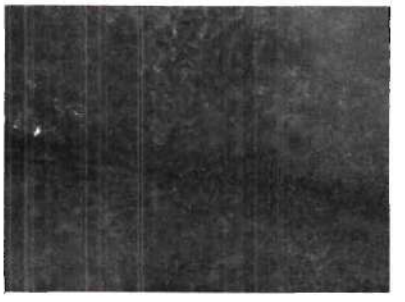

(c) PBAA Sandwich (60X).

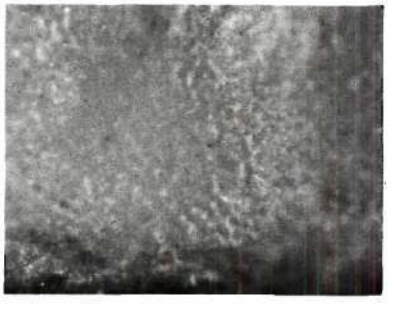

(d) CTPB Sandwich (60X).

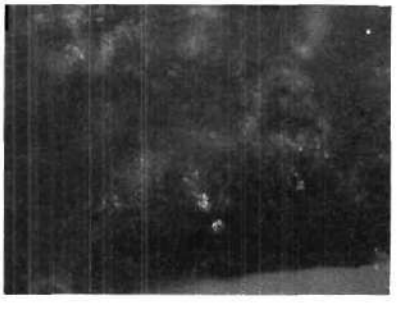

(e) CTPB Sandwich (200X).

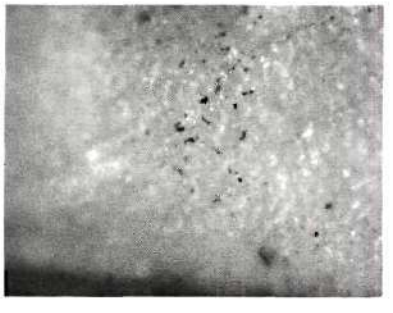

(f) PU Sandwich (60X).

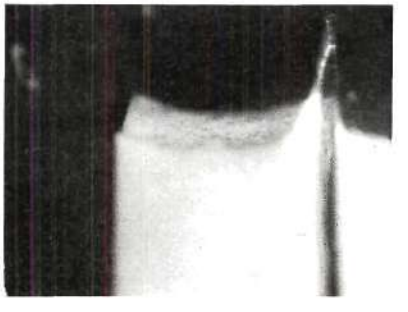

(g) PU Sandwich (60X).

Figure 39. Burned Surface of Sandwiches Quenched at 2000 psig.

Both samples exhibited a binder melt which extended 75-100 microns onto the oxidizer surface.

The CTPB surface, Figure 39d, did not possess a unified surface pattern, but rather was composed of regions of ridges and valleys and regions in which the ridges were replaced by a more intricate surface pattern. The surface adjacent to the binder layer was quite smooth and was covered by a molten binder layer, Figure 39e, which extended 100-150 microns onto the oxidizer surface.

The surface pattern of ridges and valleys exhibited by the PU sample, Figure 39f, is not well formed and appears to be inhibited by a thin, glossy melt which extends 250-300 microns from the binder interface. The oxidizer is also moderately contaminated with localized regions of carbonaceous residue, Figure 39g.

Burned Surface, 2400 psig. The oxidizer surface of the PS sandwich, Figure 40a, consists of a very tight pattern of ridges and valleys intermingled with regions of localized decomposition sites. The binder melt extends 100-150 microns onto the otherwise clean oxidizer surface.

The surfaces of PBAA and CTPB, Figures 40b and 40c, do not exhibit a uniform pattern, but generally consist of regions of localized decomposition sites with a very fine appearance. A fine binder melt was observed extending 50-75 microns onto the oxidizer surface.

The PU surface, Figure 40d, was typically one of ridges and valleys with no far reaching binder effects observed. The oxidizer surface was clean except for a 25-50 micron region near the binder interface where a fine binder melt was noted.

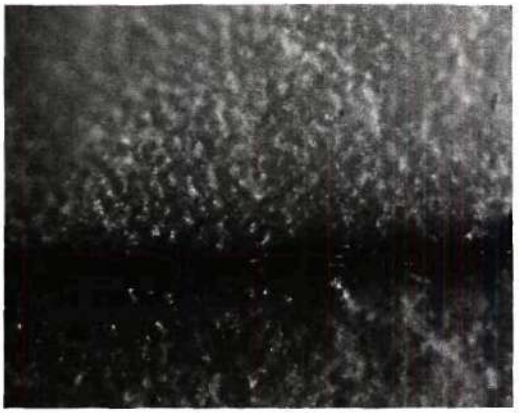

(a) PS Sandwich (60X).

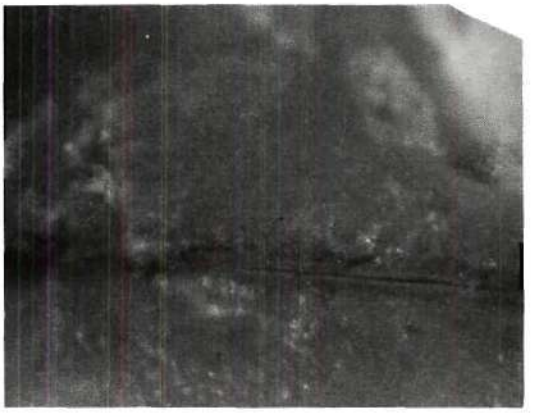

(b) PBAA Sandwich (60X).

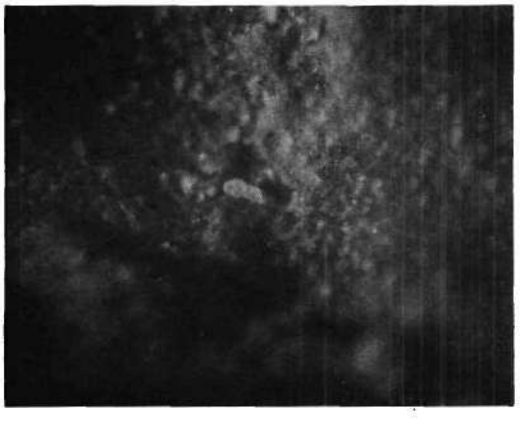

(c) CTPB Sandwich (60X).

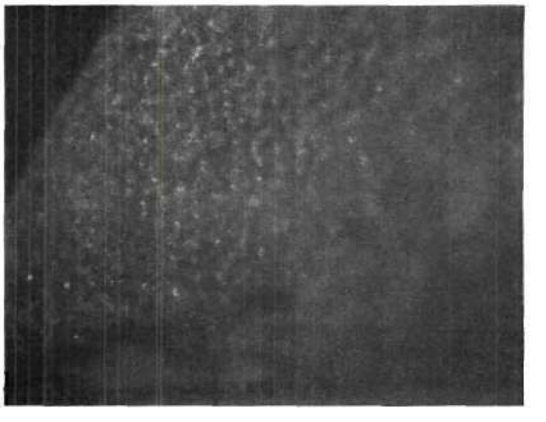

(d) PU Sandwich (60X).

Figure 40. Burned Surface of Sandwiches Quenched at 2400 psig.

Profile of the Quenched Sandwich

Profiles of the quenched propellant sandwiches were studied microscopically utilizing thin slices sectioned normal to the burning surface from sandwich replicas. The characteristics and orientation of the regressing oxidizer surface, binder-oxidizer interfacial details, and the binder regression features were carefully noted and documented with photomicrographs.

The surface profiles of the quenched propellant sandwiches were observed to have several general characteristics which were present over the entire combustion pressure range:

1. The regressing surface at the binder-oxidizer interface possessed a smooth, continuous contour.

2. The region of maximum sandwich regression was observed to occur in the oxidizer for combustion at all pressure levels, including combustion near the AP low pressure deflagration limit.

3. Binder decomposition characteristics were observed to have a pronounced effect on the sandwich profile.

An in-depth discussion of each sandwich profile investigated during this study would very quickly become redundant. The first portion of this section is, therefore, devoted to documenting the significant features of the sandwich profiles over the combustion pressure range. A summary of the quenched sandwich profile details is presented in tabular form at the end of the section.

Surface Profile, 300 psig. Combustion at 300 psig produced a sandwich profile which did not appear to be the result of uniform

deflagration, but was rather one which appeared to be strongly dependent upon the proximity of fuel products to assist the AP deflagration process.

The outer oxidizer faces of the 55 micron PS sandwiches shown in Figures 41a and 41b are sloped toward the binder layer with the leading edge of the regression front occurring approximately 150 microns from the binder interface. The oxidizer adjacent to the binder is regressing at a slower rate than the outer portion producing an inclined oxidizer trailing front which merges smoothly with the binder layer. Both the PS and PU sandwich profiles exhibit an asymmetry about the binder layer which results in one side of the sandwich clearly regressing ahead of the other side. It was not determined if the observed asymmetry was unsteady, moving back and forth over the binder layer, or if the asymmetry was steady with time. No profile differences were observed as a result of varying the binder layer thickness between 35 and 75 microns for PS and 40 to 100 microns for PU.

The PBAA sandwich profile, Figure 41c, is typical of PBAA and CTPB sandwiches with thick binder layers; the binder layer thickness in this sandwich is approximately 200 microns. The outer oxidizer faces are inclined approximately 35 degrees and the oxidizer surface adjacent to the binder is inclined approximately 45 degrees. The details of the interface, Figure 41d, reveal that the leading edge of the regression front is clearly in the oxidizer and is located approximately 40 microns from the binder interface. The observed profiles were symmetric about the binder layer for all binder thicknesses investigated.

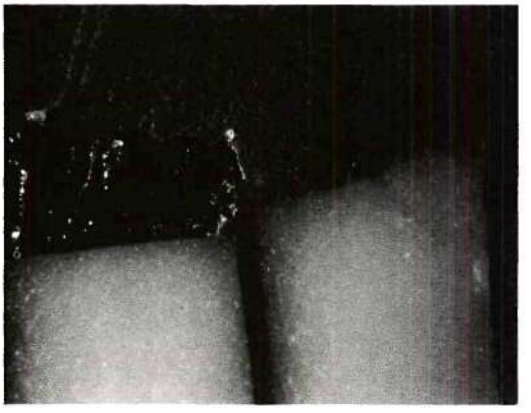

(a) PS (Crystal) Sandwich (40X).

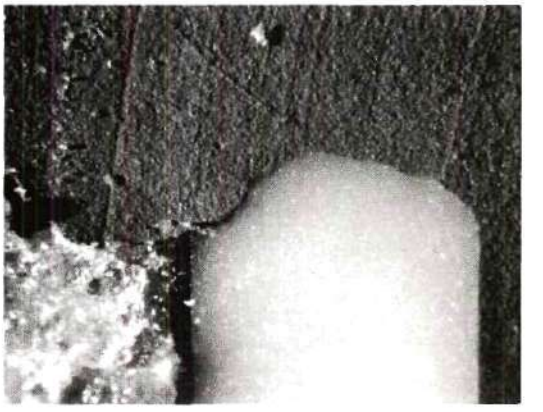

(b) PS Sandwich (40X).

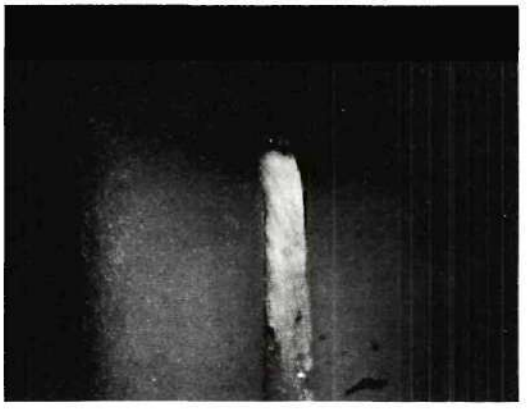

(c) PBAA Sandwich (40X).

(d) PBAA Sandwich (100X).

(e) PBAA Sandwich (60X).

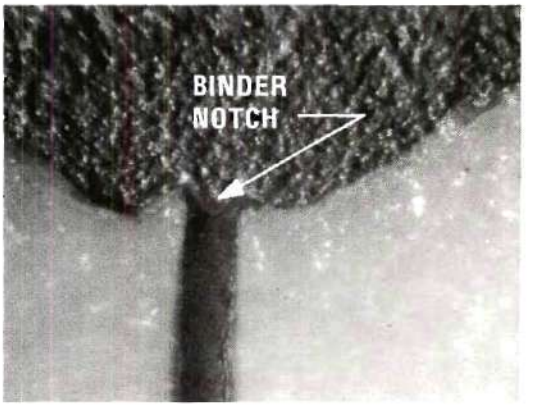

(f) PBAA Sandwich (200X).

Figure 41. Surface Profile of Sandwiches Quenched at 300 psig.

A PBAA sandwich profile for a 50 micron thick binder layer, Figure 41e, exhibited the same qualitative description as that for the thicker binder layers except that a curious binder dip was observed. The binder dip, approximately 30 microns deep, is symmetrical, Figure 41f, and the surface contour is smooth across the interface.

Surface Profile, 600 psig. The oxidizer surfaces generally regressed in a planar fashion exhibiting an upward inclination near the binder interface, the degree of inclination being greater for PBAA and CTPB binders.

The binder peak of the 55 micron PS sandwich, Figures 42a and 42b, is even with the regressing oxidizer surface whereas the binder peak of the 100 micron PBAA sandwich, Figure 42c, extends above the oxidizer surface. The results for PU and CTPB sandwiches are similar to the PBAA sandwiches.

The 25 micron binder PBAA sandwich, Figure 42d, is asymmetrical with respect to the binder layer. Inspection of the interface reveals that the lagging oxidizer surface has a very thin molten layer extending about 60 microns on the adjacent oxidizer surface. Similar asymmetric profiles were observed for thick and thin binder layers in CTPB and PU sandwiches, Figures 42e and 42f, respectively.

The large scale oxidizer surface roughness observed is the result of sectioning the sandwiches through crater locations which are present on the surface of samples burning at 600 psig.

Surface Profile, 1000 psig. The oxidizer surfaces for sandwiches made with thick binder layers (100 microns), Figure 43, regressed in a

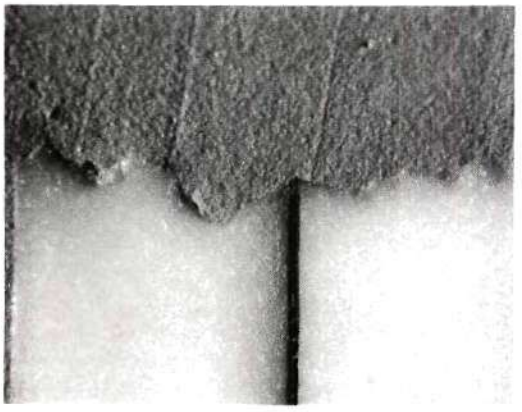

(a) PS Sandwich (40X).

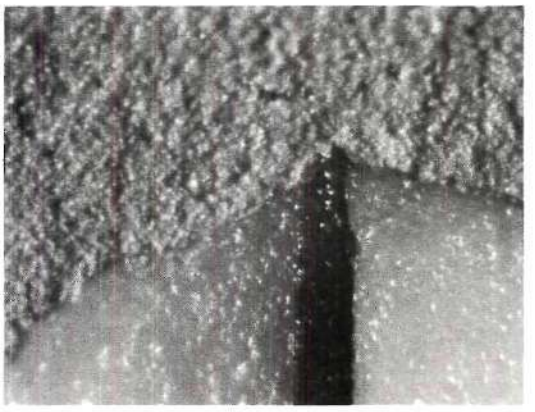

(b) PS Sandwich (200X).

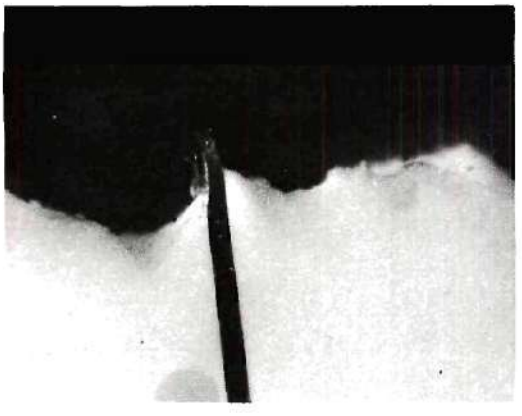

(c) PBAA Sandwich (40X).

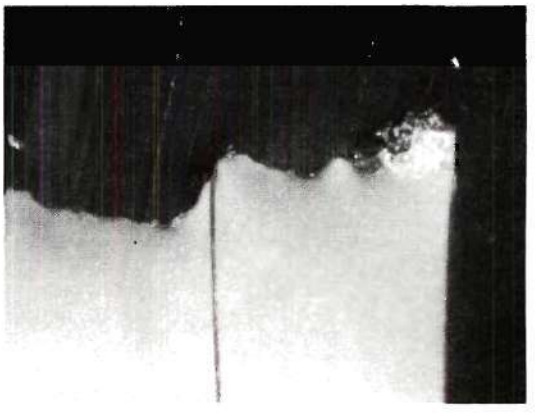

(d) PBAA Sandwich (40X).

(e) CTPB Sandwich (40X).

(f) PU Sandwich (40X).

Figure 42. Surface Profile of Sandwiches Quenched at 600 psig.

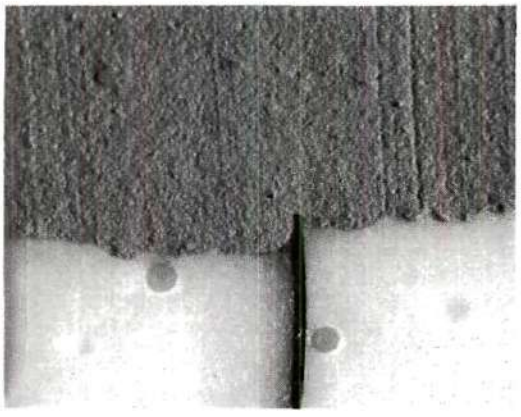

(a) PS Sandwich (40X).

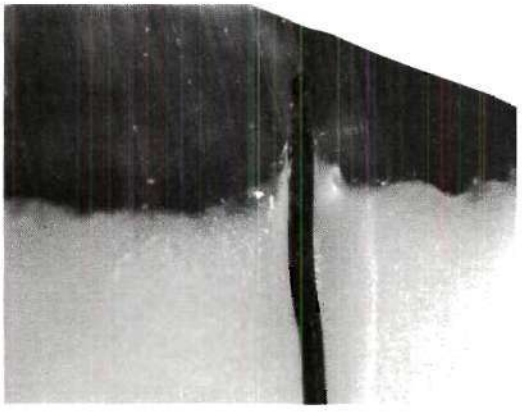

(b) CTPB Sandwich (40X).

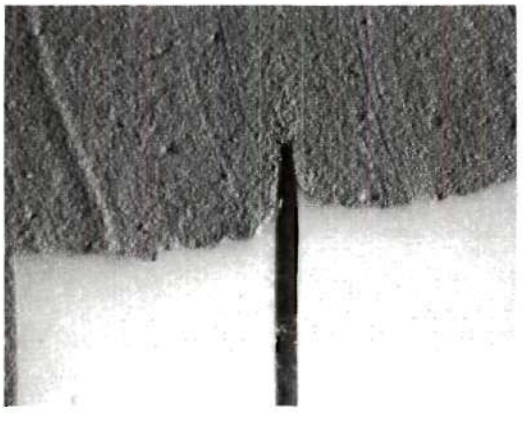

(c) PU Sandwich (40X).

Figure 43. Surface Profile of Sandwiches Quenched at 1000 psig.

planar fashion and were symmetrical with respect to the binder layer. The oxidizer surface becomes inclined upward near the binder interface, the degree of inclination being less for PS than the other binders. The binder peak of the 55 micron PS sandwich, Figure 43a, is even with the oxidizer surface while the binder peaks of the 120 micron CTPB and the 100 micron PU sandwiches, Figures 43b and 43c, respectively, extend above the oxidizer surface approximately 200 microns.

Sandwiches made with CTPB and PU binder thicknesses ranging between 30 and 75 microns also regressed planarly, but with a pronounced asymmetry. The CTPB sandwich, Figure 44a, has a binder thickness of approximately 60 microns and exhibits a stepped regression profile. The oxidizer surface leading the sandwich regression has exposed, and partially decomposed, the adjacent binder while the lagging surface is regressing evenly with the binder "peak." A magnification of the interface, Figure 44b, reveals that the binder "facing" the leading oxidizer surface is half the original binder thickness forming a step approximately 30 microns by 180 microns. The magnification of the interface also indicates that the lagging surface is coated with a thin binder melt which extends about 150 microns onto the oxidizer surface. The profile of a 40 micron binder PU sandwich, Figures 44c and 44d, indicates the same qualitative results.

Thin PS and PBAA sandwiches did not exhibit a pronounced asymmetry, although a 30 micron PBAA sandwich, Figures 44e and 44f, did possess a 10 micron binder dip and also possessed a thin molten layer extending approximately 60 microns onto the oxidizer surface.

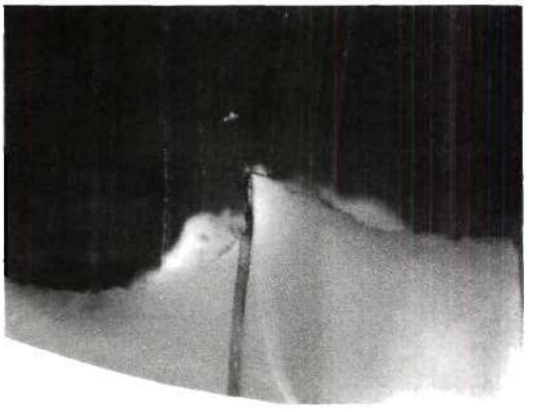

(a) CTPB Sandwich (40X).

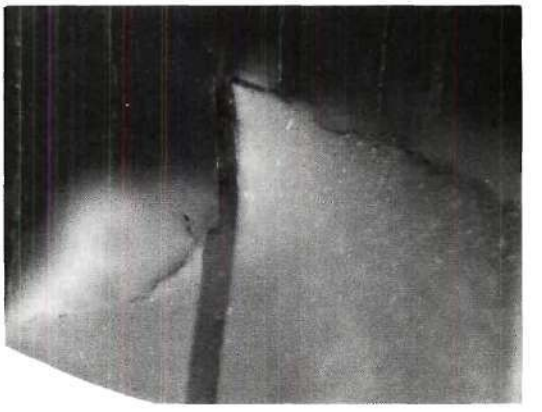

(b) CTPB Sandwich (100X).

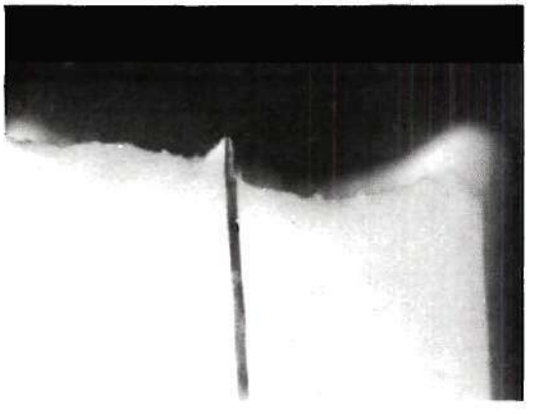

(c) PU Sandwich (40X).

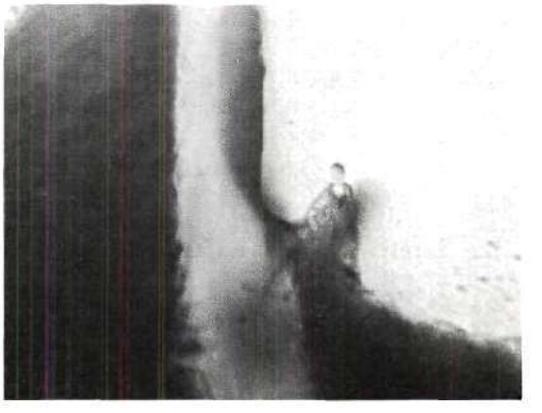

(d) PU Sandwich (400X).

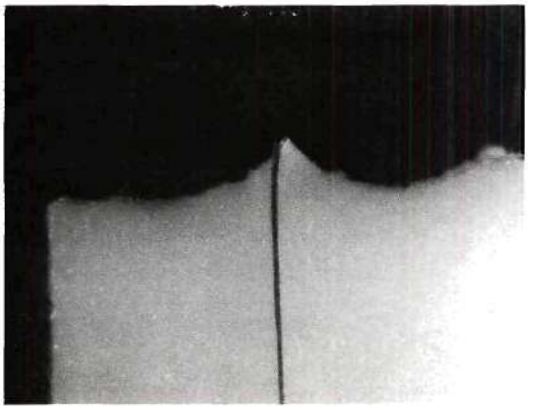

(e) PBAA Sandwich (40X).

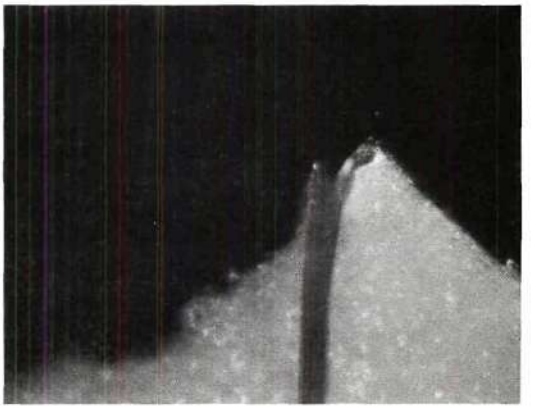

(f) PBAA Sandwich (200X).

Figure 44. Surface Profile of Sandwiches Quenched at 1000 psig.

Surface Profile, 1500 psig. Combustion at 1500 psig produced sandwiches with three distinctly different profile shapes. The oxidizer surfaces appeared to be regressing in a planar fashion for all the samples, but the binder appears to be more important in determining the surface profile in the interfacial region.

The outer surfaces of the 55 micron PS sandwich, Figure 45a, and the 35 micron PS sandwich, Figure 45b, are gently inclined (15 degrees) toward the binder with a well defined region of maximum regression located 100-150 microns from the binder interface. The thicker binder layer slightly lags the adjacent sandwich regression while the thin binder layer is regressing evenly with the nearby oxidizer surface.

The oxidizer surfaces for the 60 micron CTPB sandwich, Figures 46a to 46d, are regressing in a planar fashion with the surface sloping upward rather sharply as the binder is approached. The oxidizer surfaces adjacent to the binder are heavily coated with a melt and carbonaceous residue which extends for 125-150 microns. Figures 46b, 46c, and 46d, successive magnifications of the binder interfacial region, reveal a curious binder formation which has two cusps clearly located within the binder.

Figures 47a and 47b show the asymmetric regression profile for a 200 micron PU sandwich and the binder interfacial details, respectively. Both oxidizer surfaces are planar with a slight inclination near the binder, but one surface is regressing well ahead of the other. Binder decomposition is more complete on the side facing the leading oxidizer surface. The binder peak extends well above both oxidizer surfaces.

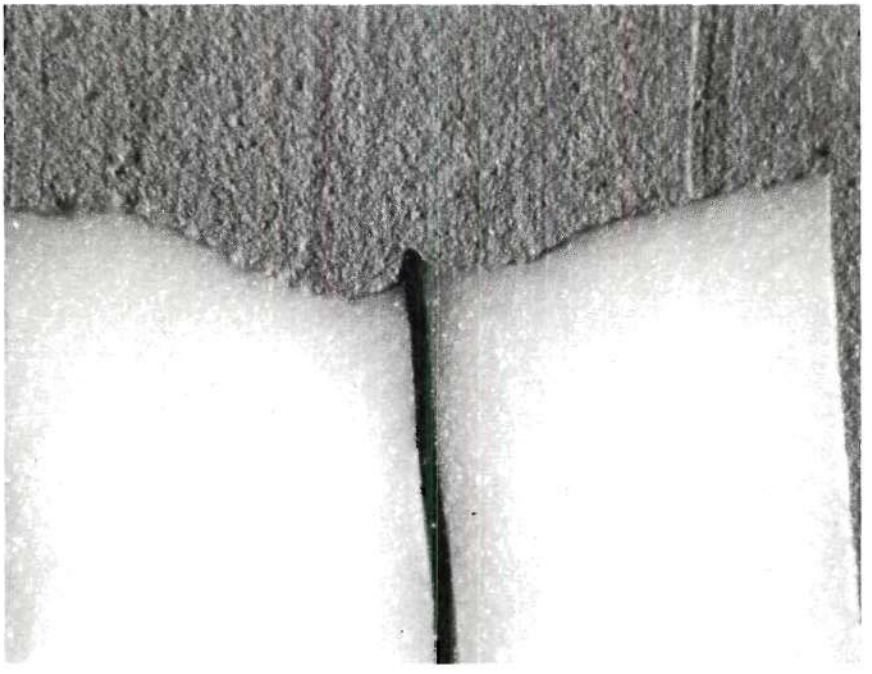

(a) PS Sandwich (40X).

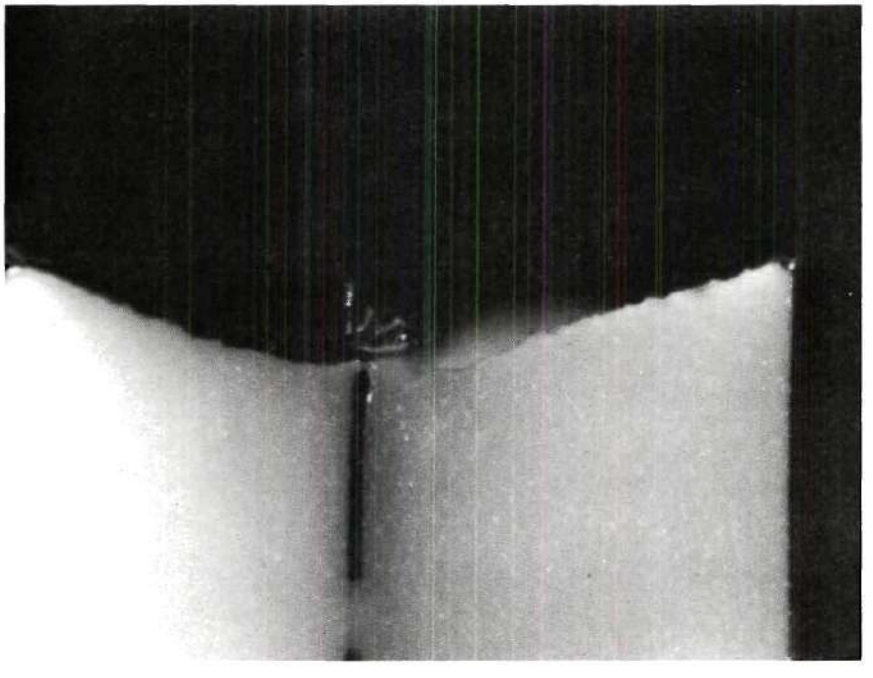

(b) PS Sandwich (40X).

Figure 45. Surface Profile of Sandwiches Quenched at 1500 psig.

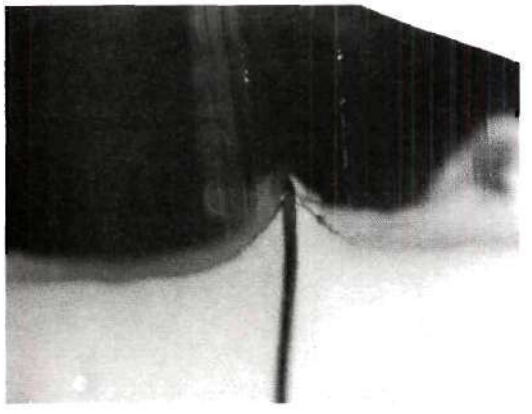

(a) CTPB Sandwich (40X).

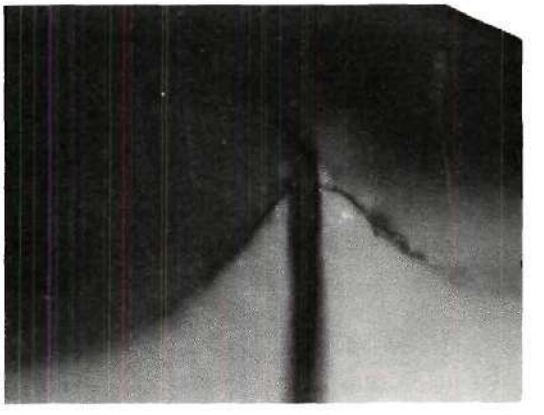

(b) CTPB Sandwich (100X).

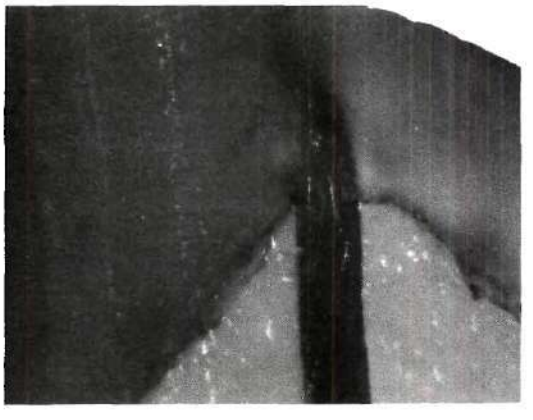

(c) CTPB Sandwich (200X).

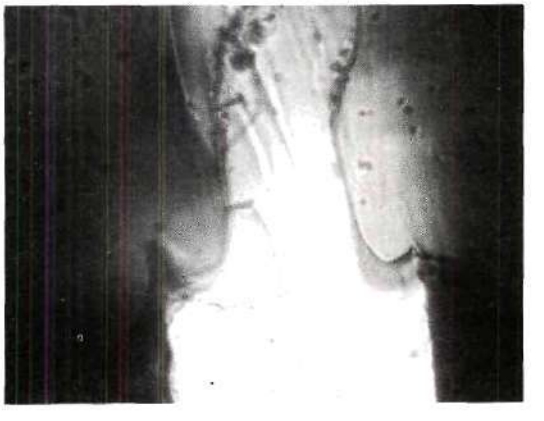

(d) CTPB Sandwich (800X).

Figure 46. Surface Profile of Sandwiches Quenched at 1500 psig.

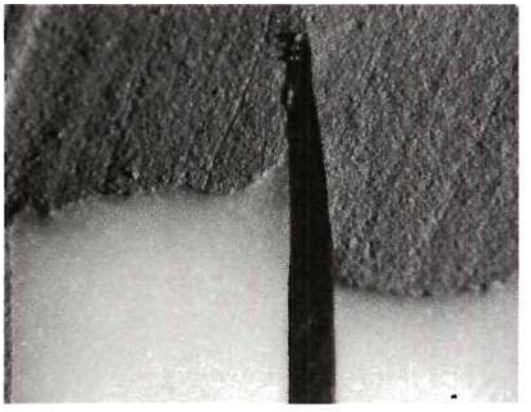

(a) PU Sandwich (40X).

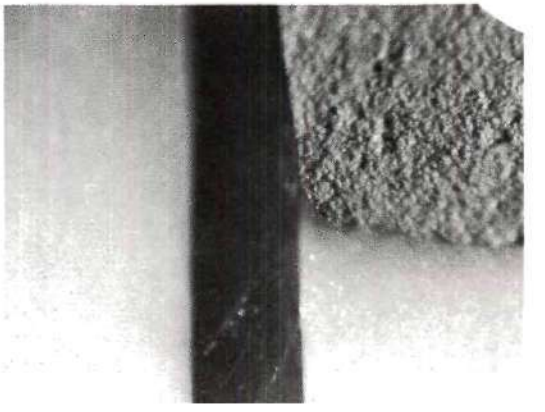

(b) PU Sandwich (100X).

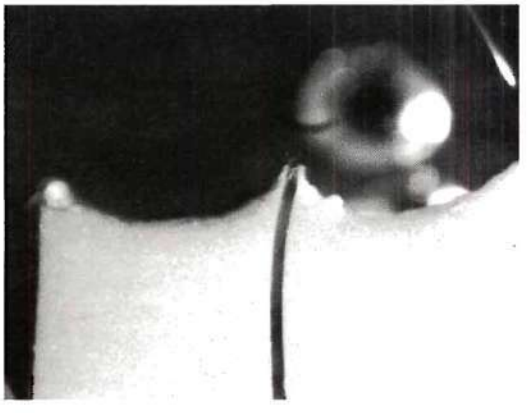

(c) PU Sandwich (40X).

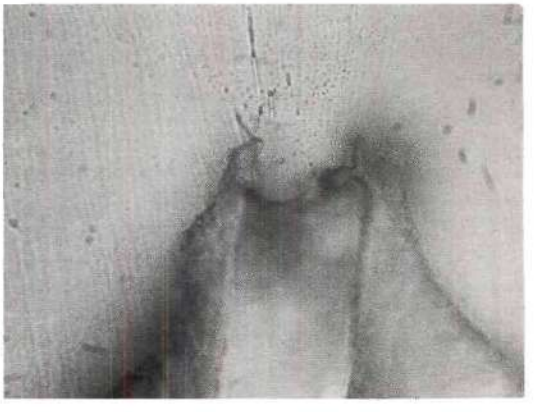

(d) PU Sandwich (400X).

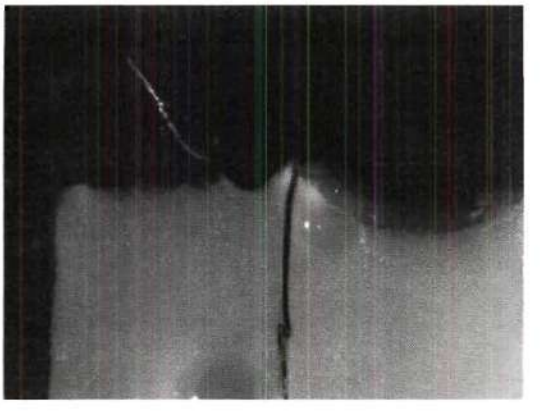

(e) PBAA Sandwich (40X).

Figure 47. Surface Profile of Sandwiches Quenched at 1500 psig.

A 60 micron PU sandwich, Figures 47c and 47d, indicates that the binder surface is regressing evenly with the adjacent oxidizer and that the surface profile is symmetrical. The central portion of the oxidizer surface is regressing in a planar fashion with a slightly increasing slope toward both the binder layer and the outer sandwich edge.

The 25 micron PBAA sandwich, Figure 47e, is slightly asymmetric, exhibiting one planar surface and one gently sloping surface similar to the 60 micron PU sandwich.

Surface Profile, 2000 psig. Oxidizer regression for the 55 micron PS sandwich, Figures 48a and 48b, is planar over the central half (600 microns half-width) of the sandwich with the outer portion of the sandwich slightly inclined upward. The surface remains planar to within 60 microns of the binder interface experiencing a very gentle inclination upward as the binder is approached. The binder extends very slightly above the adjacent oxidizer surface for the 75 micron binder but was observed to be even with the surface for the 35 micron binder thickness.

The surface regression for the 150 micron PBAA sandwich, Figure 48c, is nominally planar with the binder extending well above the oxidizer surface. Inspection of the interfacial details, Figure 48d, reveals a secondary microscopic regression front similar to the profiles observed at low pressures. This front is located near the interface with the leading edge clearly located in the oxidizer.

The 25 micron PBAA sandwich, Figure 48e, indicates that a large plateau of the oxidizer surface adjacent to the binder is regressing

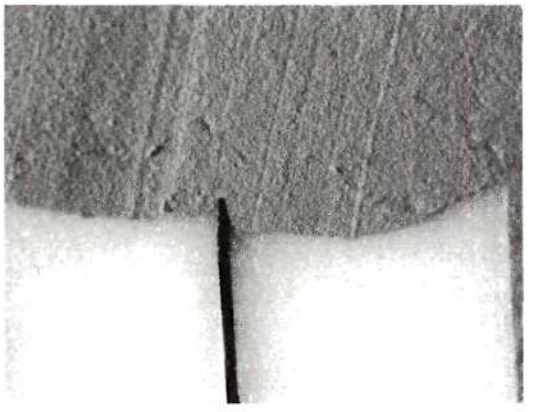

(a) PS Sandwich (40X).

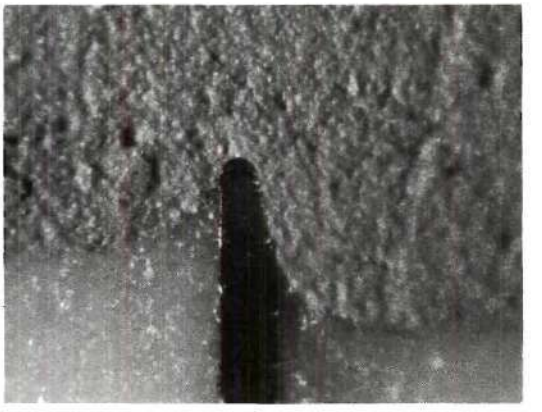

(b) PS Sandwich (200X).

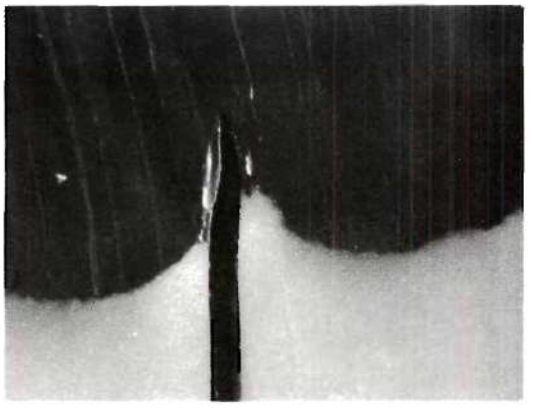

(c) PBAA Sandwich (40X).

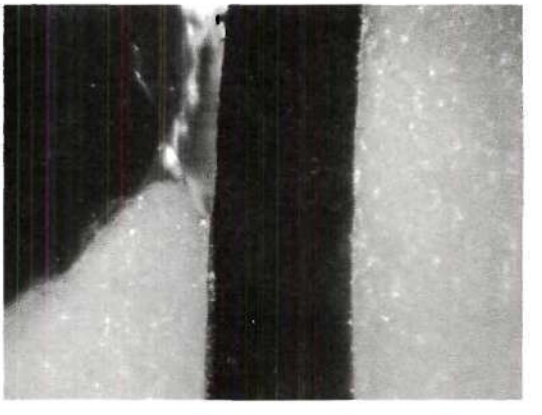

(d) PBAA Sandwich (200X).

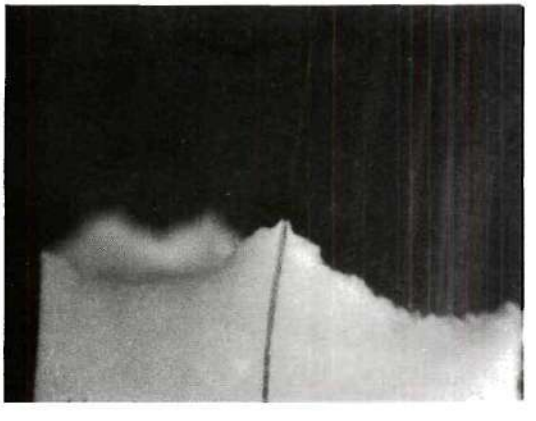

(e) PBAA Sandwich (40X).

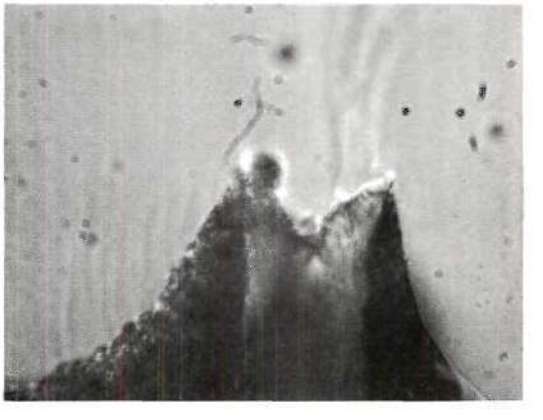

(f) PBAA Sandwich (800X).

Figure 48. Surface Profile of Sandwiches Quenched at 2000 psig.

with the overall surface regression rate. An enlargement of the binder region, Figure 48f, reveals a 10 micron binder dip and shows that the interfacial contour is smooth.

The 75 micron CTPB sandwich quenched at 2000 psig, Figure 49a, exhibits an asymmetric profile with both surfaces undergoing planar regression except adjacent to the binder interface where the surfaces incline sharply. A rather heavy melt layer extends for 100-150 microns on the lagging oxidizer surface while the leading surface is coated with a carbonaceous residue. Figure 49b indicates that binder decomposition is occurring more completely on the portion facing the leading oxidizer surface.

The 100 micron PU sandwich, Figure 49c, exhibits planar oxidizer regression except adjacent to the binder layer where the surfaces are sharply inclined. The binder layer peak extends about 500 microns above the oxidizer surface.

Surface Profile, 2400 psig. A 50 micron PS sandwich quenched at 2400 psig, Figure 50a, exhibits a planar regressing surface which gently slopes upward near the outer sandwich edge and near the binder interface. The binder peak does not extend appreciably above the oxidizer surface.

The 100 micron PU sandwich, Figure 50b, possesses the same characteristics as discussed for the 2000 psig sample except that the binder peak extension above the oxidizer surface is more exaggerated; the binder lags the surface by almost 700 microns for the sample quenched at 2400 psig.

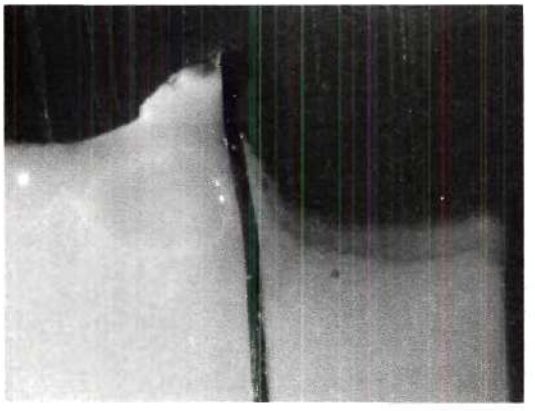

(a) CTPB Sandwich (40X).

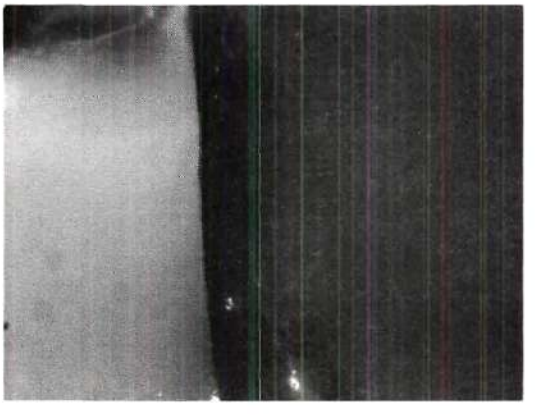

(b) CTPB Sandwich (100X).

(c) PU Sandwich (40X).

Figure 49. Surface Profile of Sandwiches Quenched 2000 psig.

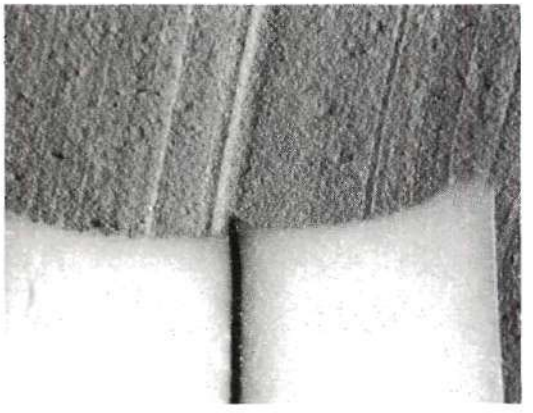

(a) PS Sandwich (40X).

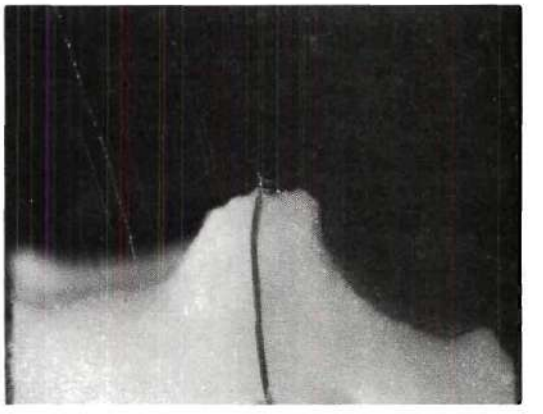

(b) PBAA Sandwich (40X).

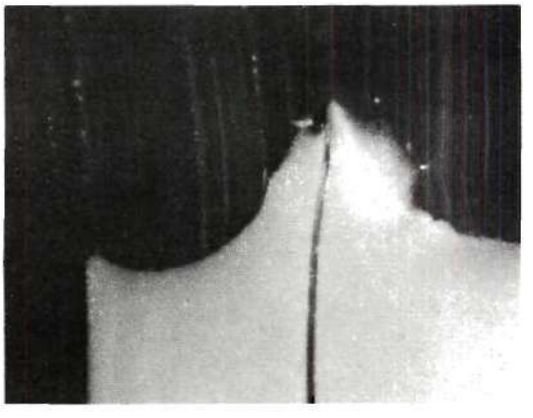

(c) CTPB Sandwich (40X).

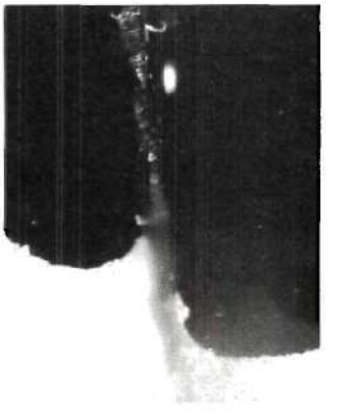

(d) PU Sandwich (40X).

Figure 50. Surface Profile of Sandwiches Quenched at 2400 psig.

The PBAA and CTPB sandwiches quenched at 2400 psig, Figures 50c and 50d, exhibit characteristics which have not previously been observed. Very little of the sandwich is regressing in planar fashion. The general surface shape is one with a steadily increasing slope, traversing from the outer edge to the binder interface with a plateau of 100-150 microns half-width adjacent to the 25-30 micron binder.

A summary of the sandwich profile details is given in Table 4 for the four binders considered in this study. Items of particular interest in Table 4 are the binder thicknesses investigated, the extent of the binder melt on the oxidizer surface, and the inclination of the oxidizer surface adjacent to the binder interface.

Contribution of the Binder to Sandwich Regression

The regression behavior of the propellant sandwiches burned and quenched in this investigation differed considerably depending upon the binder type and binder lamination thickness used in the sandwich fabrication. In general, PS resulted in sandwich regression rates greater than the AP self-deflagration rate over the entire combustion pressure range investigated. PBAA sandwich regression rates were similar to that of AP deflagration except at elevated pressures where the presence of fuel resulted in a considerable burning rate augmentation. Both CTPB and PU fuels exhibited sandwich regression rates less than that characteristic of AP deflagration at all pressure levels except 2400 psig where the addition of fuel ostensibly increased the burning rate. All four fuels were effective in increasing the AP burning rate in the high pressure region where the AP burning rate versus pressure curve possesses a negative slope.

Table 4. Summary of Sandwich Profile Details Over the Pressure Range 300 psig to 2400 psig

Binder Type	Pressure (psig)	Binder Thickness (Microns)	Extent of Binder Melt (Microns from Binder Interface)	Inclination of Oxidizer Surface Adjacent to Binder Interface (Degrees)	Point of Maximum Regression (Microns from Binder Interface)	Inclination of Oxidizer Surface Deflagrating as a Monopropellant (Degrees)
PS	300	55-75	100-125	15-25	125-150	40-50
	600	35-75	50-75	0-10	Craters	5-10
	1000	35-75	100-150	0-5	Planar	0-10
	1500	35-75	75-100	5-20	150-200	0-15
	2000	35-75	100-150	5-10	Planar	5-15
	2400	35-50	100-150	5-10	Planar	5-15
PBAA	300	50-200	300	45-50	70-40	35-40
	600	25-100	50-75	45-60	Craters	10-20
	1000	25-100	150	40-50	Planar	0-20
	1500	25-100	75-100	30-40	Planar	10-20
	2000	25-150	100-150	40-50	None*	10-20
	2400	25-150	50-75	40-50	None	5-20

* ~ Surface regression is non-planar and profile does not possess a well defined point of maximum regression.

(Continued)

Table 4. (Continued)

Binder Type	Pressure (psig)	Binder Thickness (Microns)	Extent of Binder Melt (Microns from Binder Interface)	Inclination of Oxidizer Surface Adjacent to Binder Interface (Degrees)	Point of Maximum Regression (Microns from Binder Interface	Inclination of Oxidizer Surface Deflagrating as a Monopropellant (Degrees)
CTPB	300	35-160	300	50-65	100	35-45
	600	35-160	50	15-35	Craters	10-25
	1000	35-120	50-75	20-30	Planar	0-10
	1500	60-75	75-100	25-35	Planar	0-15
	2000	35-75	100-150	15-70	None	5-15
	2400	35-75	50-75	40-55	None	5-20
PU	300	100	Not Available	Not Available	Not Available	Not Available
	600	40-100	100	15-50	Craters	10-20
	1000	40-200	50-75	10-25	Planar	0-10
	1500	40-200	250-300	15-35	Planar	5-10
	2000	40-100	250-300	15-50	Planar	5-10
	2400	40-100	25-50	15-65	Planar	5-10

PS Sandwich Regression. Sandwich regression mass flux data are shown in Figure 51 for PS sandwiches with binder lamination thicknesses ranging between 35 and 75 microns. For all binder lamination thicknesses, the sandwich regression rates were observed to increase smoothly with combustion pressure and were observed to regress more rapidly than self-deflagrating AP, except near the AP low pressure deflagration limit. Regression rates typically varied from a rate characteristic of AP at 300 psig to a rate three times that of AP at 2400 psig; increasing the binder lamination thickness increased the sandwich regression rate at every pressure level. The slope of the regression rate curve decreased slightly at elevated pressures exhibiting the underlying AP deflagration characteristics; increasing the binder layer thickness reduced this effect.

PBAA Sandwich Regression. Sandwich regression mass flux data for PBAA sandwiches with binder lamination thicknesses ranging between 25 and 200 microns are shown in Figure 52. Sandwiches prepared with binder thicknesses less than 75 microns typically exhibit regression rates characteristic of AP deflagration at every pressure level except 2400 psig where a two-fold burning rate increase was observed. Combustion of a 100 micron sandwich at 600 psig displayed a regression rate 40 per cent greater than AP deflagration while combustion at 1000 psig and 1500 psig displayed a 20 per cent augmentation and no augmentation, respectively. At 2000 psig and 2400 psig, increasing the binder thickness from 25 microns to 150 microns resulted in a significant regression rate increase; regression at 2400 psig was four times greater than the AP deflagration rate.

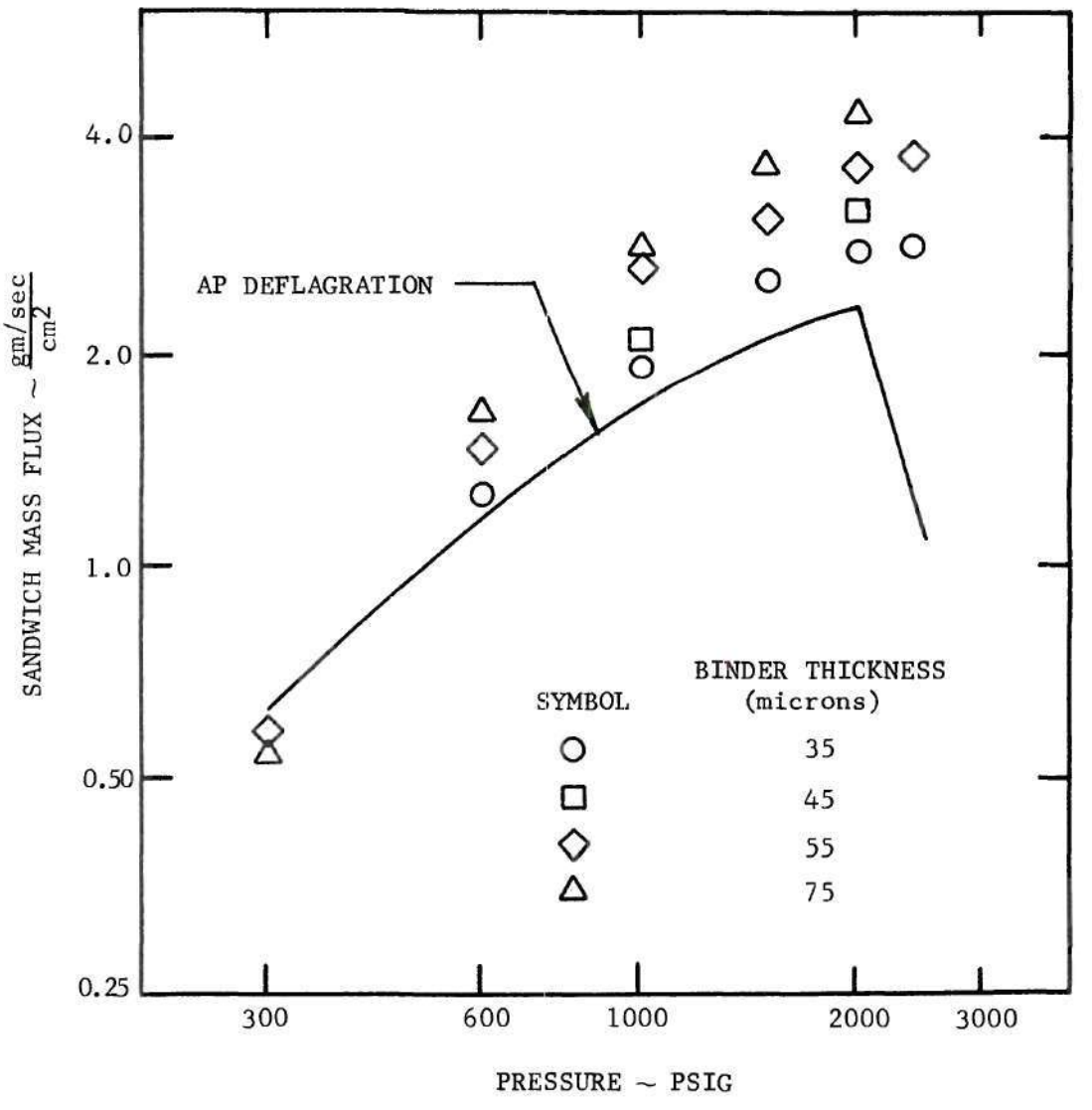

Figure 51. PS Sandwich Regression Mass Flux.

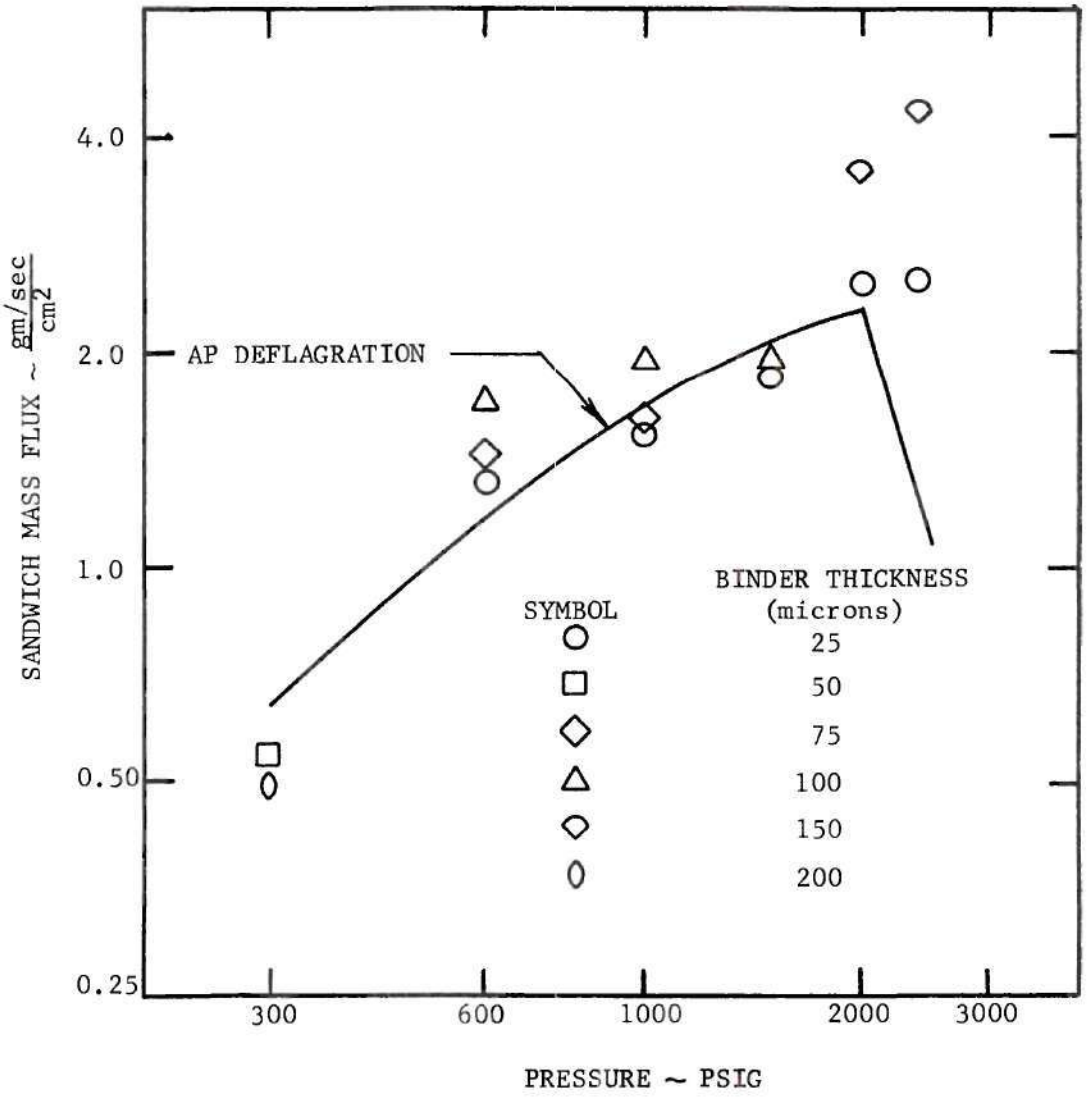

Figure 52. PBAA Sandwich Regression Mass Flux.

CTPB Sandwich Regression. Sandwich regression mass flux data, Figure 53, are shown for CTPB sandwiches with binder layer lamination thicknesses ranging between 35 and 120 microns. Sandwich regression rates for all binder thicknesses were characteristic of AP deflagration rates except for combustion at the low and high pressure extremes; low pressure regression rates were considerably below the AP deflagration rate while a doubled regression rate resulted at the high pressure extreme. Variations in binder layer thickness produced very little change in the observed sandwich regression rates.

PU Sandwich Regression. Sandwich regression mass flux data are shown in Figure 54 for PU sandwiches with binder layer lamination thicknesses ranging between 40 and 200 microns. Sandwiches with thin binder lamination layers typically exhibited regression rates similar to AP deflagration rates over the entire pressure range including the high pressure extreme. Increasing the binder lamination thickness resulted in a decreased regression rate at every pressure level below 2000 psig. Substantial increases in the regression rate occurred only at 2400 psig where the regression rate was nearly tripled.

The sandwich combustion data and the mass flux calculations generated during the quench combustion study are presented in Appendix H.

Sandwich Data Analysis

The data obtained from the combustion study were the quenched propellant sandwich and an approximate mass burning rate, as determined from the observed sandwich mass loss during combustion and the burn time. The data analysis procedure was, therefore, qualitative,

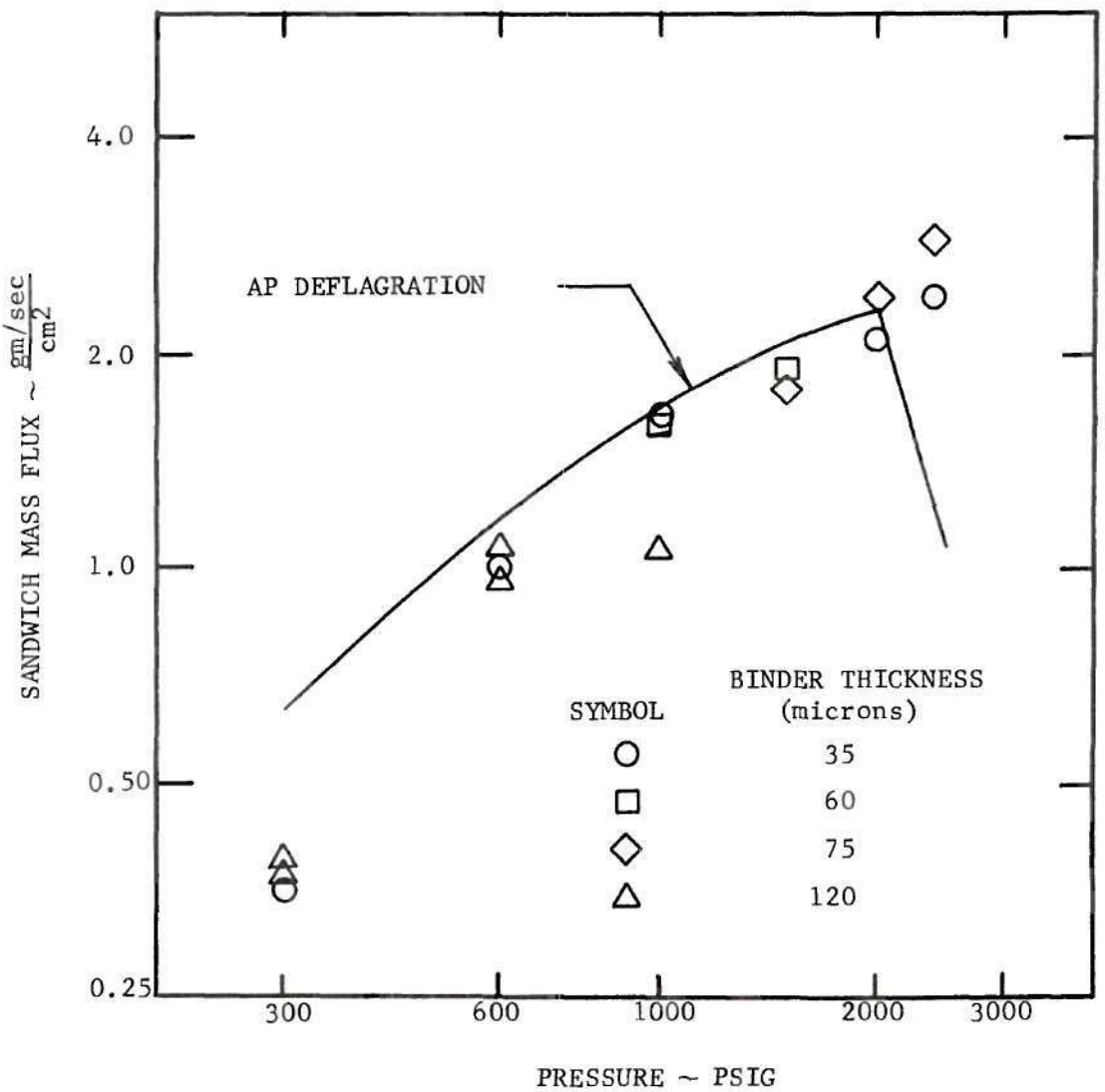

Figure 53. CTPB Sandwich Regression Mass Flux.

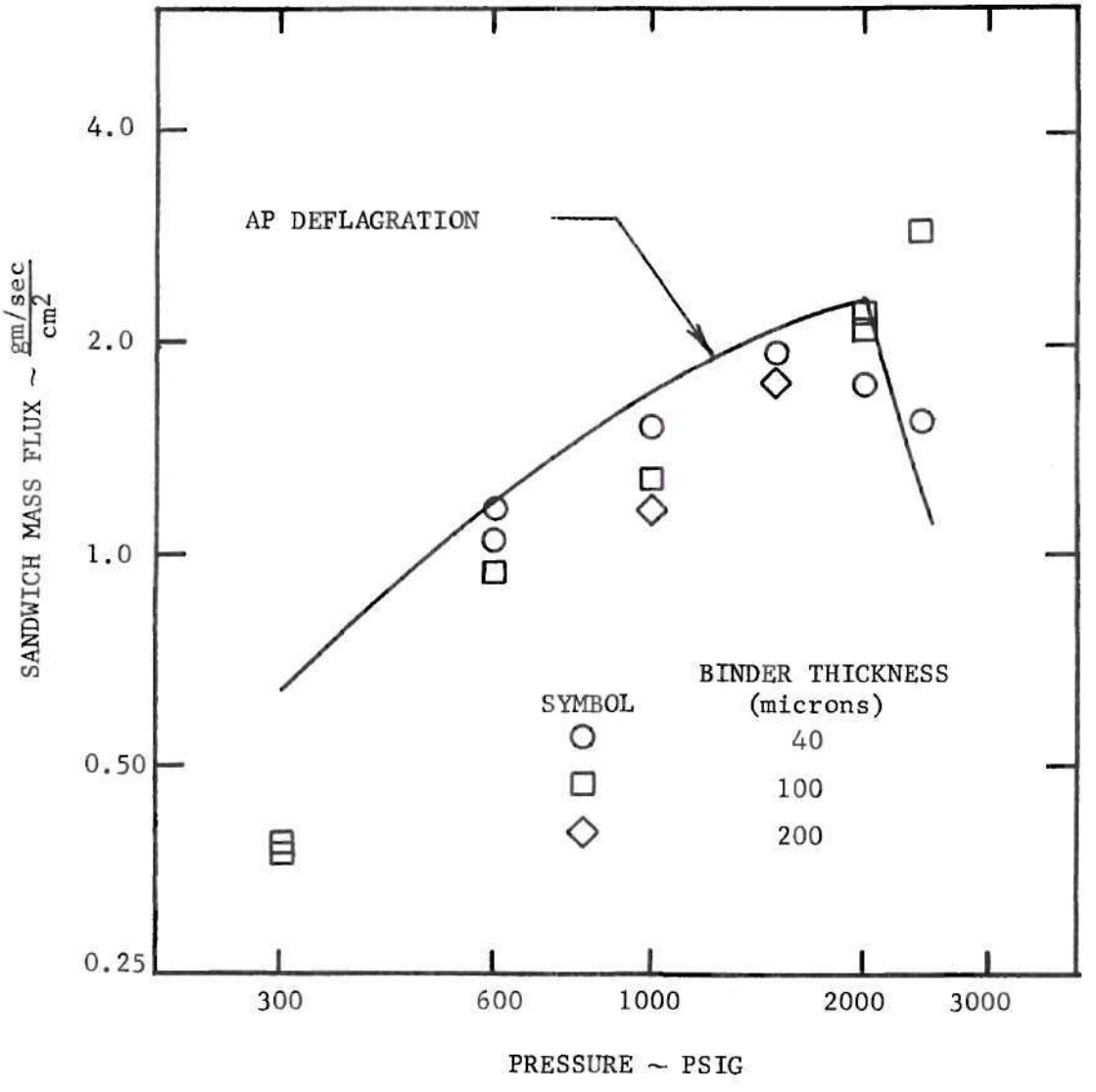

Figure 54. PU Sandwich Regression Mass Flux.

depending upon a reliable interpretation of the features and characteristics of the quenched propellant sandwich. The actual data analysis procedure was carried out in two steps:

1. The features and characteristics of the quenched propellant sandwiches were investigated over the entire pressure range.

2. An interpretation of the burned sandwich features was provided based upon combustion principles.

The surface shape of the quenched sandwich presumably represents a steady state configuration satisfying heat and mass transfer requirements; the burning rate data presented in both the Ancillary Results and the Results tend to support this assumption, but verification can be accomplished only by direct observation of the burning process. Utilizing a qualitative description of the sandwich regression process, the regression characteristics can be separated into three typical regions:

1. The first region, removed from the influence of the binder, is burning as a monopropellant and regressing as a plane wave characteristic of AP deflagration.

2. The second region, within the influence of the binder, is burning under the influence of condensed phase and/or gas phase reactions between binder and oxidizer products. This region is regressing at a rate which is typically greater than that of AP deflagration.

3. The third region, dominated by the binder, is regressing at a rate controlled by the binder decomposition energetics. This region of two-dimensional heat transfer may be regressing at a rate which is

greater or less than that of AP, depending upon the binder thermal requirements and the degree of binder-oxidizer exothermic interaction.

Using the proposed description of the sandwich burning process, the contribution of the binder to the established AP regression rate can be estimated from the sandwich profile. Since the surface profile shape, approximated by a series of straight line segments in Figure 55, presumably represents a steadily regressing configuration, each point on the surface is experiencing the same vertical (x-direction) regression rate. From physical considerations, combustion products evolve perpendicularly from the surface; that is, sandwich regression takes place locally in a direction normal to the surface. After establishing the portion of the propellant sandwich regressing as a monopropellant, the vertical regression rate, $\frac{dx}{dt}$, of the sandwich can be determined using the surface inclination, θ_{AP}, and the AP monopropellant deflagration rate, r_{AP},

$$\frac{dx}{dt} = \frac{r_{AP}}{\cos \theta_{AP}} \quad . \tag{1}$$

From the vertical regression rate and the sandwich profile geometry, the surface (normal) regression rates can be determined for the remainder of the surface profile by

$$\left(\frac{dn}{dt}\right)_i = \frac{\cos \theta_i}{\cos \theta_{AP}} r_{AP} \quad , \tag{2}$$

where n_i and θ_i refer to the normal direction and inclination of the

Segment	Inclination	Local Regression
AP Deflagration	θ_{AP}	r_{AP}
1	$\theta_1 < \theta_{AP}$	$r_1 > r_{AP}$
2	$\theta_2 \approx \theta_{AP}$	$r_2 \approx r_{AP}$
3	$\theta_3 > \theta_{AP}$	$r_3 < r_{AP}$

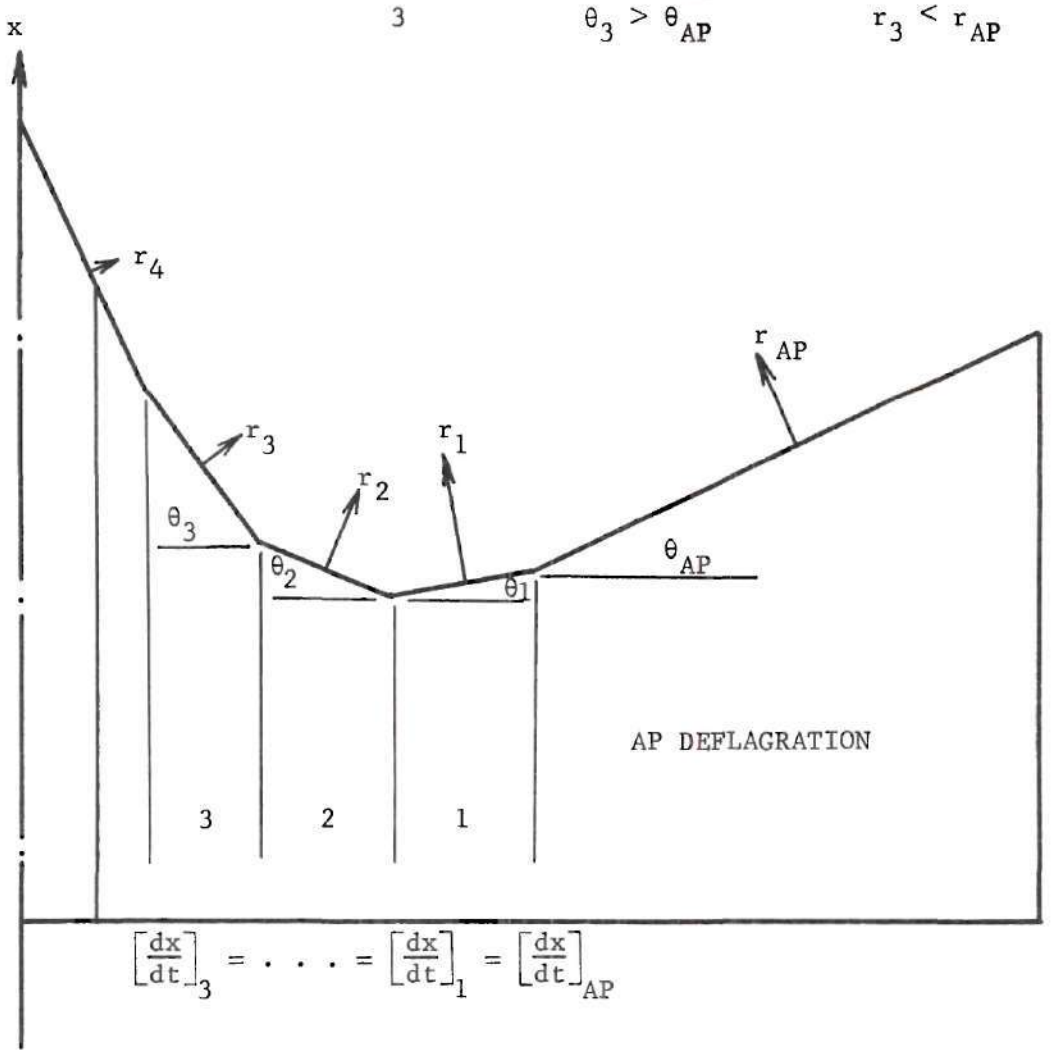

Figure 55. Approximation of Quenched Sandwich Profile Shape.

"ith" surface segment, respectively.

A comparison of the local normal regression rates provides an indication of the binder influence on the sandwich regression. A local regression rate much greater than that of self-deflagrating AP would indicate that significant gas phase binder-oxidizer heat release is occurring or that important surface processes, exothermic in nature, are occurring. A significantly reduced local regression rate would indicate that the binder serves primarily as a heat sink or that the binder products are non-reactive on or near the sandwich surface.

The net contribution of the binder to the sandwich regression rate is determined by comparing the experimentally observed sandwich mass flux with the mass flux characteristic for AP self-deflagration. An increase over the basic AP deflagration rate would imply that significant exothermic interactions were occurring between binder and oxidizer species while a decrease from the AP burning rate would indicate that the endothermic requirements of the binder were overriding any augmentation resulting from binder-oxidizer exothermic reactions.

The degree of the binder influence on sandwich regression can be qualitatively determined from the preceding argument without consideration of a combustion mechanism. Rational combustion mechanisms can be postulated from an understanding of the burning phenomena involved, but acceptable mechanisms result from uniting the observed characteristics of the quenched sandwich with the limitations imposed by principles of heat and mass transfer (e.g, conduction, diffusion, etc.). Only when a compatibility exists between the observed sandwich details and the

limitations imposed by combustion principles is a combustion mechanism considered plausible.

The possibility exists that the mechanisms influencing the sandwich regression, schematically shown in Figure 56, may be dominated by one, or a combination of:

1. Oxidizer monopropellant characteristics.

2. A gas phase flame zone resulting from binder and oxidizer products.

3. Binder decomposition characteristics and condensed phase reactions.

4. Heterogeneous binder-oxidizer interfacial reactions.

Oxidizer Monopropellant Characteristics. Domination of sandwich combustion by the AP monopropellant would be indicated by the sandwich surface and the sandwich regression rate both being similar to the established AP deflagration characteristics. Since the use of two-dimensional propellant sandwiches models the combustion only in the direction of the binder-oxidizer interface and does not simulate overall propellant features, monopropellant deflagration characteristics are expected to be dominant in the sandwich combustion. Although strong coupling between the binder and oxidizer is possible, the zone of interaction is confined by transport processes to the interfacial region.

Gas Phase Flame Zone. Evidence of a gas phase flame region can be inferred from the quenched sandwich profile. Exothermic reactions occurring in the gas phase produce an increased energy feedback to the sandwich surface which results in an increased local burning rate. For

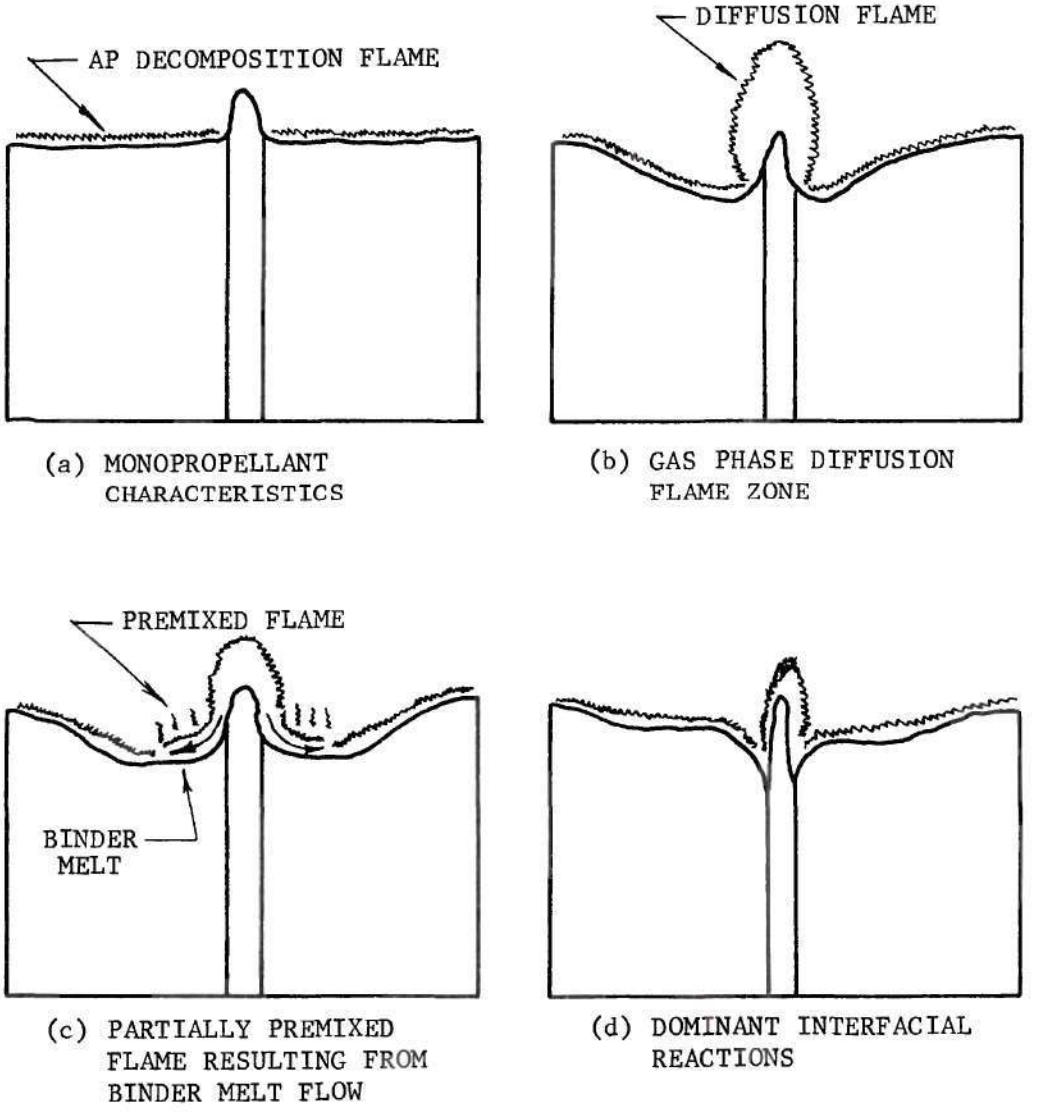

(a) MONOPROPELLANT CHARACTERISTICS

(b) GAS PHASE DIFFUSION FLAME ZONE

(c) PARTIALLY PREMIXED FLAME RESULTING FROM BINDER MELT FLOW

(d) DOMINANT INTERFACIAL REACTIONS

Figure 56. Mechanisms Influencing Sandwich Regression.

equilibrium to exist between the gas phase and the sandwich surface, the portion of the sandwich removed from the heating source must incline upward to allow the regressing surface to maintain a steady state configuration with the region of maximum regression as previously shown in Figure 55.

The location of the region of maximum regression is controlled by the lateral mixing of binder and oxidizer species from the interfacial region. High speed motion pictures and spark schlieren photographs [6] indicate that the gaseous streams evolving from a propellant surface are non-turbulent. Consequently, the process responsible for binder and oxidizer mixing is molecular in nature. In combustible gas mixtures, the Lewis number is approximately unity, implying that the energy transported by conduction and mass diffusion are of the same order of importance. The qualitative mixing argument presented in Appendix I implies that mixing, and consequently heat transfer, is confined to a very narrow region near the binder-oxidizer boundary. The quenched sandwich profiles, however, imply that the heat transfer region is much larger than the mixing analysis indicates. This may be ascribed to the existence of premixed regions caused by a binder melt flowing over the oxidizer surface or to a premixed region at the base of the diffusion flame. Since many of the details were not directly observable during the quench testing, it is highly desirable that the flame structure be investigated by high speed photography.

One final comment regarding the region of maximum regression deserves mention. If an AP slab were positioned between two non-reactive

heat sinks and ignited, the steady state burning configuration would possess a point of maximum regression which would be regressing, at most, at a rate typical of AP deflagration. The point of maximum regression in this example would be laterally positioned by equilibrium requirements satisfying heat loss to the adjacent heat sinks and the resulting configuration would be similar to the sandwich profile in which gas phase heat release was occurring.

Binder Decomposition Characteristics. The binder decomposition characteristics can play an important role in the combustion mechanism through the effects of binder melts and binder energetics.

A binder melt on the oxidizer surface can affect the sandwich combustion process in several ways depending on the energetics of the melt layer. If a molten binder is thermally stable, the melt layer can be an effective means of laterally displacing the binder-oxidizer gas phase mixing region. At least two interesting reaction mechanisms exist for the oxidizer surface which is affected by the molten binder layer:

1. The molten binder may possibly act as a thermal shield between the gas phase reaction zone and the oxidizer surface, thus inhibiting the oxidizer regression.

2. Partial binder and oxidizer pyrolysis may possibly occur producing a premixed or partially premixed flame zone above the affected region.

If the molten binder layer is thermally unstable, the melt is not as effective in the lateral displacement of the binder-oxidizer mixing

region, but may produce a more energetic situation. As the molten binder flows outward onto the oxidizer surface, the heat received from the gas phase flame region can be very effective in pyrolyzing the binder blanket and, consequently, may result in a high energy premixed flame region. The premixed nature of the flame region will be greatly enhanced if the oxidizer surface also displays a miscible melt. Also, the binder initial decomposition steps may produce active intermediates capable of undergoing exothermic reaction with the near surface oxidizer species.

The binder kinetics and thermal heat capacity determine to a large degree the sandwich profile in the interfacial region. If the binder is, in fact, experiencing steady regression, the time for a binder element to be heated from initial virgin temperature to final decomposition temperature is fixed by the sandwich regression rate. The two sandwiches in Figure 57 are undergoing identical regression rates, but the pyrolysis temperature (kinetics) of one binder is much higher than the other. (The binder in Figure 57a is presumed to have the higher pyrolysis temperature.) Since the time for a binder element to move from point A to point S is the same, the binder with the higher pyrolysis temperature must expose more surface area, increasing the total heat transfer to the binder, in order to maintain a steady regression. Since this heat is supplied to the binder material by gas phase conduction and possibly solid phase conduction through the AP, the oxidizer surface inclination adjacent to the binder-oxidizer interface is indicative of the binder kinetics and energetics. If the interfacial

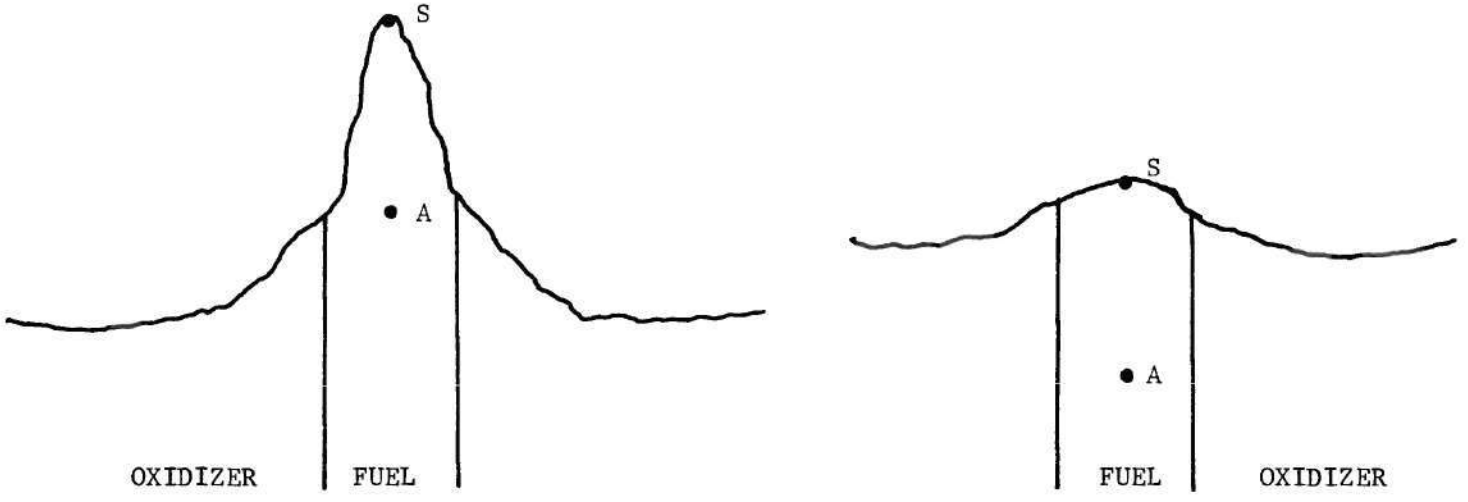

(a) HIGH PYROLYSIS TEMPERATURE

(b) LOW PYROLYSIS TEMPERATURE

Figure 57. Influence of Binder Properties on Interfacial Profile Details.

surface inclination is greater than the inclination of the sandwich surface portion deflagrating as a monopropellant, the interfacial oxidizer surface is regressing at a lesser rate than pure AP, and the binder is acting primarily as a heat sink. On the other hand, if the interfacial inclination is less than the monopropellant surface inclination, the binder-oxidizer gas phase heating contribution is overriding the binder heat capacity requirements, producing a surface which is regressing at a rate greater than pure AP.

Heterogeneous Binder-Oxidizer Interfacial Reactions. Heterogeneous reactions, either in the condensed phase or the gaseous phase, between oxidizer and binder would be strongly suggested if the leading edge of the sandwich regression front were to occur along the binder-oxidizer interface. For a self-deflagrating monopropellant like AP, the dominant interfacial reactions would likely be between active oxidizer intermediates and virgin binder material.

Mechanisms Influencing Sandwich Regression

The burning of two-dimensional propellant sandwiches appears to depend upon a balanced mechanism involving a complex interdependence between the oxidizer and binder decomposition and reaction steps. The deflagration of AP is assumed to occur in at least two stages: an endothermic solid phase reaction and an exothermic gas phase reaction. The binder decomposition is endothermic producing a molten liquid of unknown chemical composition (polymer, monomer, hydrocarbon fractions, etc.) during or before pyrolyzing. The interdependence and balance between the binder and oxidizer reaction steps was found to depend upon

both the binder type and the combustion pressure level. The controlling sandwich combustion mechanism may be considered to consist of a combination of the following steps:

1. An endothermic decomposition of the oxidizer yielding active gaseous products. An intermediate step in this process may involve a physical or chemical transition through a liquid state.

2. An endothermic decomposition of the binder material producing liquid and/or gaseous products.

3. Any of several surface processes involving binder and oxidizer species. These processes may involve liquid-liquid interaction or heterogeneous gaseous-liquid-solid interaction, either of which may be endothermic, exothermic, or purely physical.

4. An exothermic gas phase reaction involving oxidizer decomposition gaseous products establishing a flame near the oxidizer surface.

5. Exothermic gas phase binder-oxidizer reactions occurring in a premixed and/or diffusive mode. These gas phase reactions may produce species capable of further reaction in the combustion zone.

The manner in which these steps are linked and the relative importance of each step to the combustion determine the physico-chemical mechanism responsible for the sandwich burning process.

The features of the burned sandwich surface and the observed sandwich regression rates indicate that AP monopropellant deflagration is the dominating process responsible for sandwich regression, although the presence of a fuel binder can be very effective in augmenting or inhibiting the basic AP deflagration rate. Since the sandwiches burned

and quenched in this study were highly oxidizer rich in composition (Appendix J), small variations in sandwich regression rate can imply strong coupling between the binder and oxidizer decomposition steps.

The characteristics of the burned surface and the quenched sandwich profiles indicate that there was considerable interplay between the binder and oxidizer species on the surface of the oxidizer sandwich, primarily through the ability of the binder to form a melt prior to gasification. No conclusive results were observed which established the binder-surface interaction to be anything other than a physical spreading of the molten binder. In fact, the smooth interfacial sandwich profiles enforce the point of view that significant condensed heterogeneous reactions were not occurring.

The hypothesis of the existence of a diffusion flame, in many cases, explains the features of the observed sandwich profiles. At pressures near the AP low pressure deflagration limit, the existence of a well defined point of maximum regression indicated that energy release from a diffusion flame, or possibly a merged premixed-diffusion flame, was dominant in the sandwich regression process. At elevated pressures where the mixing process is slow compared to chemical processes, the contributions of a diffusion flame are less clear and are difficult to separate from contributions resulting from a premixed binder-oxidizer flame.

Sandwiches prepared with all four fuels were observed to form a surface melt during combustion at every pressure level. For all combustion tests except PU sandwiches above 1000 psig, the extent of the

binder melt on the oxidizer surface was nearly constant, ranging between 50 and 150 microns. The binder melts generally produced a situation which enhanced sandwich regression for PS and PBAA fuels, while the melts of CTPB and PU inhibited the regression rate.

The previous discussion indicates that the two-dimensional problem is extremely complex and requires more investigation and analysis than is included within the scope of this thesis. The following interpretations of the observed sandwich shapes are plausible combustion mechanisms based on the simplistic analysis previously presented, but alternate explanations may be advanced as further information becomes available. For example, it is imperative that motion pictures be taken in order to provide information on the potential role of the ignition transient in determining the final sandwich shape and the actual flame location and associated unsteadiness.

PS Sandwich Regression. Sandwiches prepared with PS fuel exhibited a uniformly increasing regression rate for all binder thicknesses at every combustion pressure level investigated. This type of behavior is indicative of a unique combustion mechanism governing the sandwich regression process. Using the binder thermal decomposition characteristics presented in Chapter II, a mechanistic argument for PS sandwich regression was developed which was consistent with the observed quench surface features and established AP deflagration characteristics.

The presence of PS fuel appeared to enhance the characteristic AP deflagration rate at every pressure level, the degree of the burning rate increase being greater for thicker binder lamination thicknesses.

The mechanism responsible for the burning rate increase probably involves two separate, but definitely coupled, heat release regions. The observed binder peak position and interfacial details would be consistent with a diffusion flame or a premixed flame located near the binder oxidizer interface. If a diffusion flame is present during combustion, gaseous binder products would presumably be combusted in a small diffusion flame region over the binder layer, thus providing energy feedback to produce the observed binder melts. The lack of a well defined point of maximum regression would imply that the contribution to sandwich regression of the diffusion flame was primarily by satisfying binder thermal requirements. It should be noted that, while heat transfer from an AP decomposition flame alone could possibly be responsible for producing the observed binder melts, exothermic reaction between binder and oxidizer species is required to produce the burning rate augmentation indicated by the mass flux data.

The sandwich details and indicated mass fluxes are best explained by hypothesizing a near surface premixed flame resulting between the binder melt products and oxidizer decomposition products. The degree to which the postulated flame zone is premixed will, of course, depend upon the nature of the oxidizer surface and may, in fact, be no more than gaseous oxidizer decomposition products percolating through the molten binder surface layer. The postulated flame zone will appear as premixed on a macroscopic scale if the degree of surface mixing (liquid-liquid or gaseous-liquid) is large, or possibly as a large number of diffusion flamelets if the mixing occurs to a lesser degree. Based on

the previously determined binder energetics, the temperature of the binder melt is between 550-650 °K and, consequently, is considerably cooler than the 750-850 °K surface temperature observed for deflagrating AP [23] [24] [53] [54]. Hence, the molten binder while flowing onto the oxidizer surface is receiving heat from at least two sources, the oxidizer surface and the AP decomposition flame. If the binder melt were non-reactive and acted as a thermal shield between the AP decomposition flame and the AP surface, the oxidizer surface in the interfacial region would be inclined (reduced local regression) for the extent of the binder melt; this was not observed. If the presence of the binder melt somehow enhanced heat transfer to the surface or produced a situation more exothermic than the AP decomposition flame alone, then the sandwich regression would be augmented relative to AP deflagration; this was observed. If the significant reactions were occurring between the molten binder and an oxidizer liquid surface layer, the increased sandwich burning rates would be expected to diminish as the presence of the liquid oxidizer layer diminishes; that is, in the neighborhood of 1000 psi where the AP surface pattern of ridges and valleys emerge [11]. The indicated mass flux rates did not show a reduction with the accompanying decrease in the liquid surface layer, but rather increased uniformly to 2400 psig. The implication is simply that the enhancement to the sandwich regression by the binder melt at low and intermediate pressure levels is not through a surface process, but rather one occurring in the gas phase.

The sandwich profiles observed at 1500 psig and above suggest

that the effects of a binder melt may extend farther than indicated by the surface photomicrographs. An extensive planar regression front adjacent to the visible binder melt was observed to be present at pressures above 1500 psig; likewise, the population of needle-like activity sites is known to characterize the AP surface beginning in this pressure region [11]. The implication is that considerable binder flow may be taking place within the needle-like sub-structure region which is not apparent from the surface and, consequently, results in a rather widely based exothermic region on, or near, the oxidizer surface.

For PS sandwiches, the significant mechanism appears to be the gasification and subsequent near surface reaction resulting from molten binder on the oxidizer surface. The question must currently be left unanswered as to the position and nature of the flame region. Heterogeneous interfacial reactions do not appear to be significant in the combustion of PS sandwiches.

PBAA Sandwich Regression. PBAA sandwiches prepared with thin binder lamination thicknesses, 50 microns or less, displayed regression rates typical of AP deflagration. The addition of fuel to the sandwiches increased the regression rate at every pressure level except 1500 psig. The oxidizer surface inclination in the interfacial region was pronounced indicating that the conductive heat loss to the binder was considerable; this is in agreement with the kinetics and energetics observed in the DSC-1B investigation. The presence of the observed surface melts indicates that an exothermic zone is present near the binder interface; further, the indicated sandwich regression rates imply that

heat release in excess of the AP decomposition flame is occurring.

The observed binder melts were not uniformly spread over the interfacial region, but rather followed the local surface contour producing a distinctive flow pattern. Considering the DSC-1B results, the relationship of the binder temperature to the oxidizer surface temperature is less clear; consequently, the binder-oxidizer surface interplay involves more uncertainty than in the PS sandwich discussion. Nevertheless, the binder flow pattern observed would seem to imply that the gas phase region over the oxidizer surface affected by the binder melts was presumably an active region of diffusion flamelets or a partially premixed flame.

The binder peak was observed to extend above the oxidizer surface for sandwiches prepared with thick binder lamination thickness. Since the flame zone resulting from the binder melts is probably close to the oxidizer surface, the matter of heat transfer to the binder extension must be resolved. At least two plausible explanations exist. An exothermic diffusion zone could presumably exist near the binder-oxidizer interface, thus supplying heat to the binder in order to maintain steady regression. Secondly, as the binder melt flows onto the oxidizer surface, oxidizer percolation through the layer could result in an exothermic region near the interface. The products of this reaction zone must flow by the binder surface, thus heating the binder with hot gases by convection. Again, high speed photography could possibly be definitive in this issue. The microscopic regression fronts observed at 2000 psig could be explained using either mechanism.

The binder peak for thin binder layer PBAA sandwiches was observed to be flush with the oxidizer surface and possessed a curious notch. Combustion at low pressure of a sandwich prepared with a 50 micron binder lamination thickness displayed a symmetrical dip in the binder surface which was approximately 30 microns deep. Similar results were observed at elevated pressure for combustion of 25 micron thick binder layers; the resulting binder dip was approximately 10 microns deep.

Using a one-dimensional heat balance for a moving surface with no decomposition reactions, the temperature at any distance below the regressing surface is related to the regression rate by

$$\frac{(T-T_0)}{(T_s-T_0)} = e^{\frac{rx}{\alpha}} , \qquad (3)$$

where x is the distance below the regressing surface, T is the temperature at any location x below the surface, r is the regression rate, α is the binder thermal diffusivity, and T_s and T_0 are the binder surface and initial temperature, respectively. Based upon the observed sandwich regression rate and an initial binder temperature of 500 $^{\circ}$K (so chosen to correspond with the AP crystal phase transition temperature), the distance below the surface at which the melting temperature, as observed in the DSC-1B study, occurred was determined using equation (3). The melting transition was predicted to occur approximately 25 microns below the surface at 300 psig and approximately 5 microns below the surface at 2000 psig. These values are in good agreement with the observed results

indicating that the binder notch may have been formed as the result of the binder melting and flowing onto the oxidizer surface. It is not known if the binder notch was present during combustion or if it was an artifact of the depressurization process used to quench the combustion. The binder heating mechanisms discussed for the thick binder sandwiches are applicable for the thin binder, but have different implications regarding the nature of the binder dip. If a diffusion flame is responsible for the binder heat feedback, Figure 58a, the binder dip apparently may be the result of a binder melt being extracted during quench. If hot gas convection exists, Figure 58b, the binder dip is possibly present during combustion, since convective heating by recirculating hot gases could supply heat transfer to maintain binder pyrolysis.

The sandwich profiles at combustion pressure levels of 2000 and 2400 psig are unexplained within the scope of this investigation. The extensive plateaus in the interfacial region and the overall oxidizer shape may be the result of an unsteady phenomenon, but this is only speculation. High speed motion pictures would provide considerable information on this problem.

The role of PBAA binder appears to change with combustion pressure. At low pressures, the binder acts more or less as a heat sink while at elevated pressures the binder-oxidizer interplay mechanism appears to become more active. The very high pressure results are unexplained by the simplistic approach taken in this investigation. Heterogeneous interfacial reactions do not appear significant although preferential interfacial regression was observed in an isolated instance.

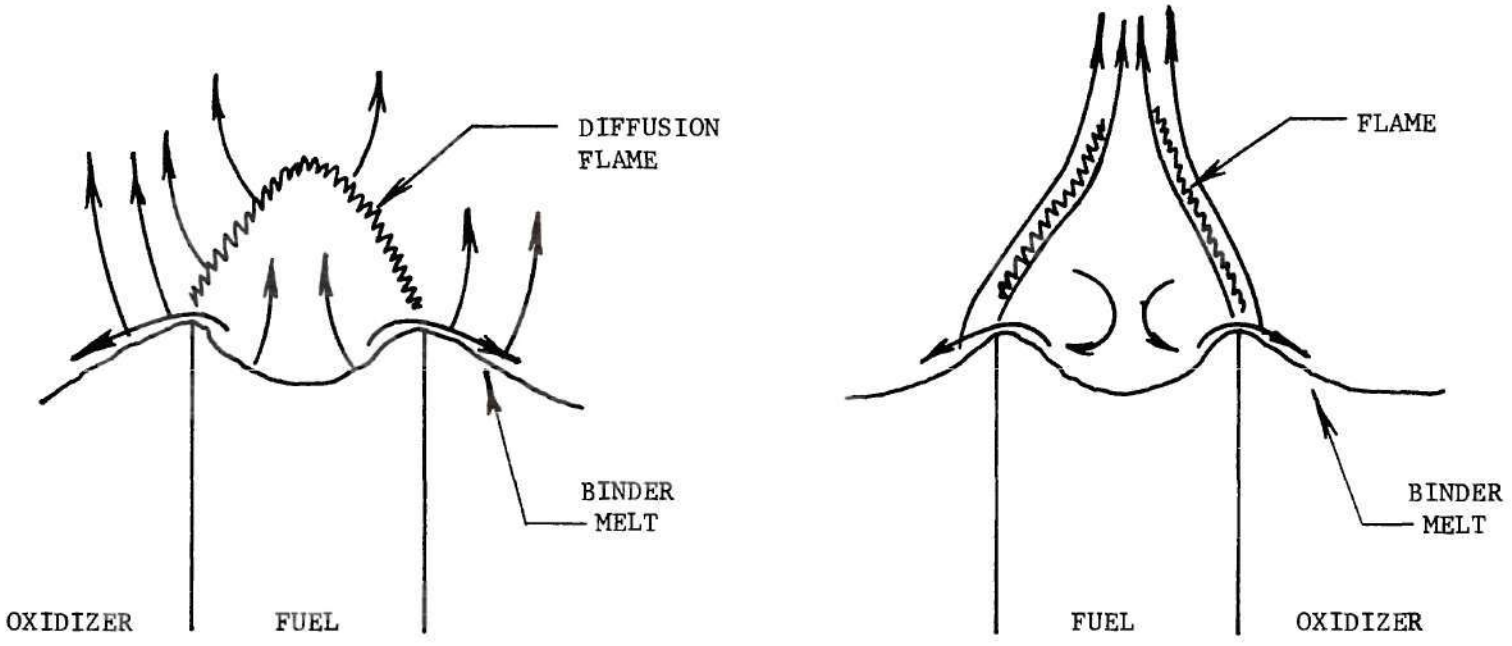

(a) DIFFUSION HYPOTHESIS

(b) CONVECTION HYPOTHESIS

Figure 58. Formation of PBAA Binder Notch.

CTPB Sandwich Regression. Sandwiches prepared with CTPB fuel generally regressed slower than rates typical of AP deflagration at every pressure level except 2400 psig. CTPB sandwiches exhibited a tendency for one side of the sandwich to considerably lag behind the other oxidizer surface. It was not determined in this study if the position of the lagging surface relative to the leading surface was time dependent or steady. Nevertheless, the lagging surface was observed to be rather heavily coated with a glossy brown substance, presumably a surface melt, whereas the leading surface was rather extensively contaminated with a carbonaceous residue. It appears that the binder melt does not readily decompose on, or near, the oxidizer surface and is capable of inhibiting, or possibly even quenching, the AP deflagration process. The excessively heavy carbonaceous contamination on the oxidizer surface is possibly an indication that thermal decomposition of the binder is only the first step in a decomposition mechanism which is oxidation limited. The rather high surface temperatures predicted using the DSC-1B thermal decomposition results seem to support this point of view.

Since sandwiches prepared with thick binder lamination thicknesses exhibited symmetrical regression profiles whereas thin binder sandwiches did not, an unsteadiness associated with an interfacial flame zone may be a plausible explanation for the observed asymmetric profiles. Evidently the thicker binder layer prevented the postulated interfacial flame from moving across the interface and enhanced heat release regions on both sides of the binder preventing the accumulation of

an inhibiting binder melt layer. The sandwich regression rates for the thick binder layer sandwiches were well below the AP deflagration rate indicating that the heat feedback (or supply of oxidative species) was considerably less than the requirements of the binder lamination layer.

The peculiar results observed at 1500 psig (Figure 46) can be explained by postulating either a diffusion flame over the binder or an eddy transfer mechanism as earlier described in the PBAA discussion. If a diffusion flame over the binder is presumed, the results shown provide a transition between the stable flame structure postulated for the thick binder layer and the unstable flame attributed to the thin lamination layers. The eddy transfer mechanism also appears plausible, particularly if the binder decomposition encompasses both thermal and oxidative decomposition steps. The possibility also exists that both mechanisms may be coupled.

The results of the CTPB quenching tests appear to involve more uncertainty than the previous PS and PBAA sandwich tests. The decomposition behavior of the CTPB binder from the DSC-1B study does not appear to be compatible with the decomposition characteristics observed in the quench tests. The uncertainty is further aggravated by the ignorance of the flame structure and the steadiness of the regression behavior. Further analysis involving high speed photography is required to eliminate some of the uncertainty involved in CTPB sandwich regression characteristics.

PU Sandwich Regression. Although the features of the burned PU sandwiches were observed to vary considerably with binder lamination

thickness and combustion pressure level, the regression rates exhibited by the PU sandwiches were generally slightly less than that of AP deflagration and did not display a marked dependence upon binder thickness.

Sandwiches prepared with thin binder lamination thicknesses of approximately 40 microns exhibited regression rates typical of AP deflagration at every pressure level including 2400 psig. The binder peak was observed to be flat indicating that there may be an energy source located near the interfacial region. The contribution of this energy source is small compared to the heat capacity of the binder as indicated by the steeply inclined interfacial oxidizer surfaces.

Sandwiches prepared with thicker binder lamination thicknesses of 100 and 200 microns displayed a rather curious behavior with combustion pressure level. Based on the observations of the binder thermal decomposition study, sandwiches prepared with PU fuel were expected to regress in a manner similar to PS sandwiches since both fuels possessed similar kinetics and energetics. At combustion pressure levels of 300 and 600 psig, the position of the binder peak relative to the oxidizer surface was nearly even with the adjacent oxidizer surface typical of the low energy level required to thermally decompose PU fuel. At combustion pressure levels from 1000 psig to 2400 psig, the position of the binder peak with respect to the oxidizer surface was observed to increase with combustion pressure; the amount the binder peak lagged the oxidizer surface was 200 microns at 1000 psig and nearly 700 microns at 2400 psig. The binder is decomposing as can be seen by comparing the binder thickness above and below the oxidizer surface, but the pyrolysis

products are not combining with the AP reaction products in a manner capable of providing heat feedback to the sandwich surface. In fact, the extensive surface melts and contamination with carbonaceous products seems to indicate that the binder pyrolysis products are relatively stable on the oxidizer surface. Although the exaggerated binder lag was noted at 2400 psig, the observed sandwich regression rate was greater than the AP deflagration rate, and the oxidizer surface was observed to be relatively clean. Apparently the increased interplay between the AP needle-like surface and the binder melt produces an energetic surface, or near surface, heat release zone capable of augmenting the sandwich regression.

The mechanism which appears important in the regression of PU sandwiches is the relatively non-reactive nature of the binder pyrolysis products. Any appreciable exothermic interplay between oxidizer and binder species, even at low pressures, does not seem to be occurring. No evidence of condensed phase or heterogeneous interfacial reactions was observed at any pressure level.

CHAPTER IV

CONCLUSIONS

The quench combustion of two-dimensional propellant sandwiches has been shown to be an effective tool for investigating the burning mechanisms of AP composite propellant ingredients. Interpretation of the quench combustion results was enhanced by an *a priori* knowledge of the individual ingredient decomposition behavior. The results of the present investigation may be summarized in the following conclusions:

1. Binder kinetics and energetics obtained by the method of differential scanning calorimetry provide a qualitative understanding of binder thermal decomposition behavior which, in some cases, may be useful for combustion analysis. Caution must be exercised in extending the low pressure, low heating rate DSC-1B decomposition characteristics to actual combustion situations by investigating the decomposition behavior in high pressure tests to detect obvious anomalous behavior (such as exhibited by PU at high pressures).

2. An effective means for compacting granular AP into polycrystalline sheets has been developed. Specimens of the compacted polycrystalline AP exhibit quantitative and qualitative deflagration behavior of pure single AP crystals over a combustion pressure range of 300 psig to 4800 psig. Also, the combustion results of sandwiches prepared with polycrystalline and single crystal AP reveal that the regression characteristics of both systems agree.

3. A reliable sandwich replica technique has been developed which permits unambiguous investigation of sandwich details.

4. Quenched combustion of propellant sandwiches prepared with PS, PBAA, CTPB, and PU polymeric binders ranging in lamination thickness from 25 to 200 microns indicated the presence of a binder melt on the oxidizer surface at combustion pressure levels from 300 psig to 2400 psig.

5. The kinetic and energetic nature of the observed binder melts has an influence on the sandwich regression behavior.

6. The presence of fuel, independent of reactive nature, was observed to augment the characteristic AP deflagration rate of a combustion pressure level of 2400 psig. Combustion at other pressure levels did not exhibit a uniform response to fuel or fuel type.

7. Smooth interfacial contours observed at the binder-oxidizer interface for every combustion pressure level indicate that significant interfacial reactions between the binder and oxidizer are not occurring.

8. The regression of two-dimensional propellant sandwiches appears to depend upon a great many interdependent events. The sandwich regression behavior was, in many cases, strikingly different, but reasonable hypotheses have been advanced to explain the observed results using the quenched sandwiches and the DSC-1B binder decomposition behavior.

9. The two-dimensional problem is extremely complex and requires more investigation than is included within the scope of this thesis. Because of the uncertainties involved in sandwich regression time history

and the actual flame structure and location, it is imperative that high speed motion pictures be taken of the sandwich combustion to provide the details unobtainable using quenching techniques.

10. Any analytical combustion models which are based upon dry propellant surfaces and/or dominant interfacial reactions are open to severe question.

11. The interpretation of the quenching results would be greatly enhanced by an analytical description of the sandwich combustion which includes the effects of two-dimensional gas and solid phase heat transfer, binder surface melts, gas and solid phase chemical kinetics, and gas phase species diffusion.

APPENDICES

APPENDIX A

OPERATING PROCEDURE FOR PERKIN-ELMER DIFFERENTIAL SCANNING CALORIMETER, MODEL DSC-1B

The procedures followed for the operation of the DSC-1B were those generally advised in the Instructions Manual [43] supplied by the Perkin-Elmer Corporation.

Cleaning the Sample Holder Assembly

Prior to conducting each series of binder decomposition tests, it was necessary to clean the sample holder assembly of decomposition products. Cleaning is usually indicated when the DSC-1B output signal characteristics possess a high noise level. The cleaning procedure is as follows:

1. Before energizing the DSC-1B unit, carefully remove the sample holder assembly from the assembly platform.

2. Hold the sample holder assembly over a laboratory basin and flood the sample holder cups and upper assembly with dimethyl formamide; gently agitate to remove decomposition products. If the sample holder was excessively dirty, the sample holder cups and upper assembly was carefully cleaned with cotton swab.

3. To assist the drying of the sample holder assembly and to insure thorough removal of the dimethyl formamide solvent, the sample holder was generously purged several times with acetone.

4. After replacing the sample holder assembly in the DSC-1B,

energize the unit and manually program the temperature to 750 °K. Following a 15-minute drying period, the temperature is manually returned to 300 °K. The DSC-1B is now ready for calibration.

Calibrating the DSC-1B

After cleaning has been performed, it is necessary to check, and reestablish if necessary, the temperature and ordinate calibration of the DSC-1B to insure optimum performance.

Differential Temperature Calibration

In order to balance the differential bridge between the sample and reference sample cups, the following procedure was used:

1. The differential temperature and average temperature controls were left in the positions indicated by the previous calibration.

2. Standard indium calibration samples of different mass were placed in the sample and reference cups and the sample holder cover was secured.

3. With the range control set at 16 and the scan control at 10 °K per minute, the temperature was manually raised to 400 °K. The temperature control was placed in the "increase" position and the indium samples were scanned through their melting point(s).

4. The temperature program was stopped by switching the temperature control to the "neutral" position, and the temperature was manually returned to 400 °K.

5. If the calibration thermogram possesses two distinct peaks, Figure A-1a, then differential temperature calibration is required. If melting in the sample cup occurred before melting in the reference cup,

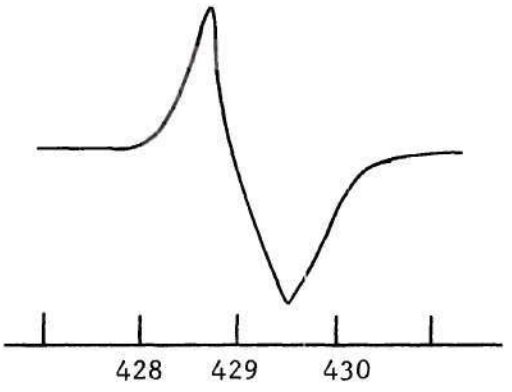

(a) NOT CALIBRATED

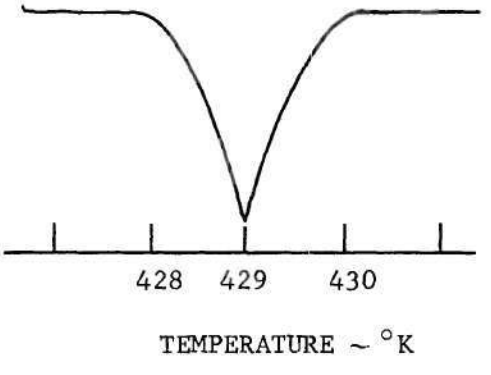

(b) CALIBRATED

Figure A-1. DSC-1B Differential Temperature Calibration Thermogram.

the differential temperature control was turned clockwise. One turn of this control will effect a change in the separation of the two peaks by approximately 10 °K.

6. Repeat steps 3 through 5 until both melting peaks appear as a single peak, Figure A-1b, and lock the calibration control.

Average Temperature Calibration

In order to insure that the indicated DSC-1B temperature is correct, within the limitations of the DSC-1B, the average temperature signal is calibrated using the known melting points of indium and lead. This procedure follows:

1. The average temperature control is left in the position used during the prior series of decomposition runs, and the differential temperature control is locked at the calibrated value.

2. Place a calibration sample metal in one holder cup and an empty reference calibration sample in the other cup.

3. Using indium first, and then lead, set the range control at 16 and the scan control at the speed of interest. Program through the melting transition, note the temperature, and return the temperature to 400 °K.

4. If the indicated indium and lead melting points are displaced from their actual values of 429 °K and 600 °K, respectively, by more than two degrees, then calibration is required.

5. If both melting points are low, or are both high, the average temperature signal can be corrected by turning the average temperature control. One full turn, clockwise, increases the temperature signal by

approximately 5 °K.

6. Repeat steps 3 through 5 until the indicated and known melting temperatures are the same and lock the calibration control.

If the correct calibration cannot be achieved in this manner, that is, one melting peak occurred early while the other occurred late, proper calibration can be made following the Instructions Manual. Correct temperature calibration in this investigation was always achieved using the steps outlined above; consequently, the additional calibration instructions will not be discussed.

Power Calibration

The DSC-1B and the recorder unit were always calibrated together using the heat of fusion of indium as a reference standard. The energy of transition of a known mass of indium was determined from the thermogram using a planimeter to measure the thermogram area at the appropriate range setting, scan rate, and chart speed.

For a range setting of 16, a one inch deviation of the ordinate pen corresponds to an energy output of 1.6 millicalories/second. Similarly, for a chart speed of 10 seconds/inch, a one inch abscissa travel corresponds to 10 seconds. Thus a one square inch thermogram area corresponds to 16 millicalories of energy. Using a 6.43 milligram indium sample, the energy of transition was determined at scan rates of 5, 10, 20, 40, and 80 °K/minute and compared with the known indium transition energy. These results are shown in Table A-1, below.

Operating the DSC-1B

After cleaning and calibration, the DSC-1B is prepared for

Table A-1. DSC-1B Power Calibration Check

Scan (°K/min)	Planimeter Area (counts/mg)	ΔH (calc) (cal/gm)	ΔH (known) (cal/gm)	Error (per cent)
5	0.0416	6.59	6.81	-3.3
10	0.0422	6.69	6.81	-1.8
20	0.0428	6.79	6.81	-0.3
40	0.0430	6.81	6.81	0
80	0.0432	6.84	6.81	+0.4

quantitative thermal decomposition work. The operating procedure is straightforward:

1. Energize the DSC-1B by turning the range control selector to the "standby" position.
2. Remove the sample holder cover.
3. Place the prepared binder sample in the sample cup (left-hand cup) and an empty pan in the reference cup (right-hand cup).
4. Place domed covers over both sample and reference cups.
5. Replace and secure the sample holder cover.
6. Select the desired range setting.
7. Manually set the temperature control to the desired starting temperature.
8. Set the scan control at the desired rate.
9. Start the temperature program by placing the temperature control switch in the "increase" position.
10. After reactions of interest have been completed, stop the

temperature program by placing the temperature control switch in the "neutral" position.

11. Remove the domed covers and the sample container.

12. Manually return the temperature to the desired level and return the range selector to the "standby" position.

13. If no further tests are planned, or if cleaning is required, manually program the temperature level to 273 $^{\circ}$K and de-energize the unit.

APPENDIX B

FORMULATION AND MIXING INSTRUCTIONS FOR PROPELLANT BINDERS

The binder preparation instructions and ingredients for the fuels used in this investigation were supplied by Mr. Ed Price of the Naval Weapons Center and Dr. Dave Flanigan of the Thiokol Chemical Corporation.

Polysulfide (Thiokol) Binder

PS binder was prepared using a liquid prepolymer and small percentages of three curing agents formulated by weight as follows:

LP-33	90.8%
GMF	6.1%
DPG	3.0%
XC-1	0.1%

where LP-33 is a Thiokol liquid polymer, GMF is p-quinonedioxime and serves as a curing rate catalyst, DPG is diphenylguanidine which promotes cure at low temperatures, and XC-1 (40 per cent sulfur and 60 per cent dibutyl phthalate) is an agent which promotes curing and aids in the dispersion of sulfur.

Mixing is accomplished in three steps:

1. Weigh the LP-33 polymer into the mixing container.
2. Add GMF and DPG while stirring; mix until homogeneous.
3. After homogeneity has been achieved, add XC-1 and mix for ten minutes.

The formulated binder is cured at 76 °C for 24 hours with the first three hours of cure being conducted under vacuum conditions in excess of 28 inches of mercury. The approximate cured formula is $C_{3.141}H_{6.58}O_{0.854}S_{0.869}$.

Polyurethane Binder

PU binder was prepared using a liquid prepolymer and small percentages of three curing agents formulated by weight as follows:

Estane	96.56%
TMP	2.32%
BD-1,4	0.72%
TEA	0.40%

where Estane (B. F. Goodrich Chemical Company) is a polyurethane prepolymer, type 5720X5, TMP is trimethyl-ol-propane which serves as a crosslinking agent, BD-1,4 is butanediol-1,4 which minimizes the heat of polymerization during cure, and TEA is triethanolamine which serves as a curing agent.

Mixing is accomplished in two steps:

1. Weigh the TMP, TEA, and BD-1,4 into the mixing container and heat to 70 °C to dissolve the TMP.

2. Add the Estane and mix for twenty minutes.

The formulated binder is cured at 72 °C for 96 hours with the first three hours of cure being conducted under vacuum conditions in excess of 28 inches of mercury. The cured formula is C_4H_8O.

Polybutadiene Acrylic Acid Binder

PBAA binder was prepared using PBAA copolymer and a curing agent formulated by weight as follows:

PBAA	84%
Epon 828	16%

where PBAA is the base copolymer and Epon 828 (Shell Oil Company) is an epoxy resin curing agent.

Mixing is accomplished in two steps:

1. Weigh the PBAA polymer into the mixing container.
2. Add Epon 828 and mix for twenty minutes.

The formulated binder is cured at 72 °C for 96 hours with the first three hours of cure being conducted under vacuum conditions in excess of 28 inches of mercury. The cured formula is $C_{22}H_{28}O$.

Carboxy Terminated Polybutadiene Binder

CTPB was prepared using Butarez polymer and a curing agent formulated by weight as follows:

Butarez	97.55%
MAPO	2.45%

where Butarez (Phillips Petroleum Company) is the base polymer and MAPO is tris [1(2) methyl aziridinyl] phosphine oxide which serves as a curing agent and promotes chain crosslinking.

Mixing is accomplished in two steps:

1. Weigh the Butarez polymer into the mixing container.

2. Add MAPO and mix for fifteen minutes.

The formulated binder is cured at 72 °C for 96 hours with the first three hours of cure being conducted under vacuum conditions in excess of 28 inches of mercury. The cured formula is C_2H_3 (with a trace of O).

APPENDIX C

DSC-1B DATA REDUCTION ANALYSIS

During the binder decomposition study, extreme variation of baseline position was observed, the variation being greater at higher scan rates. It should be noted that baseline curvature was observed to occur during scan programs when the sample and reference holders were empty; this is due to the inherent nonlinearity of the DSC-1B thermal circuitry and is indicated in the thermogram, Figure C-1, by the difference in the initial and final baseline positions. Changes in the value of the polymer heat capacity during a temperature scan will result in a change in the power necessary to maintain temperature equality between the sample and reference pan; this also results in a change in the initial and final baseline positions. A straightforward evaluation of the baseline curvature is precluded because the variation of binder thermal properties with temperature is not known. It seems reasonable that the baseline position should change more rapidly as the decomposition activity increases since the polymer specific heat is changing more rapidly in this region. The baseline position was established graphically by drawing a smooth curve between the point of initial thermogram deflection and the final baseline level after decomposition was completed (being careful to match the initial and final thermogram slopes). This procedure is schematically shown in Figure C-1.

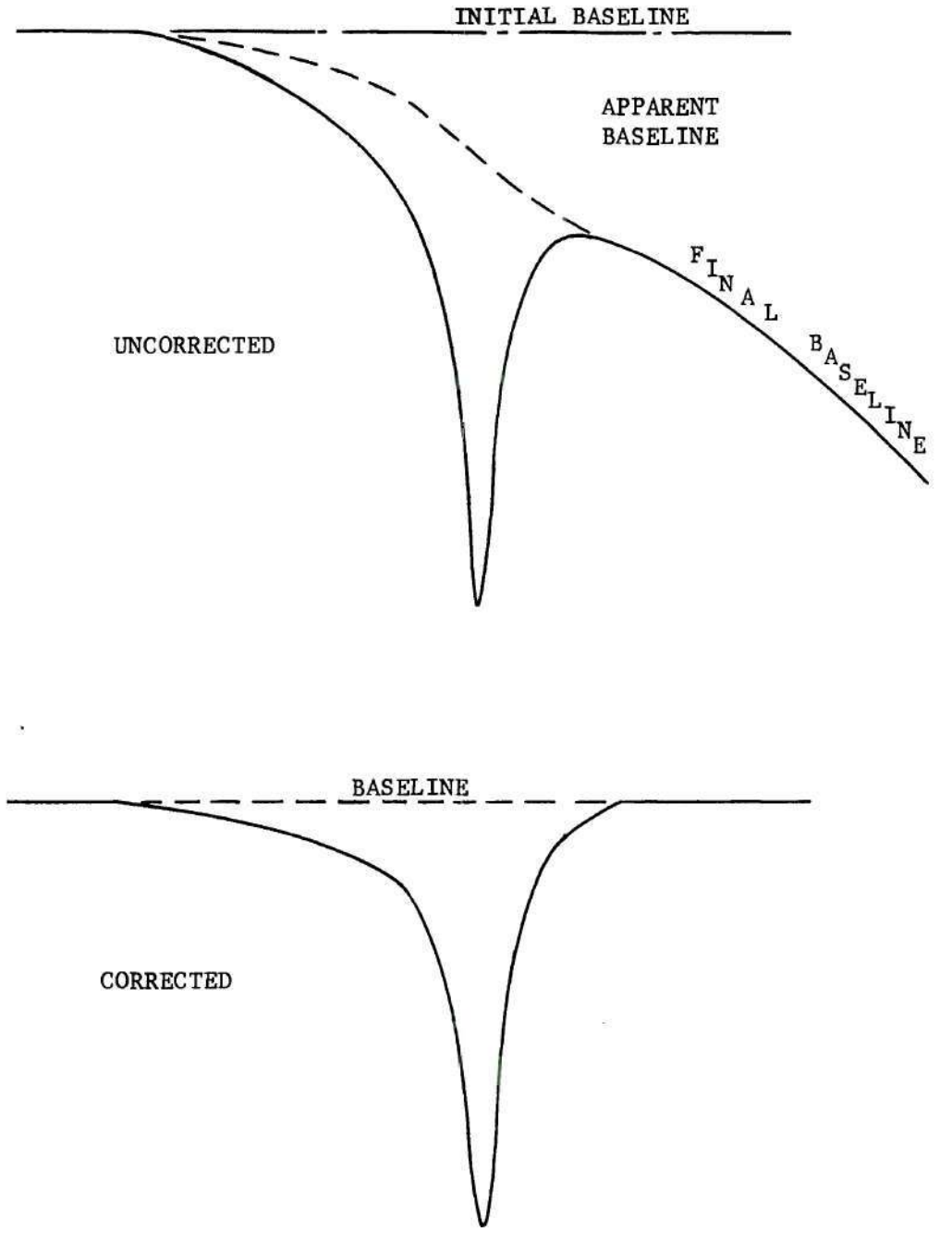

Figure C-1. Establishing the DSC-1B Thermogram Baseline Position.

Binder Decomposition Energy

The binder decomposition energy is proportional to the area enclosed by the DSC-1B thermogram and the baseline. Using a suitable metal transition, the DSC-1B response can be calibrated and the decomposition energy easily determined. Calibration curves using the transition properties of indium, Table C-1, were used to establish a proportionality constant relating the binder thermal decomposition energy to the thermogram area.

Table C-1. Indium Transition Properties

Melting Point	156.17 °C
Specific Heat	0.0652 cal/gm °C
Heat of Fusion	6.807 cal/gm

To obtain increased thermogram resolution, indium calibration curves were generated using a fast recorder speed at scan rates of 5, 10, 20, 40, and 80 °K/minute. Using a planimeter, the thermogram area was determined and initialized by the indium sample mass. These results are shown in Table C-2.

To reduce the data obtained at other recorder speeds, the effect of the abscissa contraction must be considered. The binder decomposition tests were conducted using the temperature signal from the DSC-1B to drive the abscissa instead of using a time generated sweep. Consequently, the actual sweep speed is related to the calibration sweep speed (sec/in) by

$$\text{Actual Sweep} = \frac{1920}{\text{scan}} \quad . \tag{C-1}$$

Table C-2. Indium Thermogram Calibration Areas for a Sweep Recorder Speed of 10 Seconds Per Inch

Scan (°K/min)	Transition Area (counts/milligram)
1.25	0.0405
2.5	0.0411
5	0.0416
10	0.0422
20	0.0428
40	0.0430
80	0.0438

The resulting indium calibration area for a temperature driven abscissa is given in Table C-3.

Table C-3. Indium Thermogram Areas for Temperature Driven Abscissa

Scan (°K/min)	Transition Area (counts/milligram)
1.25	0.264×10^{-3}
2.5	0.523×10^{-3}
5	1.082×10^{-3}
10	2.20×10^{-3}
20	4.46×10^{-3}
40	8.96×10^{-3}
80	18.01×10^{-3}

The indium transition area corresponds to a heat of fusion of 6.807 calories per gram. Consequently, the binder decomposition energy is related to the indium transition by

$$\Delta H_{binder} = \frac{(\Delta H)_{indium}}{(counts/mg)_{indium}} \left[\frac{counts}{mg}\right]_{binder} , \qquad (C\text{-}2)$$

where the binder thermogram area (planimeter counts) has been normalized by the binder initial mass (milligrams). The proportionality constant relating the planimeter area to the decomposition energy is given in Table C-4.

Table C-4. Proportionality Between Thermogram Area and Decomposition Energy

Scan (°K/min)	Proportionality Constant $\left[\frac{cal/gm}{(counts/mg)}\right]$
1.25	25.8×10^3
2.5	13.02×10^3
5	6.29×10^3
10	3.1×10^3
20	1.53×10^3
40	0.761×10^3
80	0.378×10^3

APPENDIX D

DSC-1B TEMPERATURE LAG

Quantitative results obtained using the DSC-1B depend quite heavily upon an accurate knowledge of the actual sample temperature during thermal decomposition. Perfect temperature accuracy is admittedly precluded by the inherent nonlinearities in the platinum sensors and other parts of the system. The net output characteristic is nonlinear with the greatest deviation between actual and indicated temperature occurring at scan speeds of 40 °K per minute and 80 °K per minute. The temperature deviation at these high scan rates may be as high as 6 °K while the deviation is less than 2 °K at all other scan rates. The inherent temperature lag is well within acceptable limits, particularly since it is an a priori lag and can be compensated.

A more disturbing feature of the DSC-1B investigation was the sensitivity of the quantitative performance to the sample size and shape. Due to the low thermal conductivity of the cured polymer and due to the sample configuration most convenient for DSC-1B use, the actual average temperature of the binder sample can be somewhat below the digital temperature indicated on the DSC-1B readout. Quite simply, a finite period of time is required for the energy supplied by the DSC-1B heaters to reach the top surface of the polymer sample; consequently, uniform sample heating is not achieved. During this heat transfer period, the temperature of the sample holder is increasing at

the programmed scan rate, and the average sample temperature is falling farther behind the indicated temperature. Presumably a steady thermal state is not achieved until the polymer sample begins to relax making more intimate contact with the sample pan. Visual observations confirmed that decomposition initiated near the base of the sample while the remainder of the sample was rapidly relaxing into a molten liquid.

In order to establish the time lag which existed between the heated surface temperature (i.e., the DSC-1B indicated temperature) and the actual temperature, a transient heating analysis was employed. Williamson and Adams [55] developed the equations for heating a body from an initial temperature under the assumption that the surface temperature is increasing proportionally to the time. These results were generalized and presented in tabular form by Jakob [46] and were used in the present analysis. From the tables of Jakob, the temperature excess, $\eta = T - T_0$, of any point of the body above the initial temperature T_0 can be found at an arbitrary instant of time if the rate of temperature increase at the surface is a given constant. The tabular results are presented in parametric form in terms of:

1. A characteristic thermal penetration time, t, normalized by s^2/α where s is depth of an insulated, infinite slab heated at the surface and α is the thermal diffusivity.

2. A dimensionless temperature excess, η/η_s, where η_s is the temperature excess between the surface and initial temperatures.

3. A dimensionless thermal penetration depth, x/s, where x is the distance away from the insulated surface.

Because of sample shape irregularities and ignorance of the true location, x/s, for the average sample temperature, the dimensionless temperature excess and the dimensionless thermal penetration depth were both taken equal to 0.5. These assumptions gave a dimensionless thermal penetration time, $\alpha t/s^2$, of approximately 0.80. For a sample approximately one millimeter thick and using a thermal diffusivity of 1×10^{-3} cm^2/sec, the time for the thermal wave to penetrate to the middle of the sample was about 18 seconds. In other words, the average sample temperature is about 18 seconds behind indicated temperature at any scan rate. Translated into a temperature lag, the difference between the indicated and actual temperature varies from one degree at a scan of 5 °K per minute to 25 degrees at a scan of 80 °K per minute.

The thermal decomposition of PU binder was characterized by a well defined melt transition which occurred at 495 °K at a scan of 5 °K/minute. As the scan rate was increased from 5 °K per minute to 80 °K per minute, the melt transition temperature indicated on the DSC-1B was delayed until nearly 530 °K, a lag of nearly 35 °K. The results tabulated from the transient analysis and the thermal lag observed in the PU binder decomposition tests are compared in Table D-1.

Table D-1. Comparison Between Calculated and Observed Binder Thermal Lag

Scan (°K/min)	ΔT_{calc} (°K)	$\Delta T_{observed}$ (°K)
5	1.5	0
10	3	5
20	6	12
40	12	16
80	24	35

These results are in accord and indicate that the analysis is qualitatively correct.

The kinetics data for both PU and PS were generated using a corrected temperature to compensate for the previously discussed thermal lag. The PU temperature correction was based on the observed melt transition temperature whereas the PS correction was based on the calculated temperature lag.

APPENDIX E

DSC-1B BINDER THERMAL DECOMPOSITION DATA

DSC-1B data are in the form of a thermogram representing the instantaneous rate of heat absorption or evolution as a function of absolute temperature. The experimental data will be presented by binder type in a manner which is consistent with the data reduction procedure. Typical thermograms are presented for a selected range of temperature scan rates. The instantaneous heating rate, the thermogram ordinate, has been initialized by the original sample mass to facilitate run to run comparisons. The data used to determine the binder kinetics are presented in tabular form in Tables E-1 through E-22.

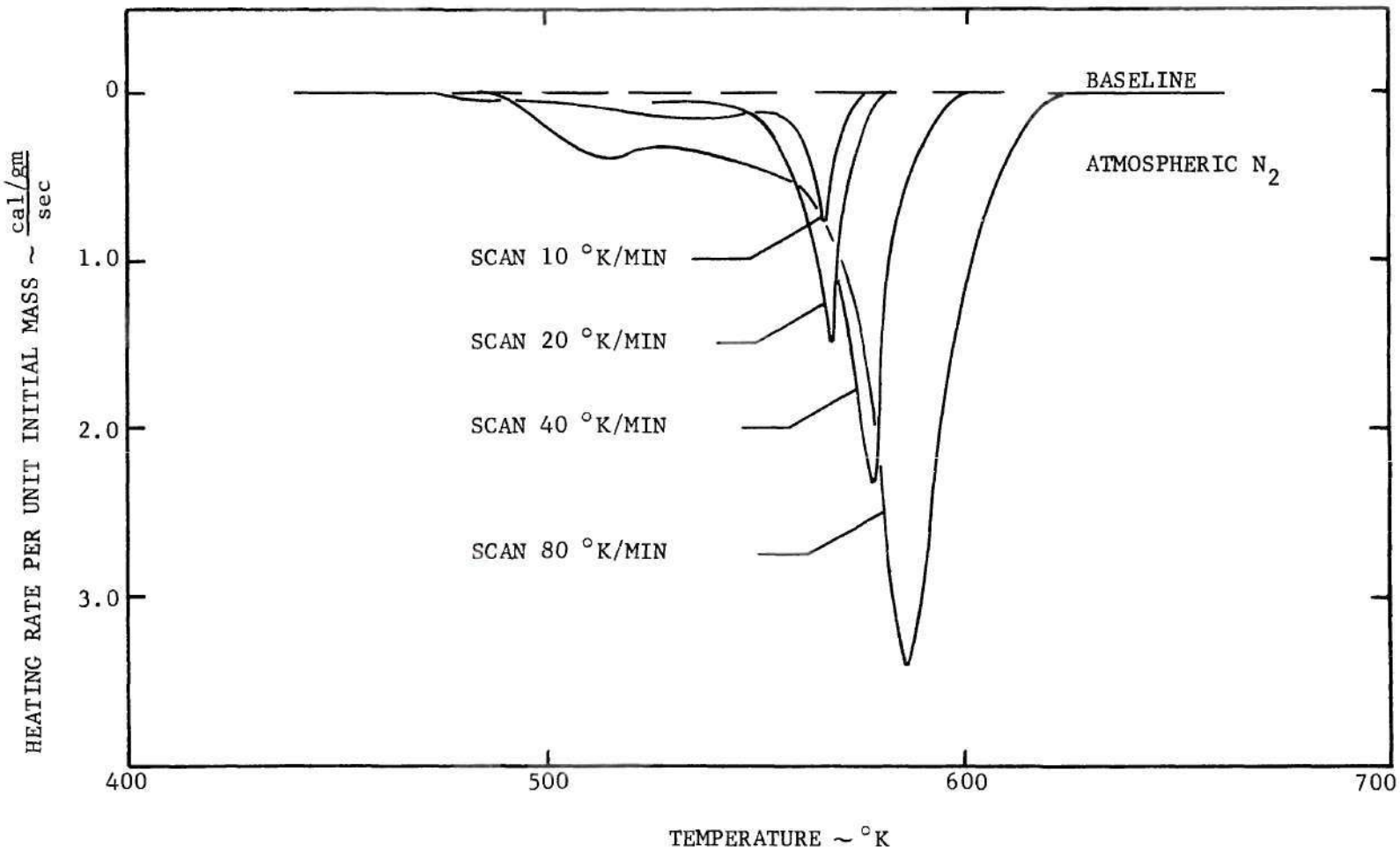

Figure E-1. Thermal Decomposition of PS.

Table E-1. Binder DSC-1B Data for PS Decomposed at a Scan Rate of 5 °K Per Minute

Initial Mass (mg)	Total Energy of Decomposition (cal/gm)	Corrected Temperature (°K)	Reciprocal Temperature ($°K^{-1} \times 10^3$)	Sample Mass Ratio Remaining (gm/gm)	DSC-1B Heating Rate (millicalories/sec)	Sample Heat Absorption Rate Per Unit Mass Remaining ($\frac{calories/sec}{gm}$)
3.3	94.0	470	2.126	.99	.103	.0315
		480	2.082	.98	.125	.0386
		490	2.04	.97	.126	.0394
		500	2.0	.96	.136	.0429
		510	1.961	.93	.07	.0229
		520	1.922	.90	.09	.03
		530	1.886	.87	.165	.0575
		540	1.851	.81	.167	.0625
		543	1.842	.79	.268	.103
		547	1.828	.75	.44	.178
		550	1.819	.72	.80	.336
		553	1.809	.68	.64	.285
		557	1.792	.61	.147	.073
		560	1.786	.54	.04	.022

Table E-2. Binder DSC-1B Data for PS Decomposed at a Scan Rate of 10 °K Per Minute

Initial Mass (mg)	Total Energy of Decomposition (cal/gm)	Corrected Temperature (°K)	Reciprocal Temperature ($°K^{-1} \times 10^3$)	Sample Mass Ratio Remaining (gm/gm)	DSC-1B Heating Rate (millicalories/sec)	Sample Heat Absorption Rate Per Unit Mass Remaining ($\frac{\text{calories/sec}}{\text{gm}}$)
1.6	69.8	473	2.116	.99	0.	-
		480	2.082	.98	.052	.033
		490	2.04	.97	.098	.063
		500	2.	.95	.112	.074
		510	1.961	.93	.127	.085
		520	1.922	.90	.102	.071
		530	1.886	.87	.114	.082
		540	1.851	.81	.163	.126
		550	1.819	.71	.202	.178
		553	1.808	.68	.254	.234
		557	1.796	.61	.397	.407
		560	1.786	.54	.583	.674
		563	1.778	.42	.945	1.41
		566.5	1.768	.21	.435	1.30
		570	1.753	.04	.173	2.7

Table E-3. Binder DSC-1B Data for PS Decomposed at a Scan Rate of 10 °K Per Minute

Initial Mass (mg)	Total Energy of Decomposition (cal/gm)	Corrected Temperature (°K)	Reciprocal Temperature ($°K^{-1} \times 10^3$)	Sample Mass Ratio Remaining (gm/gm)	DSC-1B Heating Rate (millicalories/sec)	Sample Heat Absorption Rate Per Unit Mass Remaining ($\frac{calories/sec}{gm}$)
6.1	66.4	474	-	.99	0.0	-
		480	2.082	.98	.173	.029
		490	2.04	.97	.221	.037
		500	2.0	.95	.243	.042
		510	1.961	.93	.243	.043
		520	1.922	.90	.222	.040
		530	1.886	.87	.226	.042
		540	1.851	.81	.707	.143
		550	1.819	.71	.786	.182
		556.5	1.799	.62	1.08	.286
		560	1.786	.54	1.62	.491
		563	1.778	.42	3.18	1.24
		566	1.767	.22	5.04	3.74
		566.5	1.765	.21	4.34	3.39
		568	1.759	.09	2.08	3.79
		570	1.753	.04	.96	3.93

Table E-4. Binder DSC-1B Data for PS Decomposed at a Scan Rate of 20 °K Per Minute

Initial Mass (mg)	Total Energy of Decomposition (cal/gm)	Corrected Temperature (°K)	Reciprocal Temperature ($°K^{-1} \times 10^3$)	Sample Mass Ratio Remaining (gm/gm)	DSC-1B Heating Rate (millicalories/sec)	Sample Heat Absorption Rate Per Unit Mass Remaining ($\frac{calories/sec}{gm}$)
1.5	83.5	477	2.1	.98	-	-
		481	2.08	.98	.037	-
		491	2.038	.97	.213	.145
		501	1.998	.96	.226	.157
		511	1.958	.93	.218	.156
		521	1.920	.91	.115	.085
		531	1.883	.88	.157	.119
		541	1.848	.82	.238	.193
		551	1.816	.74	.228	.206
		561	1.781	.58	.506	.582
		563	1.778	.52	1.02	1.31
		567	1.762	.38	2.13	3.74
		569	1.758	.30	2.66	5.91
		571	1.749	.20	1.51	5.04
		573	1.747	.12	.72	4.0

Table E-5. Binder DSC-1B Data for PS Decomposed at a Scan Rate of 20 °K Per Minute

Initial Mass (mg)	Total Energy of Decomposition (cal/gm)	Corrected Temperature (°K)	Reciprocal Temperature ($°K^{-1} \times 10^3$)	Sample Mass Ratio Remaining (gm/gm)	DSC-1B Heating Rate (millicalories/sec)	Sample Heat Absorption Rate Per Unit Mass Remaining ($\frac{\text{calories/sec}}{\text{gm}}$)
1.9	65.2	477	2.1	.98	0.	-
		481	2.08	.98	.052	-
		491	2.038	.97	.13	.071
		501	1.998	.96	.13	.071
		511	1.958	.93	.133	.075
		521	1.920	.91	.088	.051
		531	1.883	.88	.126	.075
		541	1.848	.82	.282	.181
		551	1.816	.74	.44	.313
		557	1.794	.65	.64	.518
		561	1.781	.58	1.03	.951
		563	1.778	.52	1.41	1.43
		567	1.762	.38	2.33	3.23
		569	1.758	.30	2.80	4.91
		570	1.755	.22	2.37	5.66
		573	1.747	.12	.82	3.60

Table E-6. Binder DSC-1B Data for PS Decomposed at a Scan Rate of 40 °K Per Minute

Initial Mass (mg)	Total Energy of Decomposition (cal/gm)	Corrected Temperature (°K)	Reciprocal Temperature ($°K^{-1} \times 10^3$)	Sample Mass Ratio Remaining (gm/gm)	DSC-1B Heating Rate (millicalories/sec)	Sample Heat Absorption Rate Per Unit Mass Remaining ($\frac{calories/sec}{gm}$)
1.9	64.5	486	2.059	.97	0.0	-
		496	2.018	.95	.227	.126
		506	1.977	.93	.302	.171
		516	1.938	.90	.357	.208
		526	1.902	.87	.307	.186
		536	1.867	.83	.350	.222
		546	1.831	.77	.507	.347
		556	1.799	.70	.876	.659
		566	1.768	.55	1.28	1.22
		572	1.749	.44	2.21	2.64
		576	1.734	.19	3.24	8.99
		580	1.723	.15	3.25	9.0
		582	1.718	.09	1.93	11.3
		586	1.704	.04	.65	8.55

Table E-7. Binder DSC-1B Data for PS Decomposed at a Scan Rate of 40 °K Per Minute

Initial Mass (mg)	Total Energy of Decomposition (cal/gm)	Corrected Temperature (°K)	Reciprocal Temperature ($°K^{-1} \times 10^3$)	Sample Mass Ratio Remaining (gm/gm)	DSC-1B Heating Rate (millicalories/sec)	Sample Heat Absorption Rate Per Unit Mass Remaining ($\frac{\text{calories/sec}}{\text{gm}}$)
1.9	66.1	486	2.059	.97	0.0	-
		496	2.018	.95	.253	.140
		506	1.977	.93	.23	.130
		516	1.938	.90	.194	.113
		526	1.902	.87	.189	.114
		536	1.867	.83	.323	.205
		546	1.831	.77	.508	.347
		556	1.799	.70	.639	.48
		566	1.768	.55	1.26	1.21
		574	1.742	.37	2.57	3.66
		576	1.734	.19	3.6	9.97
		579	1.728	.18	4.34	12.7
		582	1.718	.09	2.76	16.1
		586	1.704	.04	1.03	13.6

Table E-8. Binder DSC-1B Data for PS Decomposed at a Scan Rate of 80 °K Per Minute

Initial Mass (mg)	Total Energy of Decomposition (cal/gm)	Corrected Temperature (°K)	Reciprocal Temperature ($°K^{-1} \times 10^3$)	Sample Mass Ratio Remaining (gm/gm)	DSC-1B Heating Rate (millicalories/sec)	Sample Heat Absorption Rate Per Unit Mass Remaining ($\frac{calories/sec}{gm}$)
1.3	64.5	492	2.037	.99	0.0	-
		507	1.971	.96	.472	.378
		517	1.932	.93	.531	.44
		527	1.897	.89	.546	.472
		537	1.861	.86	.381	.341
		547	1.828	.81	.456	.433
		557	1.793	.76	.712	.72
		567	1.761	.69	1.06	1.18
		577	1.731	.58	1.48	1.96
		579	1.728	.53	1.62	2.35
		582	1.718	.47	2.78	4.55
		587	1.702	.32	3.86	9.29
		592	1.689	.17	3.13	14.2
		597	1.674	.07	1.50	16.5

Table E-9. Binder DSC-1B Data for PS Decomposed at a Scan Rate of 80 °K Per Minute

Initial Mass (mg)	Total Energy of Decomposition (cal/gm)	Corrected Temperature (°K)	Reciprocal Temperature ($°K^{-1} \times 10^3$)	Sample Mass Ratio Remaining (gm/gm)	DSC-1B Heating Rate (millicalories/sec)	Sample Heat Absorption Rate Per Unit Mass Remaining ($\frac{\text{calories/sec}}{\text{gm}}$)
1.8	68	491	2.038	.99	0.0	-
		497	2.012	.98	.138	-
		507	1.971	.96	.578	.336
		517	1.932	.93	.725	.433
		527	1.897	.89	.579	.362
		537	1.861	.86	.579	.374
		547	1.828	.81	.694	.475
		557	1.793	.76	.91	.664
		567	1.761	.69	1.36	1.09
		577	1.731	.58	2.31	2.22
		582	1.718	.46	3.99	4.81
		587	1.702	.32	6.14	10.7
		597	1.674	.07	3.40	22.

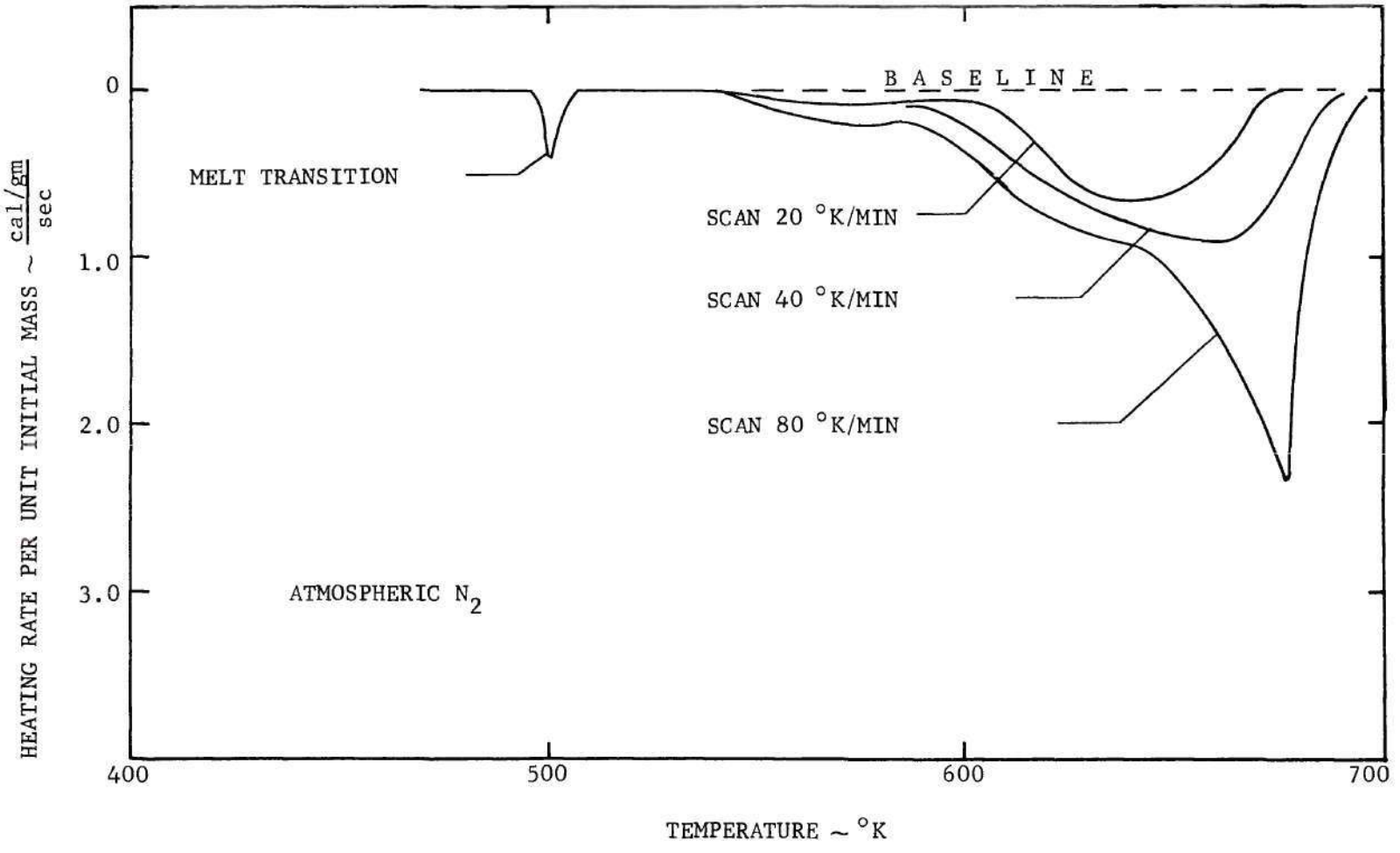

Figure E-2. Thermal Decomposition of PU.

Table E-10. Binder DSC-1B Data for PU Decomposed at a Scan Rate of 10 °K Per Minute

Initial Mass (mg)	Total Energy of Decomposition (cal/gm)	Corrected Temperature (°K)	Reciprocal Temperature ($°K^{-1} \times 10^3$)	Sample Mass Ratio Remaining (gm/gm)	DSC-1B Heating Rate (millicalories/sec)	Sample Heat Absorption Rate Per Unit Mass Remaining ($\frac{\text{calories/sec}}{\text{gm}}$)
1.3	78.8	585	1.719	.82	.104	.122
		595	1.680	.77	.16	.158
		605	1.653	.69	.128	.143
		615	1.628	.65	.104	.123
		625	1.60	.53	.256	.372
		630	1.588	.47	.304	.497
		635	1.575	.38	.432	.874
		640	1.562	.28	.545	1.50
		645	1.55	.06	.656	8.4

Table E-11. Binder DSC-1B Data for PU Decomposed at a Scan Rate of 20 °K Per Minute

Initial Mass (mg)	Total Energy of Decomposition (cal/gm)	Corrected Temperature (°K)	Reciprocal Temperature ($°K^{-1} \times 10^3$)	Sample Mass Ratio Remaining (gm/gm)	DSC-1B Heating Rate (millicalories/sec)	Sample Heat Absorption Rate Per Unit Mass Remaining ($\frac{\text{calories/sec}}{\text{gm}}$)
2.2	79.4	568	1.761	.95	.208	.099
		578	1.730	.9	.208	.105
		588	1.701	.86	.192	.102
		598	1.671	.82	.272	.151
		608	1.645	.78	.208	.121
		618	1.619	.65	.752	.526
		628	1.592	.54	.769	.648
		638	1.569	.40	.976	1.11
		648	1.544	.24	1.01	1.91
		658	1.520	.13	.85	2.98
		668	1.498	.01	.176	8.

Table E-12. Binder DSC-1B Data for PU Decomposed at a Scan Rate of 40 °K Per Minute

Initial Mass (mg)	Total Energy of Decomposition (cal/gm)	Corrected Temperature (°K)	Reciprocal Temperature ($°K^{-1} \times 10^3$)	Sample Mass Ratio Remaining (gm/gm)	DSC-1B Heating Rate (millicalories/sec)	Sample Heat Absorption Rate Per Unit Mass Remaining ($\frac{calories/sec}{gm}$)
2.2	78.1	570	1.755	.97	.112	.053
		590	1.695	.93	.176	.086
		600	1.667	.91	.642	.32
		610	1.639	.83	1.12	.615
		620	1.613	.72	1.27	.801
		630	1.588	.61	1.28	.955
		640	1.562	.50	1.43	1.3
		650	1.539	.38	1.70	2.04
		655	1.528	.30	1.82	2.76
		660	1.515	.21	1.84	3.98
		665	1.503	.13	1.67	5.84
		670	1.492	.07	1.36	8.85
		680	1.470	.01	.256	11.6

Table E-13. Binder DSC-1B Data for PU Decomposed at a Scan Rate of 40 °K Per Minute

Initial Mass (mg)	Total Energy of Decomposition (cal/gm)	Corrected Temperature (°K)	Reciprocal Temperature ($°K^{-1} \times 10^3$)	Sample Mass Ratio Remaining (gm/gm)	DSC-1B Heating Rate (millicalories/sec)	Sample Heat Absorption Rate Per Unit Mass Remaining ($\frac{calories/sec}{gm}$)
1.6	73.1	560	1.785	.97	.128	.083
		570	1.755	.95	.176	.116
		580	1.725	.92	.256	.174
		590	1.695	.88	.384	.273
		600	1.667	.83	.496	.374
		610	1.639	.77	.656	.533
		620	1.613	.68	.768	.706
		630	1.588	.59	.80	.849
		640	1.562	.49	.816	1.04
		650	1.539	.39	.896	1.44
		654	1.530	.35	.832	1.48
		660	1.515	.27	1.3	3.01
		665	1.503	.14	1.33	5.94
		670	1.492	.05	1.06	13.2

Table E-14. Binder DSC-1B Data for PU Decomposed at a Scan Rate of 80 °K Per Minute

Initial Mass (mg)	Total Energy of Decomposition (cal/gm)	Corrected Temperature (°K)	Reciprocal Temperature ($°K^{-1} \times 10^3$)	Sample Mass Ratio Remaining (gm/gm)	DSC-1B Heating Rate (millicalories/sec)	Sample Heat Absorption Rate Per Unit Mass Remaining ($\frac{\text{calories/sec}}{\text{gm}}$)
2.0	74.8	565	1.77	.99	.464	.234
		575	1.739	.97	.608	.314
		585	1.719	.95	.752	.396
		595	1.68	.92	.928	.504
		605	1.653	.83	1.14	.686
		615	1.628	.77	1.43	.936
		625	1.60	.69	1.63	1.18
		635	1.575	.59	1.75	1.48
		645	1.55	.49	2.18	2.22
		655	1.528	.37	2.48	3.35
		665	1.503	.24	3.01	6.26
		668	1.498	.17	3.35	9.86
		675	1.481	.08	2.5	15.6
		681	1.469	.02	1.01	25.2
		685	1.460	.01	.448	22.4

Table E-15. Binder DSC-1B Data for PU Decomposed at a Scan Rate of 80 °K Per Minute

Initial Mass (mg)	Total Energy of Decomposition (cal/gm)	Corrected Temperature (°K)	Reciprocal Temperature ($°K^{-1} \times 10^3$)	Sample Mass Ratio Remaining (gm/gm)	DSC-1B Heating Rate (millicalories/sec)	Sample Heat Absorption Rate Per Unit Mass Remaining ($\frac{\text{calories/sec}}{\text{gm}}$)
2.6	77.9	565	1.77	.98	.384	.151
		575	1.739	.96	.40	.160
		585	1.719	.95	.496	.201
		595	1.680	.93	.704	.291
		605	1.653	.91	1.25	.529
		615	1.628	.88	1.86	.813
		625	1.60	.76	2.18	1.10
		635	1.575	.68	2.32	1.31
		645	1.55	.59	2.56	1.67
		655	1.528	.48	3.23	2.58
		660	1.515	.41	3.64	3.42
		665	1.503	.30	4.76	6.11
		670	1.492	.17	5.92	13.4
		675	1.481	.10	4.02	15.8
		680	1.470	.01	1.17	45.

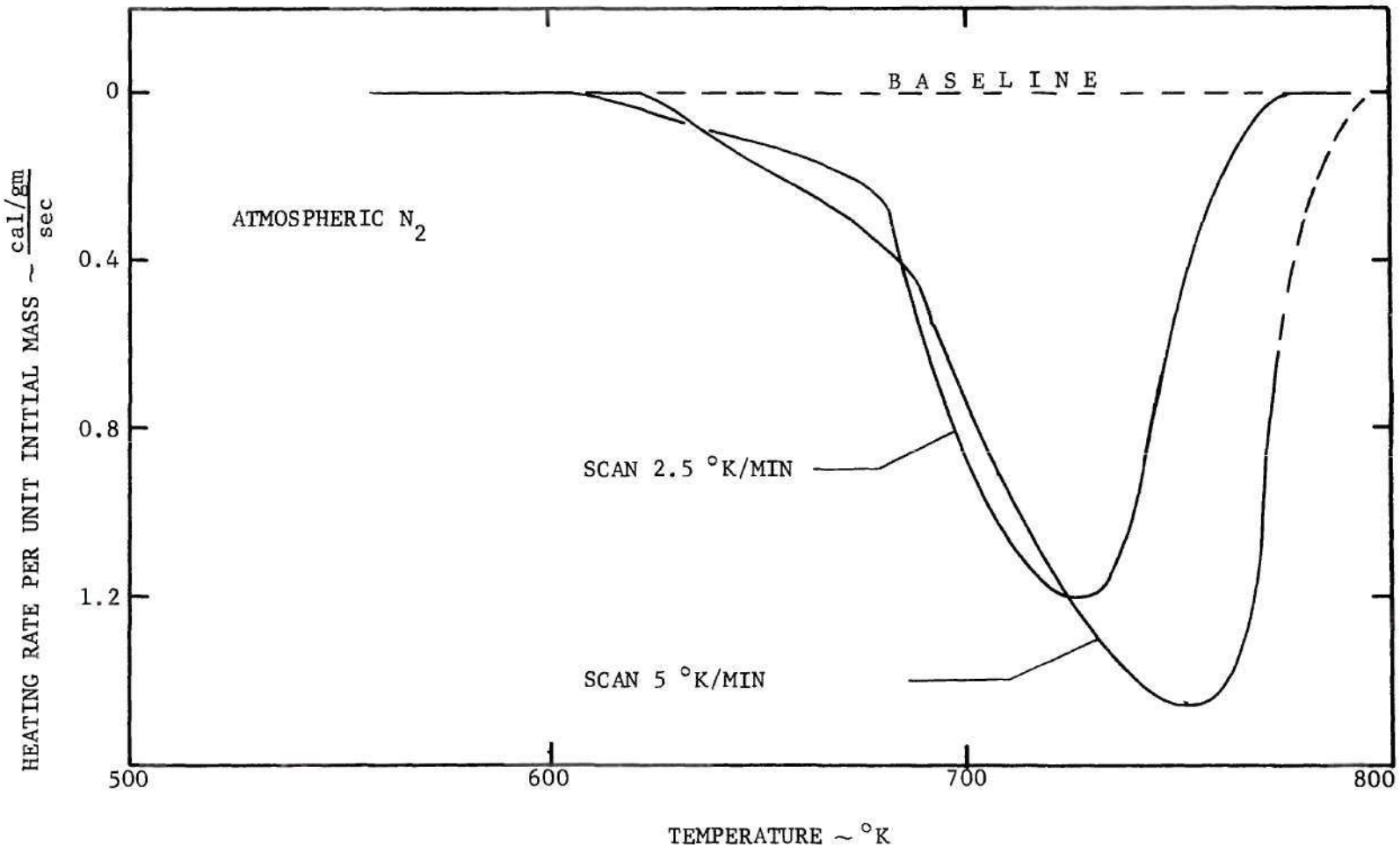

Figure E-3. Thermal Decomposition of PBAA.

Table E-16. Binder DSC-1B Data for PBAA Decomposed at a Scan Rate of 2.5 °K Per Minute

Initial Mass (mg)	Total Energy of Decomposition (cal/gm)	Corrected Temperature (°K)	Reciprocal Temperature ($°K^{-1} \times 10^3$)	Sample Mass Ratio Remaining (gm/gm)	DSC-1B Heating Rate (millicalories/sec)	Sample Heat Absorption Rate Per Unit Mass Remaining ($\frac{\text{calories/sec}}{\text{gm}}$)
2.8	1980	640	1.562	.98	.38	.139
		650	1.539	.96	.54	.201
		660	1.516	.93	.72	.276
		670	1.491	.89	.90	.361
		680	1.470	.85	1.07	.573
		690	1.449	.79	1.52	.689
		700	1.428	.71	1.97	.99
		710	1.408	.60	2.29	1.37
		720	1.389	.48	2.56	1.90
		730	1.369	.36	2.76	2.74
		740	1.350	.22	2.61	4.24
		750	1.333	.11	2.1	6.82
		760	1.315	.04	1.2	10.7

Table E-17. Binder DSC-1B Data for PBAA Decomposed at a Scan Rate of 2.5 °K Per Minute

Initial Mass (mg)	Total Energy of Decomposition (cal/gm)	Corrected Temperature (°K)	Reciprocal Temperature ($°K^{-1} \times 10^3$)	Sample Mass Ratio Remaining (gm/gm)	DSC-1B Heating Rate (millicalories/sec)	Sample Heat Absorption Rate Per Unit Mass Remaining ($\frac{calories/sec}{gm}$)
2.2	1940	640	1.562	.98	.22	.102
		650	1.539	.97	.31	.145
		660	1.516	.95	.34	.163
		670	1.491	.93	.4	.196
		680	1.470	.90	.54	.272
		690	1.449	.85	1.14	.61
		700	1.428	.76	1.65	.99
		710	1.408	.64	2.22	1.58
		720	1.389	.49	2.64	2.45
		730	1.369	.33	2.66	3.68
		740	1.350	.18	2.03	5.13
		750	1.333	.08	1.19	6.76
		760	1.315	.03	.496	7.51

Table E-18. Binder DSC-1B Data for PBAA Decomposed at a Scan Rate of 5 °K Per Minute

Initial Mass (mg)	Total Energy of Decomposition (cal/gm)	Corrected Temperature (°K)	Reciprocal Temperature ($°K^{-1} \times 10^3$)	Sample Mass Ratio Remaining (gm/gm)	DSC-1B Heating Rate (millicalories/sec)	Sample Heat Absorption Rate Per Unit Mass Remaining ($\frac{calories/sec}{gm}$)
2.4	1930	650	1.539	.97	.82	.35
		660	1.516	.94	1.07	.48
		670	1.491	.93	1.31	.59
		680	1.470	.87	1.6	.77
		690	1.449	.83	1.7	.85
		700	1.428	.77	2.35	1.27
		710	1.408	.70	2.8	1.67
		720	1.389	.62	3.17	2.13
		730	1.369	.52	3.44	2.76
		740	1.350	.43	3.65	3.54
		750	1.333	.33	3.6	4.55
		760	1.315	.23	3.34	5.8
		770	1.299	.14	3.01	8.95

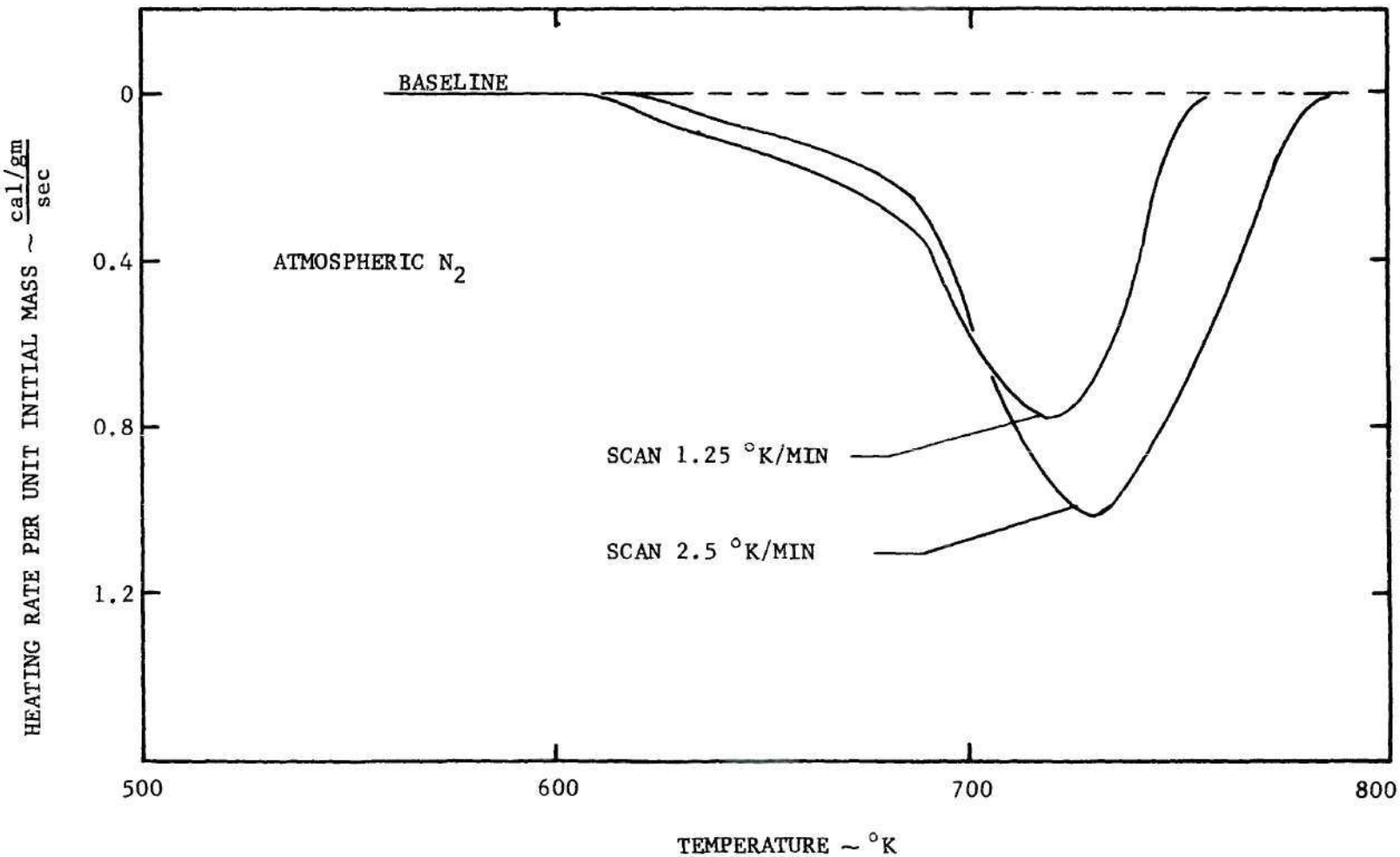

Figure E-4. Thermal Decomposition of CTPB.

Table E-19. Binder DSC-1B Data for CTPB Decomposed at a Scan Rate of 1.25 °K Per Minute

Initial Mass (mg)	Total Energy of Decomposition (cal/gm)	Corrected Temperature (°K)	Reciprocal Temperature ($°K^{-1} \times 10^3$)	Sample Mass Ratio Remaining (gm/gm)	DSC-1B Heating Rate (millicalories/sec)	Sample Heat Absorption Rate Per Unit Mass Remaining ($\frac{calories/sec}{gm}$)
2.6	1880	680	1.470	.98	.13	.051
		686	1.458	.97	.21	.098
		690	1.449	.94	1.07	.44
		700	1.428	.80	1.54	.74
		710	1.408	.62	1.81	1.12
		720	1.389	.41	2.05	1.92
		730	1.369	.20	1.52	2.92
		740	1.350	.07	.88	4.84
		750	1.333	.01	.24	9.24

Table E-20. Binder DSC-1B Data for CTPB Decomposed at a Scan Rate of 2.5 °K Per Minute

Initial Mass (mg)	Total Energy of Decomposition (cal/gm)	Corrected Temperature (°K)	Reciprocal Temperature ($°K^{-1} \times 10^3$)	Sample Mass Ratio Remaining (gm/gm)	DSC-1B Heating Rate (millicalories/sec)	Sample Heat Absorption Rate Per Unit Mass Remaining ($\frac{calories/sec}{gm}$)
2.6	1920	640	1.562	.99	.18	.073
		650	1.539	.97	.24	.095
		660	1.516	.96	.35	.146
		670	1.491	.94	.43	.183
		680	1.470	.91	.58	.255
		690	1.449	.88	.74	.336
		700	1.428	.83	1.46	.705
		710	1.408	.74	1.91	1.03
		720	1.389	.62	2.45	1.58
		730	1.369	.48	2.64	2.2
		740	1.350	.36	2.16	2.4
		750	1.333	.25	1.71	2.74
		760	1.315	.17	1.39	3.27

Table E-21. Binder DSC-1B Data for CTPB Decomposed at a Scan Rate of 2.5 °K Per Minute

Initial Mass (mg)	Total Energy of Decomposition (cal/gm)	Corrected Temperature (°K)	Reciprocal Temperature ($°K^{-1} \times 10^3$)	Sample Mass Ratio Remaining (gm/gm)	DSC-1B Heating Rate (millicalories/sec)	Sample Heat Absorption Rate Per Unit Mass Remaining ($\frac{\text{calories/sec}}{\text{gm}}$)
3.2	1940	640	1.562	.97	.38	.122
		650	1.539	.95	.48	.158
		660	1.516	.93	.56	.188
		670	1.491	.90	.66	.229
		680	1.470	.87	.82	.295
		690	1.449	.83	1.01	.38
		700	1.428	.78	1.73	.694
		710	1.408	.70	2.29	1.02
		720	1.389	.59	2.68	1.42
		730	1.369	.47	2.96	1.97
		740	1.350	.35	2.56	2.28
		750	1.333	.25	2.16	2.7
		760	1.315	.17	1.71	3.14
		770	1.299	.09	1.25	4.34

Table E-22. Binder DSC-1B Data for CTPB Decomposed at a Scan Rate of 5 °K Per Minute

Initial Mass (mg)	Total Energy of Decomposition (cal/gm)	Corrected Temperature (°K)	Reciprocal Temperature ($°K^{-1} \times 10^3$)	Sample Mass Ratio Remaining (gm/gm)	DSC-1B Heating Rate (millicalories/sec)	Sample Heat Absorption Rate Per Unit Mass Remaining ($\frac{\text{calories/sec}}{\text{gm}}$)
2.5	1910	660	1.516	.96	.74	.308
		670	1.491	.93	.94	.404
		680	1.470	.91	1.1	.484
		690	1.449	.87	1.46	.672
		700	1.428	.83	1.79	.863
		710	1.408	.78	2.51	1.29
		720	1.389	.70	2.98	1.70
		730	1.369	.61	3.4	2.23
		740	1.350	.52	3.84	2.96
		750	1.333	.41	3.8	3.71
		760	1.315	.30	3.46	4.61
		770	1.299	.21	3.05	5.81

APPENDIX F

QUENCH COMBUSTION SYSTEM RUN PROCEDURE

The general procedures used in the combustion tests were those outlined in Chapter III. A detailed run procedure, including electrical and mechanical checks, follows.

Preliminary Checks

Mechanical

1. N_2 supply cylinder valves (3) closed.
2. System control valve MOV-1 closed.
3. System bleed valve MOV-2 closed.
4. System metering valves NV-1 and NV-2 closed.

Electrical

1. Cam timer actuator switch in OFF position.
2. Ignition circuit armed.
3. Quench circuit armed.
4. Primary power circuit connected.

Run Procedure

1. Open N_2 supply cylinder valves (3).
2. Note manifold pressure level.
3. Open system control valve MOV-1.
4. Adjust combustion vessel pressure level via panel mounted hand loader.

5. Note combustion pressure level.

6. Open system metering valve(s) NV-1 and/or NV-2.

7. Switch cam timer actuator ON.

8. Following quench (a loud discharge), switch cam timer actuator OFF.

9. Close system control valve MOV-1.

10. Close N_2 supply cylinder valves (3).

11. Open system bleed valve MOV-2.

12. Open system control valve MOV-1.

13. Note manifold pressure; all gauges should indicate zero psig.

Post-Run Checks

Mechanical

1. Relieve hand loader internal pressure.

Electrical

1. Disconnect primary power.

2. Quench circuit disarmed.

3. Ignition circuit disarmed.

APPENDIX G

MYLAR DIAPHRAGM RUPTURE EVALUATION TEST

In order to achieve successful rupture with the mylar quenching device, Figure G-1a, it was desirable to use a diaphragm which was stressed near the failure point. To preclude any premature failures, it was decided to establish a diaphragm rupture curve and operate slightly below the failure curve. Since the diaphragm total thickness was achieved by placing several laminae of 5 mil mylar discs into the retainer, the operating thickness was established by simply adding one additional 5 mil disc to the critical rupture thickness. The results of the rupture test and the recommended operating curve are shown in Figure G-1b.

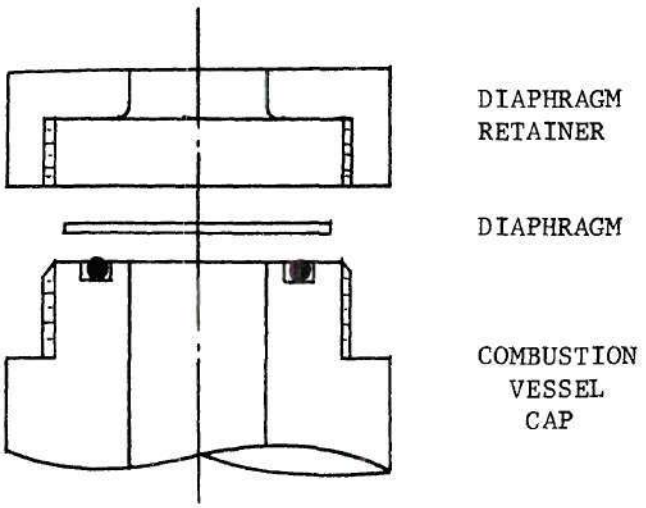

(a) QUENCHING SCHEMATIC

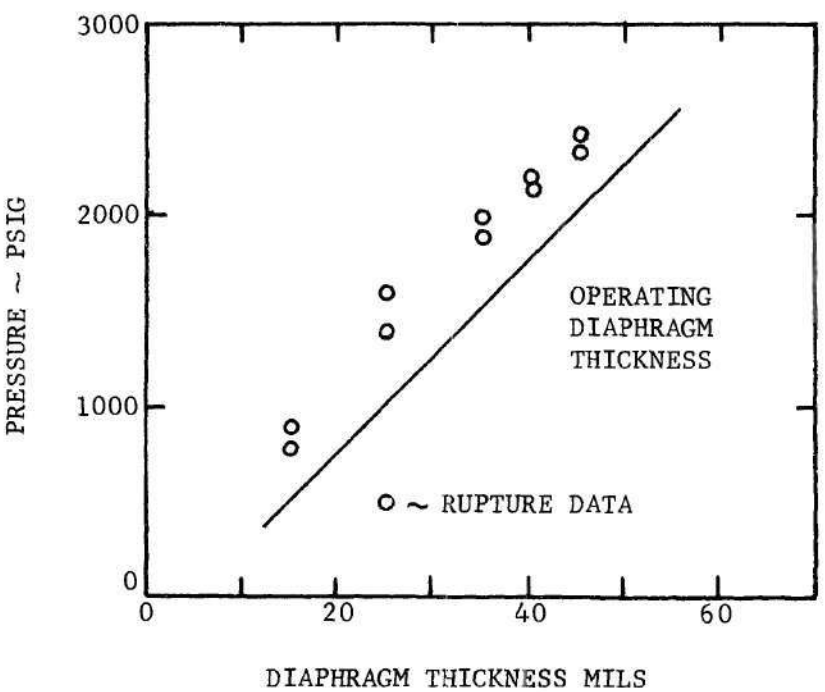

(b) OPERATING DIAPHRAGM THICKNESS

Figure G-1. Mylar Diaphragm Rupture Analysis.

APPENDIX H

QUENCH COMBUSTION STUDY DATA

The data obtained in the quench combustion study were the quenched sample, a sample mass loss during combustion, and the sample burn time. Prior to combustion, the laminated sandwich width and thickness were measured and used to calculate an approximate sandwich regression area. These data were then used to determine the sandwich regression mass flux (mass loss per unit time per unit area) for comparison with the mass flux of deflagrating AP. The quench combustion data and the calculated parameters are tabulated in Tables H-1, H-2, H-3, and H-4 for PBAA, PS, CTPB, and PU sandwich regression, respectively.

Table H-1. PBAA Sandwich Quench Data

Pressure (psig)	Sandwich Thickness (cm)	Binder Thickness (microns)	Mass Loss (gm)	Burn Time (sec)	Regression Area (cm^2)	Mass Flux ($\frac{gm/sec}{cm^2}$)
300	0.328	50	0.2070	1.725	0.216	0.55
300	0.296	200	0.1342	2.525	0.109	0.49
600	0.250	25	0.1441	1.225	0.089	1.33
600	0.326	75	0.3200	1.725	0.128	1.45
600	0.332	100	0.3836	1.725	0.131	1.70
1000	0.252	25	0.1458	0.975	0.097	1.54
1000	0.271	75	0.2237	1.225	0.113	1.61
1000	0.292	100	0.2145	0.975	0.112	1.96
1500	0.248	25	0.1231	0.725	0.093	1.84
1500	0.302	100	0.1598	0.725	0.112	1.96
2000	0.252	25	0.1100	0.475	0.093	2.50
2000	0.327	150	0.2058	0.475	0.120	3.60
2400	0.252	25	0.1106	0.475	0.092	2.52
2400	0.254	150	0.1930	0.475	0.094	4.32

Table H-2. PS Sandwich Quench Data

Pressure (psig)	Sandwich Thickness (cm)	Binder Thickness (microns)	Mass Loss (gm)	Burn Time (sec)	Regression Area (cm^2)	Mass Flux ($\frac{gm/sec}{cm^2}$)
300	0.308	55	0.1775	1.725	0.177	0.582
300	0.312	75	0.1730	1.725	0.184	0.545
600	0.248	35	0.1426	1.225	0.093	1.26
600	0.318	55	0.2043	1.225	0.115	1.46
600	0.292	75	0.2168	1.225	0.109	1.64
1000	0.254	35	0.1858	0.975	0.100	1.91
1000	0.312	45	0.2460	0.975	0.120	2.1
1000	0.314	55	0.3287	0.975	0.128	2.63
1000	0.306	75	0.3148	0.975	0.115	2.8
1500	0.250	35	0.1726	0.725	0.095	2.52
1500	0.282	55	0.2370	0.725	0.106	3.09
1500	0.306	75	0.3078	0.725	0.116	3.64
2000	0.248	35	0.1202	0.475	0.091	2.78
2000	0.294	45	0.1613	0.475	0.107	3.18
2000	0.259	55	0.1589	0.475	0.092	3.65
2000	0.308	75	0.2319	0.475	0.113	4.31
2400	0.248	35	0.1207	0.475	0.091	2.8
2400	0.276	55	0.1769	0.475	0.100	3.71

Table H-3. CTPB Sandwich Quench Data

Pressure (psig)	Sandwich Thickness (cm)	Binder Thickness (microns)	Mass Loss (gm)	Burn Time (sec)	Regression Area (cm^2)	Mass Flux ($\frac{gm/sec}{cm^2}$)
300	0.274	35	0.0589	1.225	0.132	0.358
300	0.302	120	0.1190	1.225	0.256	0.378
300	0.324	120	0.1483	1.225	0.310	0.39
600	0.270	35	0.1222	1.225	0.099	1.01
600	0.312	120	0.1353	1.225	0.102	1.08
600	0.312	120	0.1312	1.225	0.112	0.96
1000	0.268	35	0.1660	0.975	0.103	1.66
1000	0.320	60	0.1634	0.975	0.104	1.61
1000	0.316	120	0.1244	0.975	0.116	1.08
1500	0.314	60	0.1655	0.725	0.118	1.94
1500	0.318	75	0.1554	0.725	0.119	1.8
2000	0.258	35	0.1007	0.475	0.100	2.12
2000	0.314	75	0.1307	0.475	0.114	2.41
2400	0.268	35	0.1022	0.475	0.089	2.42
2400	0.270	75	0.1364	0.475	0.098	2.92

Table H-4. PU Sandwich Quench Data

Pressure (psig)	Sandwich Thickness (cm)	Binder Thickness (microns)	Mass Loss (gm)	Burn Time (sec)	Regression Area (cm^2)	Mass Flux ($\frac{gm/sec}{cm^2}$)
300	0.298	100	0.0446	1.225	0.097	0.375
300	0.298	100	0.0612	1.225	0.129	0.388
600	0.294	40	0.1529	1.225	0.132	1.16
600	0.262	40	0.1286	1.225	0.101	1.04
600	0.292	100	0.0925	0.975	0.099	0.94
1000	0.254	40	0.1430	0.975	0.097	1.51
1000	0.296	100	0.1414	0.975	0.113	1.28
1000	0.302	200	0.1291	0.975	0.114	1.16
1500	0.262	40	0.1381	0.725	0.098	1.95
1500	0.284	200	0.1445	0.725	0.113	1.76
2000	0.254	40	0.0776	0.475	0.094	1.75
2000	0.294	100	0.1243	0.475	0.125	2.09
2000	0.290	100	0.1400	0.475	0.134	2.2
2400	0.254	40	0.0684	0.475	0.093	1.55
2400	0.302	100	0.1681	0.475	0.123	2.88

APPENDIX I

BINDER AND OXIDIZER PYROLYSIS PRODUCTS MIXING REGION

In an effort to determine the region of the sandwich surface which could possibly be affected by heat transfer from a gas phase diffusion flame, the width of the diffusion mixing region was determined. In this simple analysis, binder-oxidizer species mixing is considered to occur by molecular diffusion only. The effect of a binder melt has not been included.

Define the width of the mixing region at any position x above the interface to be f. The mixing region boundary, Figure I-1, represents the lateral spread of oxidizer and binder species by diffusion while being swept upward by the mean gas velocity. The binder and oxidizer are assumed to contribute equally to the gaseous evolution velocity although this most certainly is not true. The lateral and vertical position of a point on the mixing boundary is simply a vector sum of the mean vertical velocity, u, and the diffusion velocity, v. If the binder-oxidizer concentration gradient is taken as unity, the diffusion velocity based on the characteristic width of the mixing region is approximated by

$$v \approx \frac{G}{f} , \qquad \text{(I-1)}$$

where G is the diffusion coefficient. The flow velocity and diffusion

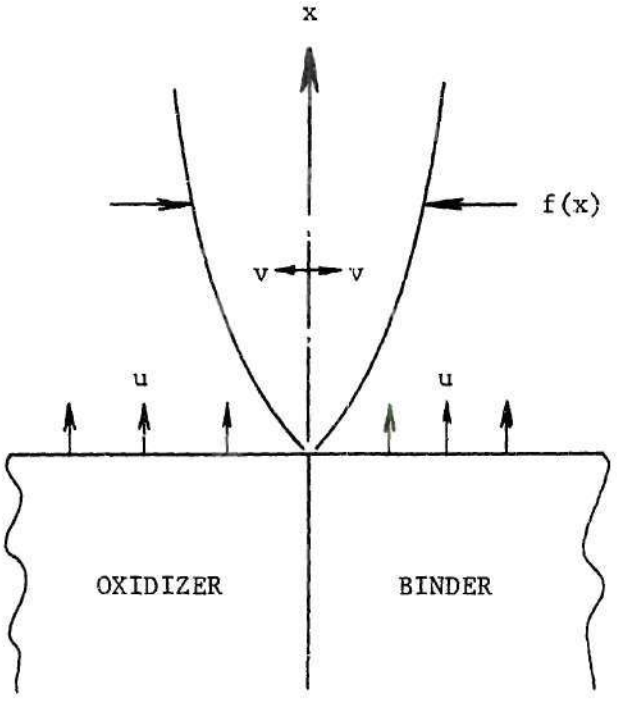

Figure I-1. Width of Binder and Oxidizer Products Mixing Region.

velocity can be expressed in terms of the mixing boundary by

$$v \approx \frac{df}{dt} \tag{I-2}$$

$$u \approx \frac{dx}{dt} .$$

Combining equations (I-1) and (I-2) and integrating gives

$$f^2 \approx \frac{2Gx}{u} . \tag{I-3}$$

If the diffusion coefficient and gas velocity are taken as 1×10^{-3} cm^2/sec and 600 cm/sec, respectively, then the mixing boundary f(x) is

$$f^2(x) \approx 3 \times 10^{-6} x . \tag{I-4}$$

For a point 200 microns above the interface, the predicted mixing zone width is only two microns.

APPENDIX J

SANDWICH STOICHIOMETRIC BALANCE

Stoichiometric relations describing the presumed chemical reaction between AP oxidizer and the polymeric fuels are presented. The stoichiometric products will be defined as CO_2, H_2O, HCl, N_2, and SO_2 (where applicable). The polymer formulae used are open to some question and, consequently, the results presented are only intended to provide an indication of the stoichiometry achieved in the sandwich fabrication.

$$NH_4ClO_4 + \upsilon_1(\text{Polymer})_n = \upsilon_2 CO_2 + \upsilon_3 H_2O + \upsilon_4 HCl + \upsilon_5 N_2 + \upsilon_6 SO_2 \ , \quad \text{(J-1)}$$

where the υ are the stoichiometric coefficients of the reaction and N is the degree of polymerization. The stoichiometric coefficient for the polymer was determined from an elemental balance and used to calculate the stoichiometric mass ratio, O/F, for the reaction. The ratio of the sandwich thickness, τ, to binder thickness, δ, for stoichiometric conditions was calculated using

$$\left(\frac{\tau}{\delta}\right)_{ST} = \frac{\rho_p}{\rho_{ox}}\left(O/F\right) + 1 \ . \quad \text{(J-2)}$$

The results of the calculations and the τ/δ ratios achieved in the sandwich fabrication indicate that the sandwich composition is highly oxidizer rich.

Table J-1. Sandwich Stoichiometric Balance

Reactant	Molecular Weight	Binder Stoichiometric Coefficient	Stoichiometric Mass Ratio (O/F)	Sandwich Oxidizer to Binder thickness Ratio(τ/δ)	
				Calculated	Formulated
AP	117.5	5/22N	7.2	5.3	15-60
PU	72N	5/114N	13	8	10-80
PBAA	308N	5/13N	7.1	5.4	10-80
CTPB	43N	2.5/10.5N	5.7	4.7	25-70
PS	87N				

BIBLIOGRAPHY

1. Wilfong, R. E., Penner, S. S., and Daniels, F., Journal of Physical Chemistry, 54 (1950)

2. Schultz, R. D., and Dekker, A. O., Aerojet-General Corporation, Report Number 576 (1952).

3. Chaiken, R. F., "A Thermal Layer Mechanism of Combustion of Solid Composite Propellants: Application to Ammonium Nitrate," Combustion and Flame, 3 (1959).

4. Chaiken, R. F., and Andersen, W. H., "The Role of Binder in Composite Propellant Combustion," Solid Propellant Rocket Research, 1, ed. by Martin Summerfield, Academic Press, New York (1960).

5. Sutherland, G. S., "The Mechanism of Combustion of an Ammonium Perchlorate-Polyester Resin Composite Solid Propellant," Ph.D. Thesis, Princeton University (1956).

6. Summerfield, Martin, Sutherland, G. S., Webb, M. J., Taback, H. J., and Hall, K. P., "Burning Mechanism of Ammonium Perchlorate Propellants," Solid Propellant Rocket Research, 1, ed. by Martin Summerfield, Academic Press, New York (1960).

7. Blair, D. W., Bastress, E. K., Hermance, C. E., Hall, K. P., and Summerfield, M., "Some Research Problems in the Steady State Burning of Composite Solid Propellants," Solid Propellant Rocket Research, 1, ed. by Martin Summerfield, Academic Press, New York (1960).

8. Steinz, J. A., Stang, P. L., and Summerfield, M., "The Burning Mechanism of Ammonium Perchlorate-Based Composite Solid Propellants," Princeton University Aerospace and Mechanical Sciences Report Number 830, Princeton University (1969).

9. Shannon, Larry J., "Composite Solid Propellant Ignition by Radiant Energy," AIAA Journal, 8 (1970).

10. Boggs, T. L., Derr, R. L., and Beckstead, M. W., "Surface Structure of Ammonium Perchlorate Composite Propellants," AIAA Journal, 8 (1970).

11. Boggs, T. L., "The Deflagration of Pure Single Crystals of Ammonium Perchlorate," AIAA Paper Number 69-142, New York (1969).

12. Nachbar, W., "A Theoretical Study of the Burning of a Solid Propellant Sandwich," Solid Propellant Rocket Research, 1, Academic Press, New York (1960).

13. Schultz, R. D., Green, L., and Penner, S. S., "Studies of the Decomposition Mechanism, Erosive Burning, Sonance, and Resonance for Solid Composite Propellants," Combustion and Propulsion, Pergamom Press, New York (1958).

14. Fenn, J. B., "A Phalanx Flame Model for the Combustion of Composite Solid Propellants," Combustion and Flame, 12 (1968).

15. Hermance, Clarke E., "A Model of Composite Propellant Combustion Including Surface Heterogeneity and Heat Generation," AIAA Journal, 4 (1966).

16. Hermance, Clarke E., "A Detailed Model of the Combustion of Composite Solid Propellants," AIAA Solid Propellant Propulsion Conference, Anaheim (1967).

17. Culick, F. E. C., and Dehority, G. L., "An Elementary Calculation for the Burning Rate of Composite Solid Propellants," Combustion Science and Technology, 1 (1969).

18. Wenograd, J., "Study of the Kinetics and Energetics of Propellant Decomposition Reactions and Application to Steady State Combustion Mechanism," Third ICRPG Combustion Conference, CPIA Publication Number 138, 5 (1966).

19. Waesche, R. H. W., and Wenograd, J., "The Effects of Pressure and Additives on the Kinetics of Decomposition of Ammonium Perchlorate," Combustion Institute Meeting, Western States Section, San Diego (1967).

20. Waesche, R. H. W., Wenograd, J., and Feinauer, L. R., "Investigation of Solid Propellant Decomposition Characteristics and Their Relation to Observed Burning Rates," ICRPG-AIAA Solid Propulsion Conference, San Diego (1967).

21. Waesche, R. H. W., "Research Investigation of the Decomposition of Composite Solid Propellants," United Aircraft Research Laboratories, Report Number F-910476-12 (1967).

22. Waesche, R. H. W., "Research Investigation of the Decomposition of Composite Solid Propellants," United Aircraft Research Laboratories, Report Number G-910476-24 (1968).

23. Caveny, L. H., and Pittman, C. U., "Contribution of Solid Phase Heat Release to AP Composite Propellant Burning Rate," AIAA Journal, 6 (1968).

24. Beckstead, M. W., and Hightower, J.D., "On the Surface Temperature of Deflagrating Ammonium Perchlorate Crystals," AIAA Journal, 5 (1967).

25. Pittman, C. U., "The Mechanism of Decomposition of Ammonium Perchlorate: A Review," U.S. Army Missile Command Report Number RK-TR-66-13 (1966).

26. Jackobs, P.W.M., "Kinetics and Mechanism of the Decomposition of Ammonium Perchlorate," Third ICRPG Combustion Conference, CPIA Publication Number 138, 5 (1966).

27. Friedman, R., Nugent, R. C., Rumbel, K. E., and Scurlock, A. C., "Deflagration of Ammonium Perchlorate," Sixth Symposium (International) on Combustion, Reinhold Publishing Corporation, New York (1957).

28. Powling, J., "Experiments Relating to the Combustion of Ammonium Perchlorate Based Propellants," Eleventh Symposium (International) on Combustion, The Combustion Institute, Pittsburgh (1967).

29. Price, E. W., "Solid Propellant Combustion: State of Knowledge 1967," Sixty-Second National Meeting of the American Institute of Chemical Engineers, Paper Number 3b, Salt Lake City (1967).

30. Grassie, Norman, Chemistry of High Polymer Degradation Processes, Butterworths Scientific Publications, London (1956).

31. Wall, W. A., "Pyrolysis," Analytical Chemistry of Polymers, High Polymers Series, 12, Interscience Publishers, New York (1962).

32. Grassie, Norman, "Thermal Degradation," Chemical Reactions of Polymers, High Polymers Series, 19, Interscience Publishers, New York (1964).

33. Madorsky, S. I., "Thermal Degradation of Organic Polymers," Mechanism of Polymer Reactions, High Polymers Series, 20, Interscience Publishers, New York (1964).

34. Jellinek, H. H. G., Degradation of Vinyl Polymers, Academic Press, New York (1955).

35. Howard, B. C., "Pyrolysis of Some Composite Propellant Fuel Binders," Explosives Research and Development Establishment Report Number 13-R-65, Waltham Abbey, Essex, England (1965).

36. Sammons, George D., "Application of Differential Scanning Calorimetry to the Study of Solid Propellant Decomposition," Third ICRPG Combustion Conference, CPIA Publication Number 138, 5 (1966).

37. Shannon, L. J., and Erickson, J. E., "Thermal Decomposition of Composite Solid Propellant Binders," Sixth ICRPG Combustion Conference, CPIA Publication Number 192, 1 (1969).

38. Hightower, J. D., and Price, E. W., "Two-Dimensional Experimental Studies of the Combustion Zone of Composite Solid Propellants," Second ICRPG Combustion Conference, CPIA Publication Number 105, 1 (1966).

39. Hightower, J. D., and Price, E. W., "Experimental Studies Relating to the Combustion Mechanism of Composite Propellants," Astronautica Acta, 14, Pergamon Press, London (1968).

40. Powling, J., "The Combustion of Ammonium Perchlorate-Based Composite Propellants: A Discussion of Some Recent Experimental Results," Explosives Research and Development Establishment Report Number 15-R-65, Waltham Abbey, Essex, England (1965).

41. Austin, T. D., "Flame Temperature Profile of Ammonium Perchlorate Fuel Binder Sandwiches," Fourth ICRPG Combustion Conference, CPIA Publication Number 162, 1 (1967).

42. Nadaud, L., "Models Used at ONERA to Interpret Combustion Phenomena in Heterogeneous Solid Propellants," Combustion and Flame, 12 (1968).

43. Instructions, Differential Scanning Calorimeter, Perkin-Elmer Document Number 990-9556, Norwalk (1967).

44. Encyclopedia of Chemical Technology, 11, John Wiley and Sons, New York (1966).

45. Roff, J. W., Fibers, Plastics, and Rubbers, Academic Press, New York (1956).

46. Jakob, Max, Heat Transfer, John Wiley and Sons, Inc., New York (1949).

47. Finlayson, B. G., and Scriven, L. E., "The Method of Weighted Residuals and its Relation to Certain Variational Principles for the Analysis of Transport Processes," Chemical Engineering Science, 20 (1965).

48. Boggs, Thomas L., Private Communication, March (1970).

49. Boggs, T. L., and Zurn, D. E., "The Deflagration of Pure and Doped Ammonium Perchlorate," Sixth ICRPG Combustion Conference, CPIA Publication Number 192, 1 (1969).

50. Cieplucn, C. C., "Effect of Rapid Pressure Decay on Solid Propellant Combustion," ARS Journal, 31 (1961).

51. Mantilla, R., Baer, A., and Ryan, R., "Extinction by Rapid Depressurization: A Means to Other Ends," Third ICRPG Combustion Conference, CPIA Publication Number 138, 5 (1966).

52. Horton, M. D., Bruno, P. S., and Graesser, E. C., "Depressurization Induced Extinction of Burning Solid Propellant," AIAA Journal, 6 (1968).

53. Powling, J., and Smith, W. A. W., "The Surface Temperature of Burning Ammonium Perchlorate," Combustion and Flame, 7 (1963).

54. Powling, J., and Smith, W. A. W., "The Surface Temperature of Ammonium Perchlorate Burning at Elevated Pressures," Tenth International Symposium on Combustion, Combustion Institute, Pittsburgh (1965).

55. Williamson, E. D., and Adams, L. H., "Temperature Changes in the Manufacture of Optical Glass," Physics Review, 14 (1919).

VITA

Al Michael Varney was born in Sanford, Florida, on June 15, 1941. He attended elementary schools in Williamson, West Virginia and DeLand, Florida and was graduated from DeLand High School in June, 1959. In September of 1959, Mr. Varney entered the Georgia Institute of Technology and received the degree of Bachelor of Aerospace Engineering in June, 1963.

From 1963 to 1965, Mr. Varney was employed with Pratt & Whitney Aircraft in West Palm Beach, Florida. In September of 1965, he returned to the Georgia Institute of Technology as a graduate student and received the degree of Master of Science in Aerospace Engineering in December of 1966.

After working for a year with the Martin-Marietta Corporation, Orlando, Florida, as a senior engineer, Mr. Varney returned to the Georgia Institute of Technology and was awarded an NDEA Fellowship to study under the doctoral program. He was a member of The Society of The Sigma Xi, Tau Beta Pi, Sigma Gamma Tau, Phi Eta Sigma, American Institute of Aeronautics and Astronautics, and Delta Tau Delta Social Fraternity. Mr. Varney has been chosen to attend the von Karman Institute for Fluid Dynamics, Rhode-Saint-Genese, Belgium, during 1970-1971 academic year.

On September 19, 1962, Mr. Varney married the former Marolyn Frances Marcum of Eustis, Florida; they have one child, Pamela Carrole.